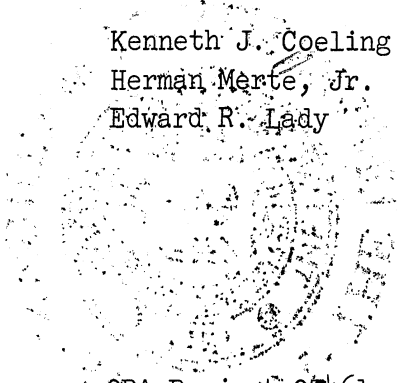# THE UNIVERSITY OF MICHIGAN

COLLEGE OF ENGINEERING
Department of Mechanical Engineering
Heat Transfer Laboratory

Technical Report No. 3

INCIPIENT BOILING OF CRYOGENIC LIQUIDS

Kenneth J. Coeling
Herman Merte, Jr.
Edward R. Lady

ORA Project 07461

under contract with:

NATIONAL AERONAUTICS AND SPACE ADMINISTRATION
GEORGE C. MARSHALL SPACE FLIGHT CENTER
CONTRACT NO. NAS 8-20228
HUNTSVILLE, ALABAMA

administered through:

OFFICE OF RESEARCH ADMINISTRATION   ANN ARBOR

January 1968

This report was also a dissertation submitted by
the first author in partial fulfillment of the require-
ments for the degree of Doctor of Philosophy in The
University of Michigan, 1967.

TABLE OF CONTENTS

TABLE OF CONTENTS (Concluded)

LIST OF TABLES

LIST OF FIGURES

vi

LIST OF FIGURES (Continued)

LIST OF FIGURES (Concluded)

NOMENCLATURE

Units indicated are the units normally used, other units indicated locally where needed.

Symbol   Definition

A area, cm^2

c_p specific heat, joules/gm°K

D diameter of heat transfer surface, cm

d diameter, cm or in.

g gravitational acceleration, cm/sec^2 or ft/sec^2

Gr Grashof number, $\rho^2 g\beta \Delta T L^3/\mu^2$

h heat transfer coefficient, watts/cm°K

h_{fg} heat of vaporization, erg/gm

L length, cm

Nu Nusselt number, hL/k

P pressure, $dynes/cm^2$ or $lbf/in.^2$

Pr Prandtl number $c_p\mu/k$

q heat rate, watts

q'' heat flux, $watts/cm^2$

r radius, cm or in.

T temperature, °K or °F

v_{fg} specific volume increase during vaporization, cm^3/gm

β thermal coefficient of volume expansion, 1/°K

NOMENCLATURE (Concluded)

Symbol	Definition
δ	thickness, cm or in.
δT_{corr}	temperature drop from surface thermocouple to the surface, °K
μ	viscosity, poise
ρ	density, gm/cm^3
σ	surface tension, $ergs/cm^2$

Subscripts

c	cavity
f	liquid
g	gas
l	liquid
L	loss
M	measured
s	surface—saturation
sat	saturation
sur	surface
v	vapor

ABSTRACT

The purpose of this work was to determine the heat flux and surface superheat necessary to initiate nucleate boiling, i.e., form the initial vapor, on a flat surface heating into a pool of saturated liquid hydrogen. Some incipient boiling data were also obtained with liquid nitrogen, used to check out the system. Natural convection and nucleate boiling heat transfer data were obtained with both liquids when the incipient boiling tests were conducted. The variables investigated are surface material, surface roughness, and orientations. The surface materials used are stainless steel, copper, Teflon, and a special surface consisting of a glass fiber web covered with epoxy cement. The stainless steel and copper surfaces were tested in both a polished and roughened condition. The orientations investigated are horizontal upwards, vertical, and horizontal downwards.

An instrumented test surface was placed in the cryogenic liquid and heated by a dc resistance wire heater. After steady state conditions were established, the heater power and surface superheat were measured and visual observations of the surface made. The visual observations were to determine if vapor was being formed and, if so, the pattern of the boiling. The heater power was then stepped to a new value, steady state conditions established, and new measurements and observations made.

Natural convection and nucleate boiling heat transfer data from surfaces heating upwards and vertically in liquid hydrogen are presented. The range of heat fluxes is from less than 10×10^{-3} watts/cm^2 to 1500×10^{-3} watts/cm^2. For liquid nitrogen, natural convection heat transfer data for surfaces heating upwards and downwards and nucleate boiling heat transfer data for surfaces heating upwards are presented. The range of heat fluxes is from 10×10^{-3} watts/cm^2 to $10,000 \times 10^{-3}$ watts/cm^2. The surface superheat and heat flux when the initial observable vapor was formed are reported for 15 combinations of surfaces, liquids and orientations. The surface superheats at the initial vapor point range from almost 0°K for an epoxy coated surface heating upwards in liquid hydrogen to over 6°K for a polished stainless steel surface heating upwards in liquid nitrogen.

During nucleate boiling of liquid hydrogen, the rate of heat transfer at a given surface superheat was as much as 25 times greater from a copper surface than from a stainless steel surface prepared in an identical manner. Over the range of boiling heat fluxes investigated, the rate of heat transfer from a surface at a given surface superheat was greater when heating vertically than when heating upwards. When boiling liquid hydrogen, the roughest stainless steel surface tested required a larger surface superheat than a smoother stainless steel surface for a given heat flux. The smoothest stainless steel surface required the largest surface superheat. It is postulated

that the liquid hydrogen wets the larger surface cavities. The roughest surface has many large cavities on it, so the wetting results in a number of potentially active sites being inactive and the surface superheat at a given heat flux increases.

The surface superheat and heat flux at which the initial vapor was observed to form on a given surface in a given orientation were reproducible to within $\pm 25\%$ of the average values. The initial vapor formation in liquid hydrogen and liquid nitrogen is primarily a function of the surface superheat and is not a strong function of orientation or heat flux. In general, the lower the surface superheat needed to form the initial vapor on a uniform surface, the lower the surface superheat at a given nucleate boiling heat flux.

I. INTRODUCTION AND LITERATURE SURVEY

A. INTRODUCTION

Boiling liquids, although used for centuries, received relatively little attention from researchers until the last several decades. When a large quantity of heat is generated in a small volume, nucleate boiling is especially attractive for removing the heat as it permits a large heat flux to be transferred from a solid surface (or nonboiling liquid) to a boiling liquid with a relatively small temperature difference between them. The development of nuclear reactors, jet engines and rocket motors has been responsible for much of the recent interest in nucleate boiling.

In nucleate boiling, the liquid is in contact with the heated surface and vapor is formed at (or very near) the surface. An understanding of the vapor formation process at a heated surface is thus necessary for an understanding of nucleate boiling. In many instances, it is also desirable to know under what conditions the very efficient heat transfer mechanism of nucleate boiling replaces the less efficient mechanism of natural convection.

The increased use of cryogenic liquids in recent years creates a need for reliable data for heat transfer from a solid surface to cryogenic liquids. A critical review of the data available in the literature indicates that much of it is either questionable because potentially large heat losses and temperature differences between the surface and measuring device where neglected, or of limited practical use because of unusual test geometry or test procedures.

The cryogenic liquids can also serve as a rather severe test of correlations and theories as their physical properties are considerably different than those of the "normal" liquids usually used for comparison. The problem of dissolved gases is eliminated or minimized with certain cryogenic liquids. No gas can go into solution in liquid helium and only helium can go into solution in liquid hydrogen. Being available in high purity, the cryogenic liquids are excellent for heat transfer studies.

The incipient boiling of liquid hydrogen is of particular interest in the space program. For the long term storage of liquid hydrogen under near zero gravity conditions, it is important to know the heat flux and temperature at the container wall at which nucleate boiling will be initiated.

The purpose of this work was to determine the heat flux and surface temperature necessary to initiate nucleate boiling, i.e., form the initial vapor, on a flat surface heating into a saturated pool of liquid hydrogen. Some incipient boiling data were also recorded with liquid nitrogen, while checking out the system. Natural convection and nucleate boiling heat transfer data were recorded for both liquids when the incipient boiling tests were made. The variables investigated are surface material, suface roughness and orientation. The surface materials investigated are stainless steel, copper, Teflon, and a special surface consisting of a glass fiber web coated with epoxy cement. The stainless steel and copper surfaces were tested in both a polished and roughened condition. The orientations investigated are horizontal upwards, vertical, and horizontal downwards.

B. LITERATURE SURVEY

The immense amount of literature available on nucleate boiling and on the

inception of boiling makes it impractical to attempt here a complete review of the literature. Instead the reader is referred to one of the many reviews that are available[e.g.,1-4] and only that literature of direct interest for the present work will be reviewed here.

The formation of a vapor nucleus from the liquid phase and the conditions for the growth of a vapor nucleus have been investigated both analytically and experimentally. Bankoff[5] applied nucleation theory to a superheated liquid at a solid surface and made an order of magnitude comparison between superheats observed in boiling and those theoretically necessary to form a new vapor nucleus at different locations. From these comparisons he concluded that during nucleate boiling no new nuclei form within the homogeneous liquid, on a flat surface, at a projection on the surface or in a well wetted cavity. Instead, nucleation occurs preferentially in nonwetted cavities, and it is likely that ebullition normally results from the growth of existing nuclei. By microphotography, Clark, Strenge and Westwater[6] found that active nucleation sites were located at surface imperfections such as pits and scratches. Howell and Siegel[13] reported that photographs of water boiling from artificial sites drilled in stainless steel surfaces show a vapor nucleus remaining in the site after a bubble leaves.

Analyses for the growth of a vapor nucleus are given by many authors.[e.g.,7-13] The general procedure is to first relate the difference between the pressure of the vapor in the nucleus and the liquid pressure to the radius of curvature of the nucleus and the fluid properties. Gibbs equation for the static equilibrium of a bubble,

$$\Delta P = \frac{2\sigma}{r} \qquad (1)$$

is usually used for this purpose. The pressure differential is then related

to the increase in the saturation temperature of the vapor in the nucleus by

means of the Claperyon relation,

$$\frac{dP}{dT} = \frac{h_{fg}}{Tv_{fg}} \ . \qquad (2)$$

This temperature increase is a liquid superheat if referred to the liquid

pressure.

Analyses differ owing to the assumption of various equilibrium shapes of

the vapor nucleus, various criterion for determining when the vapor nucleus will

grow and various temperature distributions in the liquid. The equilibrium shape

of the vapor nucleus is that shape which it assumes before it begins to grow.

All of the analyses assume that the vapor fills the cavity and extends into the

liquid as a truncated sphere, a common case being a hemisphere. The radius of

the truncated sphere and the amount of truncation depend upon the cavity

radius, the angle of the cavity wall, and the liquid contact angle. For a

hemispherical nucleus, the radius of the hemisphere is equal to the cavity

radius. Generally the criterion for growth of the vapor nucleus is that the

temperature at some critical location exceeds the saturation temperature of

the vapor inside the nucleus.

Corty and Foust[7] formulated a general expression for the radius of curvature

of the vapor-liquid interface of a vapor nucleus in a conical cavity. Assuming

that the nuclei were truncated spheres, that the surface cavities had cone angles

of 120° and that the critical temperature location is at the solid-liquid interface,

boiling heat transfer data were used to calculate the size of the surface cavities

theoretically serving as nucleation sites on two different surfaces. The cavity

sizes so computed from data for three different liquids boiling on each surface

agreed resonably well with each other.

The analysis of Griffith and Wallis[8] assumes a hemispherical nucleus and

that the critical temperature location is the solid-liquid interface. The analysis

was compared with data for water boiling from a polished copper surface on which

37 artificial conical sites of uniform size had been placed. Two possibilities are

given for the discrepancy between the 20°F superheat needed to form vapor from

the sites and the 3°F predicted. It is postulated that either the nuclei are

not hemispheres or else that the surface temperature in the immediate vicinity

of a site is considerably below the average surface temperature, which is measured.

When the liquid was uniformly superheated by a bath, rather than being heated by

the solid surface, good agreement was found between theory and experiment. Here

the surface served only to supply the surface cavities which acted as nucleation

sites. The superheat was slowly reduced by reducing the bath temperature and

the conditions when vapor was no longer generated from the surface site recorded.

It should be noted that the foregoing analyses[7,8] place no upper limit

on the size of an active cavity. They indicate that the larger the surface

cavity, the lower the superheat necessary for vapor growth, approaching zero

for large cavities. It would appear to be physically reasonable that there should

exist a size beyond which a surface cavity could no longer function as an active

nucleation site.

Hsu[10] made an analysis of the growth of a vapor nucleus in a surface cavity which is based on the observation by Hsu and Graham[9] that as a vapor bubble leaves the surface, cool liquid from the bulk replaces the warm liquid in the thermal boundary layer. He assumed that the vapor nucleus is a truncated sphere and that the critical temperature location is the outer edge of the vapor nucleus. A limiting thickness for the thermal boundary layer, beyond which it does not grow because of turbulence in the bulk liquid, is assumed. The time that it takes for a transient conduction process in the liquid to heat the fluid at the critical location to the saturation temperature of the vapor in the nucleus is the waiting period, or dead time, between bubbles. The limiting temperature distribution resulting from the transient conduction process is assumed to be linear from the wall to the edge of the limiting thermal boundary layer. The analysis, using the limiting temperature distribution, predicts a range of cavity sizes that will be active. Very small nuclei do not grow as they have a small radius of curvature and are therefore at a high pressure and the vapor in them have a high saturation temperature. Very large nuclei do not grow as their outer edge is located in the relative cool liquid away from the surface. If cavities of all sizes are present on the surface, the initial boiling with theoretically occur when conditions are such that the theoretical maximum active cavity size is equal to the theoretical minimum active cavity size. It is necessary to know the limiting thermal boundary layer thickness in order to use this analysis.

A modification to the above analysis[10] was made by Bergles and Rohsenow.[11] A linear temperature distribution in the liquid, determined by the surface temperature, the heat flux and the thermal conductivity of the liquid, was assumed

along with a hemispherical vapor nucleus. By using conventional correlations

for the heat transfer coefficient, it is possible to predict the surface super-

heat at a given heat flux and then the size range of active cavities.

The interface between the vapor nucleus and the liquid was considered

by Han and Griffith[12] to be both adiabatic and isothermal, before the vapor

nucleus grows. Satisfying only the adiabatic condition, the critical temperature

location is taken to be the outer edge of the nucleus. They concluded from results

of potential flow theory and the analogy between isothermal lines in conduc-

tion and potential lines in fluid flow, that the critical temperature location

is $3r/2$ from the solid surface. Their analysis assumes that the temperature

distribution in the liquid, at any given time, is linear with a gradient equal

to the gradient computed at the wall for a transient conduction process in the

initially uniform temperature liquid. The temperature distribution is assumed

to be limited by the maximum thermal boundary layer thickness that is present

in natural convection. The results and limitations are similar to those for

Hsu's theory,[10] with a smaller range of cavity sizes predicted to be active at

a given surface temperature.

Howell and Siegel[13] boiled water from polished stainless steel surfaces

that contained artificial sites. Most of the surfaces contained two nominally

identical sites, but some contained up to six sites of various sizes. The analy-

sis of Griffith and Wallis[8] predicts that all of the sites will be active at

a lower surface superheat than was observed to be necessary. The difference

between the theory and experiment is especially large for the larger sites. The

analysis of Hsu[10] correctly predicts the minimum surface superheat necessary

to form vapor from a surface, if cavities of all sizes are present on the surface. The analyses of both Hsu and Han and Griffith[12] predict that the smaller sites will be active at a lower surface superheat than observed to be necessary and that the larger sites will not be active at any value of surface superheat.

Howell and Siegel observed that after a vapor bubble left the larger sites a vapor nucleus that extended outside the thermal boundary layer remained at the site. An analysis was developed, assuming that the vapor nucleus was an isothermal hemisphere at the temperature of the saturated vapor in it and that it would grow whenever the net heat transferred across the liquid-vapor interface is positive. The analysis predicts superheats for the growth of vapor nuclei closer to the observed values than those predicted by the analysis of Griffith and Wallis. However, the predicted values are still less than the observed values and there is no upper limit to the size of the cavities predicted to be active. This analysis could be used to predict a lower limit for the superheat necessary for a cavity to become active.

It is important to note that all of the analyses considered for incipient vapor formation assume a vapor nucleus in a surface imperfection. The maximum cavity size that will be active in any given situation may be determined by the ability of the cavity to hold a vapor nucleus. The replacement of the vapor in a cavity by liquid has been examined by Bankoff.[14] He concluded that when a liquid front moves over a surface cavity containing vapor, the liquid will replace the vapor in the cavity whenever the liquid contact angle, measured from inside the liquid, is less than the enclosed angle at the bottom of the cavity. If a

vapor front moves over a surface cavity containing liquid, the vapor will not replace the liquid whenever the sum of the liquid contact angle and the cavity angle is less than 180°.

Additional data on the inception of boiling can be found in the literature. Marto and Rohsenow[15] boiled liquid sodium from a surface that contained twelve re-entrant cavities with an outside radius of 0.002 in. A superheat of 48°F was required to initiate boiling from these sites. The analysis of Bergles and Rohsenow[11] predicts that for the same conditions a cavity with radius of 0.0028 in. will become active at 48°F.

Hutton and Hall[16] boiled water from a chrome plated stainless steel rod on which small (maximum radius of 0.0025 in.) artificial sites had been made by acid etching. Much higher temperatures than predicted by the analyses of Hsu[10] and Griffith[12] were needed for the sites to become active. The site sizes were well within the range predicted to be active under the conditions that they did become active.

Defining the incipient boiling point as the intersection of the extensions of the natural convection and fully developed nucleate boiling curves, Merte and Clark[17] indicate that for saturated water boiling in an accelerating system the incipient boiling point appears to be independent of acceleration level.

Working with a cryogenic liquid, Lyon[22] found that the heat flux and super-heat necessary to initiate boiling in liquid helium was not reproducible. Even when the surface was not removed from the liquid, large variations were noted between runs.

An interesting observation concerning incipient boiling is an apparent difficulty in activating the first site.[7,15,18] If the heat flux is increased from a low value, natural convection can be maintained at a heat flux which produces vigorous nucleate boiling when decreasing the heat flux from a higher value. The surface temperature under such conditions is much larger than when boiling is present at the same heat flux. Once boiling begins, the surface temperature drops to a value characteristic of nucleate boiling. Corty and Foust[7] report that the rougher the surface, the larger the superheat that could be obtained before boiling begins. The opposite trend was found by Marto and Rohsenow.[15]

Corty and Foust also reported that once the initial site became active, patchwise boiling occurred, i.e., there was a clustering of active sites in some areas of the surface while other areas of the surface were void of active site. Patchwise boiling also occurred if the heat flux was decreased from a vigorous nucleate boiling level until natural convection was established, and then immediately increased again. The last sites active while decreasing the heat flux became active again while increasing the heat flux and served as centers for the patches of active sites. Gaertner[19] postulates that patchwise boiling does not actually occur and quotes Feller[46] as saying, it is an "established fact that to the untrained eye randomness appears as regularity or tendency to cluster."

It is well known that the position and slope of the nucleate boiling heat transfer curve is strongly affected by the surface.[e.g.,7,15,16,20,21,28,41] An increase in roughness generally decreases the surface temperature needed for a given heat transfer rate. Corty and Foust[7] found that for n-pentane boiling

from nickel surfaces, the ΔT needed for a given heat transfer coefficient cor-
related reasonably well with the RMS roughness of the surface. A limit to
the effect of increasing surface roughness is postulated. Berenson[20] also boiled
n-pentane from a number of different surfaces and reports that the RMS roughness
is not a significant number in correlating the effect of roughness. It is also
reported by Berenson that materials with higher thermal conductivity require
a lower ΔT to transfer a given heat flux. Kurihara and Myers[21] boiled a number
of different liquids from copper surfaces polished with emery paper. They found
that as roughness is increased, the incremental effect of an incremental increase
in roughness becomes smaller. It is estimated that the limit in roughness above
which the boiling heat transfer coefficient will not be changed by an increase
in roughness is about 30 μin.

The effect of orientation on nucleate boiling is not clear. Githinji and
Saberski[23] found that in subcooled nucleate boiling of isopropyl alcohol, a
vertical heater had a larger heat transfer coefficient than a horizontal heater
heating upward. The heat transfer coefficient for a horizontal heater heating
downward was considerably lower than for the other two cases. Marcus and Dropkin[24]
report that for saturated pool boiling of water, the heat transfer coefficient
at a low heat flux decreases as the surface is rotated from horizontal to ver-
tical. The opposite effect was found when vigorous boiling was taking place.
Using liquid hydrogen, Class, et al.,[28] report that for a smooth surface there
was very little difference between the boiling curves when the surface was hori-
zontal, inclined 45° or vertical. For the same surface roughened with emery

paper the heat transfer coefficient at a low heat flux decreased as it was rotated from horizontal to vertical. Covering the surface with a light coat of grease produced the opposite effect.

In 1961 Richards, Steward and Jacobs[25] collected the available heat transfer data for all cryogenic liquids and, when possible, compared them to theories and correlations. The only natural convection data found for liquid hydrogen were from a vertical wire and no natural convection data were found for liquid nitrogen.

Much of the data presented in Ref. 25 are applicable only to the special conditions of the tests. Two sets are considered important for the present work. Mulford and Nigon[26] boiled liquid hydrogen from the outside of a vertical copper cylinder. The test pressure was 0.73 atmospheres and the heat flux was varied from low nucleate boiling values to film boiling values. After data were recorded for the smooth surface, the surface was sand blasted to roughen it. The heat transfer data from the roughened surface were within the scatter of the data from the smooth surface. Class, et al.,[27] boiled liquid hydrogen from an electrically heated resistance ribbon 1 in. wide, 22 in. long and 5 mils thick. The test pressure was varied from 0.82 to 8.7 atmospheres and the heat flux from low nucleate boiling values to film boiling values. The temperatures were measured at various locations on the back side of a 5 mil Mylar film to which the heater ribbon was cememted. The complete report[28] indicates that an estimate was made of the heat loss from the back side of the heater ribbon and of the temperature drop across the Mylar film. Other heat losses and the temperature drop across the heater ribbon were not considered. Data are presented for the ribbon in the

vertical, 45° up, and horizontal positions. The ribbon was tested in an "as received" condition, roughened with emery paper and covered with a light coat of grease. The effect of orientation on the heat transfer data was mentioned above. In all of the positions, there was very little difference between the roughened and smooth surface at nucleate boiling heat fluxes near burnout. At a low nucleate boiling heat flux, the ΔT was smaller for the roughened surface than for the smooth surface. In the vertical position, the greased surface had a smaller ΔT than the other two surfaces at a low heat flux and a larger ΔT than the other two surfaces at a large heat flux. In the other positions, the greased surface had a larger ΔT than the other two surfaces at all heat fluxes.

Other significant pool boiling data for liquid hydrogen have been reported since 1961. Drayer and Timmerhaus[29] boiled from the outside of a vertical brass tube. The test pressure was 0.82 atmospheres and the heat flux limited to low values in the nucleate boiling range. Sherley[32] boiled from a lead film deposited on a horizontal glass slide. Data were taken at one atmosphere pressure over the entire nucleate boiling range for both normal gravity and zero-gravity conditions. The temperatures were measured by resistance changes of the lead film, also used as the heater, and represent an average across its thickness. Of particular interest to the present study, it was indicated that a heat flux of between 250 and 500 Btu/hr ft^2 was required to initiate boiling under normal gravity conditions. The corresponding surface superheat was about 2.5°F. Nearly the same incipient boiling results were found under zero-gravity conditions, but they might have been different if zero-gravity times longer than the maximum of 15 sec had been available.

Data are presented by Graham, et al.,[30] for liquid hydrogen boiling from an electrically heated resistance ribbon. Pressures ranged from 60 to 260 psi and accelerations from 1 to 10 g. The temperatures were measured on the back side of the heater ribbon. In the only run that the temperature drop across the ribbon was estimated, the correction to the measured temperature, to obtain the surface temperature, amounts to about 50% of the measured temperature. No corrections were made for heat losses.

Steinle[33] indicates that Tusk[34] conducted tests on incipient boiling of liquid hydrogen. Zero-gravity conditions were simulated by heating liquid hydrogen with a surface facing downward. Boiling began on a rough surface with a temperature rise of less than 0.2°F and on a very smooth surface with a temperature rise of 6°F.

Hord, et al.,[40] investigated the superheats that could be obtained in liquid hydrogen by rapidly reducing the pressure above the liquid. It appeared that the larger the rate of pressure reduction the larger the superheat that could be obtained, but the rate of pressure reduction depended upon the initial conditions so the effect could have been that of the initial conditions. An acid cleaned glass container was used as an "ideal" system. For a given set of initial conditions, there was no apparent change in the obtainable superheat when rods of aluminum, stainless steel or brass, with surface roughnesses of from 4 to 78 μin., were placed in the liquid. A very rough (200 μin.) stainless steel rod reduced the nucleation superheat. Contaminants, consisting of solid nitrogen and water particles, also reduced the superheat at nucleation. The theories discussed previously do not correctly predict the results obtained.

A number of authors have compared existing hydrogen nucleate boiling heat transfer data with theories and correlations.[e.g.,25,27,29,35,36,42] A comprehensive work is that of Drayer[35] in which 11 equations from the literature are compared with experimental data. The equations predict heat transfer rates, at a given ΔT, that cover 7-1/2 orders of magnitude. Of those tested, three equations appear to be applicable over a limited range, those of Forster-Zuber,[37] Forster-Greif,[38] and Cryder-Gilliland.[39]

II. EXPERIMENTAL APPARATUS

A schematic of the experimental apparatus is shown in Fig. 1. The system was designed specifically for the investigation of heat transfer from a solid surface to a saturated pool of a cryogenic liquid. An instrumented test surface was mounted in a holder and immersed into the test liquid which was contained in a vacuum insulated pyrex dewar. Heat was supplied to the test surface by an electrical dc resistance wire heater. Constant vapor pressure over the test liquid was maintained by a pressure control system which vented the vapor as it was formed.

A. DEWARS

The test fluid was contained in the inner one of the two concentric pyrex dewars shown in Fig. 2. This dewar was designed to be suspended from above by a metal flange attached to a single walled section of the dewar. This section supported the portion of the dewar which held the test liquid and which was surrounded by the outer dewar. The liquid section was double walled and vacuum insulated. Its volume was 5 liters with an I.D. and length of approximately 10 cm and 65 cm respectively. The interior of the vacuum space was silvered except for two 1 in. wide strips that were diametrically opposite.

The outer dewar was supported from the bottom. It surrounded the liquid portion of the inner dewar and was of similar construction. Liquid nitrogen was placed in the outer dewar to form a heat shield for the test liquid. There was no direct contact between the two dewars.
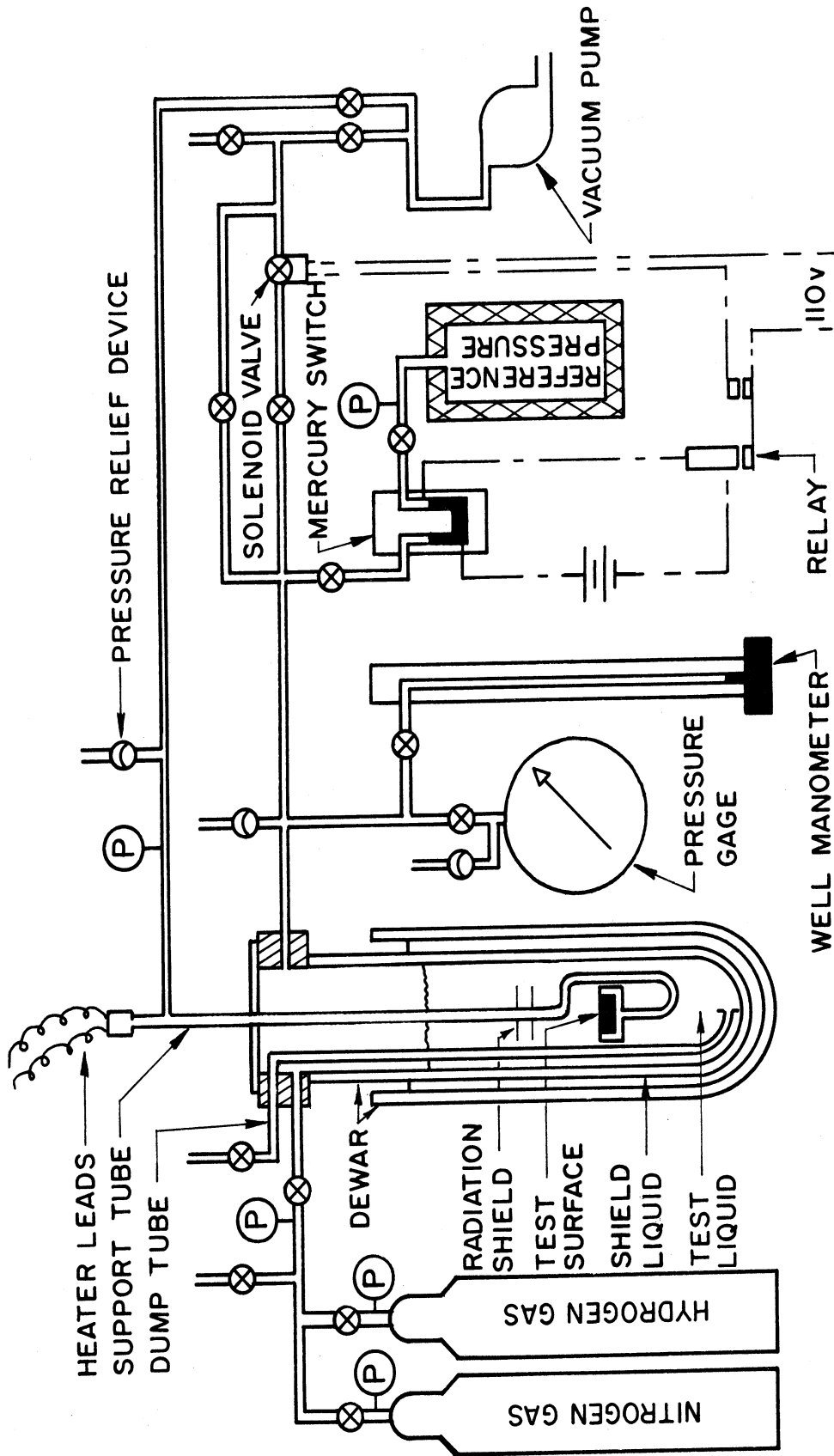
Fig. 1. Schematic of test apparatus.

When the two sets of unsilvered strips were aligned with each other, it was possible to visually observe the interior of the inner dewar. Reflecting paper was mounted behind the dewars to permit indirect lighting for visual observations. When the unsilvered strips were not aligned, the silvered surfaces formed an effective radiation barrier.

All permanent connections (vent line, gas pressurization lines, etc.) to the test dewar were made through a manifold ring mounted on the metal flange. This is shown in Figs. 2 and 3. The manifold ring did not restrict the access to the interior of the test dewar as it had an I.D. approximately the same size as the dewar I.D. This design permitted the test surface to be changed with a minimum of effort as only the connections to the surface itself had to be broken.

A dump tube extended through the manifold ring to the bottom of the test dewar. This provided a means of removing the test liquid after a test. By pressurizing the test dewar, the liquid could be forced out through the dump tube and then through a heat exchanger to vaporize it. The vapor was exhausted into the atmosphere.

B. PRESSURE CONTROL

The controlling device in the pressure control system was a mercury switch. This was a small U-tube, mercury manometer with an electrical contact in each leg. One contact was located at the bottom of its leg so it was always wetted by the mercury and the other contact was located above the normal mercury level. External to the manometer, a relay circuit was wired between the contacts. When the mercury wetted both contacts, the circuit was completed and the relay closed.

Manifold Ring

Single Walled Section of Inner Dewar

Dump Tube

Outer Dewar

Fig. 2. Liquid dewars.

Vacuum Line

Support Tube

Thermocouple Leads
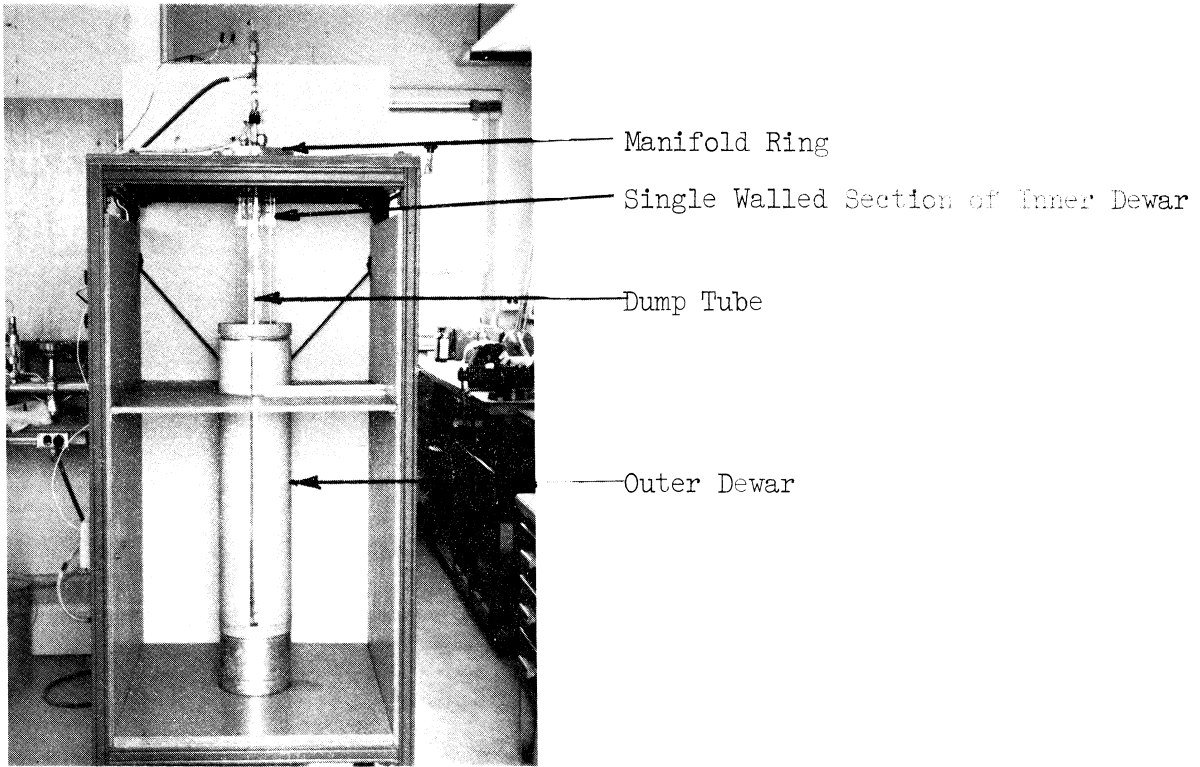
Cover Plate
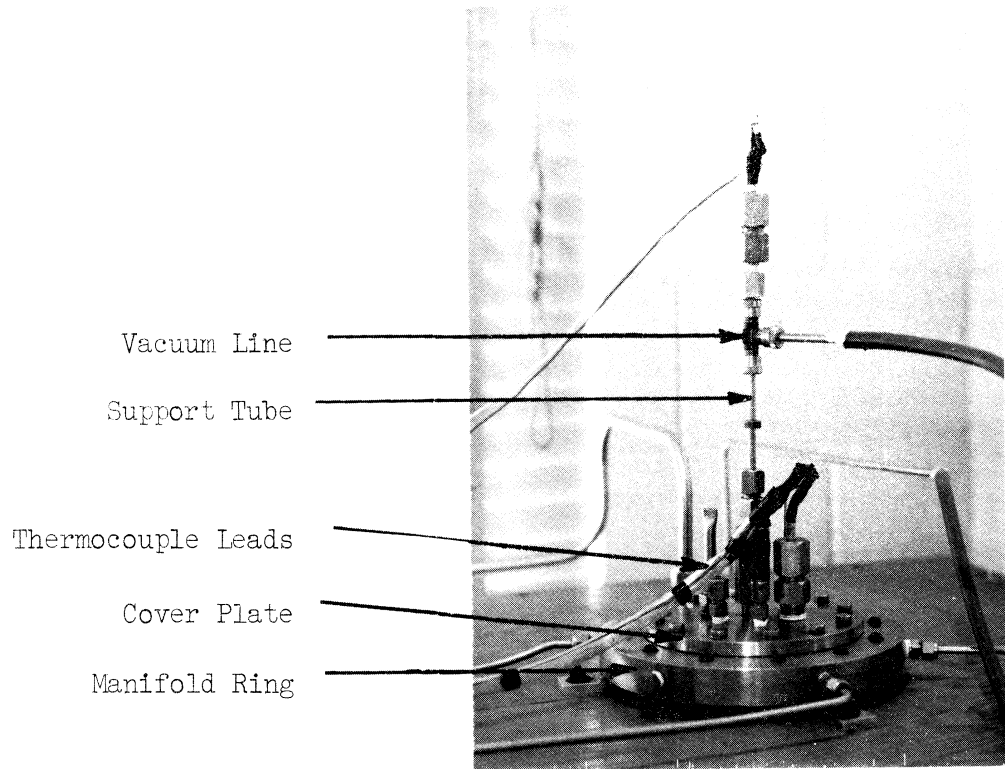
Manifold Ring

Fig. 3. Manifold ring and cover plate.

The test liquid vapor pressure (dewar pressure) was applied to the manometer leg with the wetted contact and a reference pressure was applied to the other leg. As heat was transferred to the saturated test liquid, its temperature and vapor pressure increased. The pressure increase forced the mercury into the leg with the unwetted contact. When the mercury level reached the contact, the relay circuit was completed and the relay closed, opening a solenoid valve in a vent line.

Two needle valves were used in conjunction with the solenoid valve; one in parallel used as a variable vent and one in series used as a flow restriction. The variable vent was adjusted to vent the vapor almost as fast as it was formed. This permitted operation over a wide range of venting rates as the solenoid valve vented only the excess vapor. Tilting the mercury switch from a vertical plane towards the horizontal increased the sensitivity of the pressure control. The actual system controlled the pressure to ± 0.02 psi.

Sparking between the mercury and the make and break contact was at first a problem. A layer of silicone oil was placed over the mercury to prevent the spark from reaching any hydrogen gas that might be present, but the sparking decomposed the oil, contaminating the mercury and resulting in poor wetting of the contacts. A variable resistance was placed in parallel with the mercury between the two contacts and its resistance adjusted so it did not operate the relay, but did offer a lower resistance than the spark gap. This reduced the sparking to a tolerable level.

The reference pressure was supplied by a constant mass of nitrogen gas contained in an insulated cylinder. Changes in the ambient temperature produced

a slow drift in the reference pressure which, for long runs, was as large as ±0.1 psi. As the liquid was maintained in a saturated condition, this pressure drift is reflected only in small changes in the saturated physical properties of the liquid and vapor. Not shown in Fig. 1 are provisions for purging the reference cylinder and pressurizing it with nitrogen gas.

C. SURFACE MOUNTING

The original and final designs of the heat transfer surface and its holder are shown in Fig. 4. The difficulties encountered with the original design and the details of the surface preparation are discussed in Section IV.A.

In the final design, the heat transfer surface is back by a disc of copper 1/2 in. thick and 1 in. in diameter, which served as a heater block. A 1 mil thick stainless steel fin was attached to the copper disc to eliminate the physical discontinuity at the edge of the heater surface. A typical stainless steel surface, backed by the copper disc, is shown in Fig. 5.

The fin was backed with a Teflon ring to make it more rigid for mounting. Teflon was chosen for the backing material because it has a small thermal conductivity and thus contributes very little to the heat loss. The surface was mounted by clamping the Teflon backed fin and a loading ring between a housing cup and a clamping ring (see Fig. 6-8). A seal between mating members permitted a vacuum to be drawn inside the housing cup. This insulated the back side of the Teflon ring, the heater block and the leads to the surface thermocouple. The members of the clamping assembly were covered with a light coat of vacuum grease to aid in sealing.

HEAT TRANSFER SURFACE

SOLDER FILLET

STAINLESS STEEL FIN

LOADING RING

CLAMPING RING

TEFLON BACKING RING

COPPER DISC

SOLID DISC OF SURFACE MATERIAL

TEFLON HOUSING CUP

STAINLESS STEEL HOUSING CUP

HEATER

INSULATION DISC

SHEATHED SURFACE THERMOCOUPLE

BACKING DISC

ORIGINAL DESIGN | FINAL DESIGN
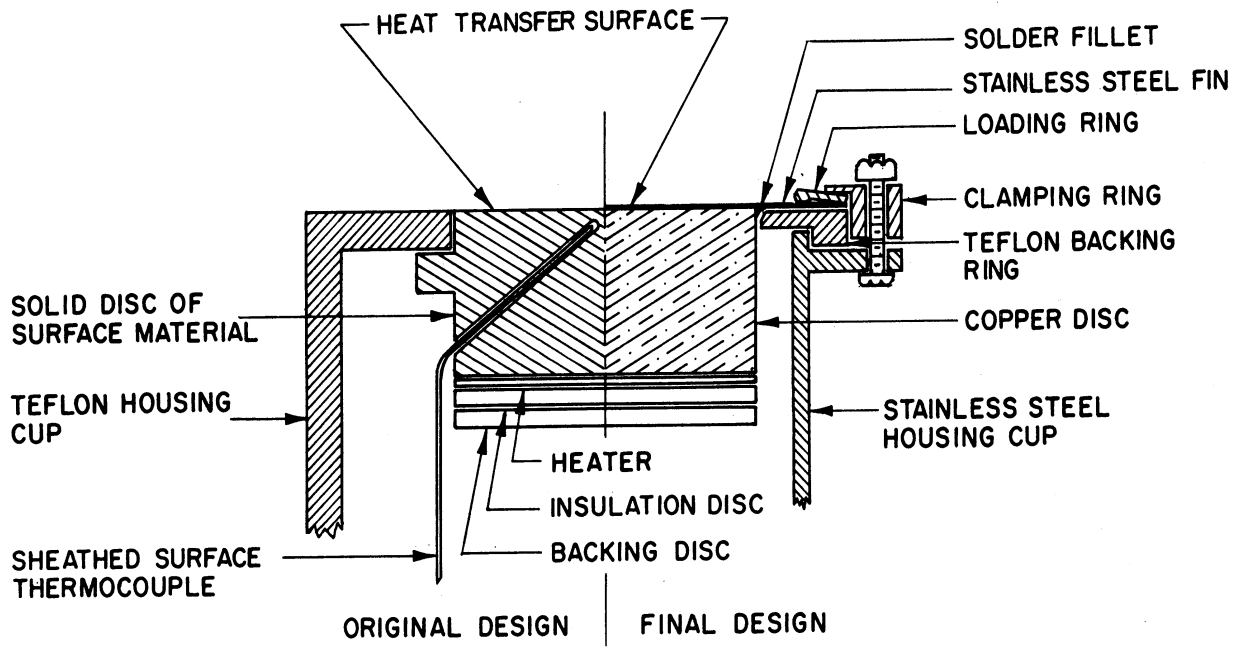
Fig. 4. Schematic of test surfaces and mountings.

Heat Transfer Surface

Fin

Fig. 5. Test surface.

Heater Block
Teflon Ring
Loading Ring
Clamping Ring
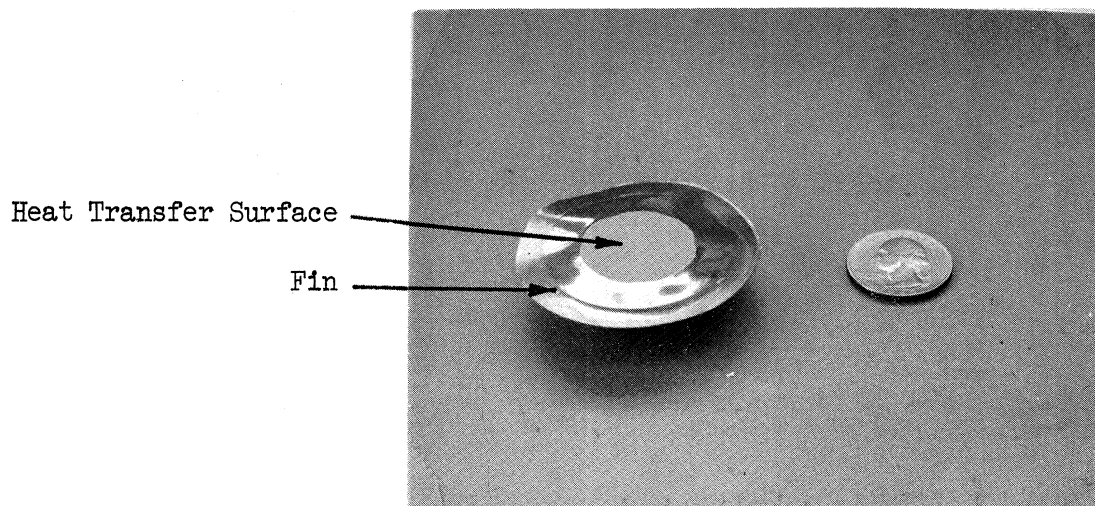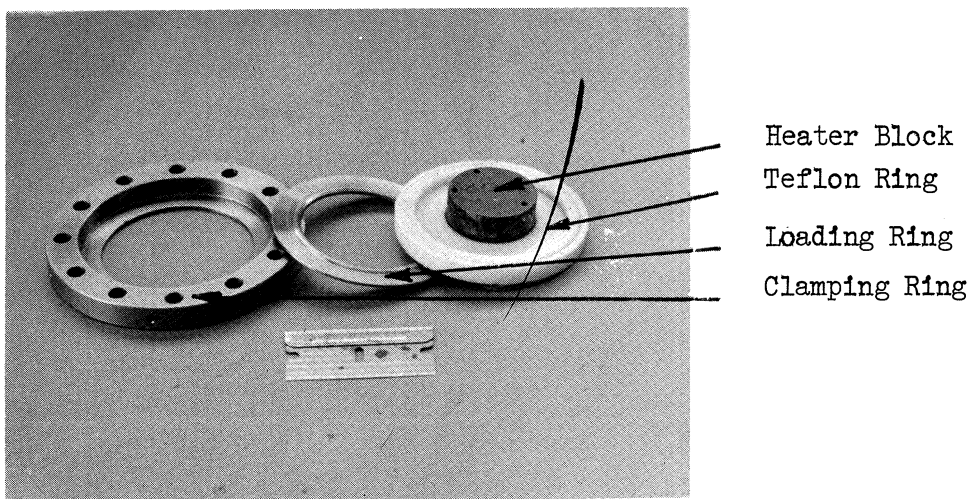
Fig. 6. Clamping arrangement.

Heater

Housing Cup

Support Tube
Surface Thermocouple

Fig. 7. Housing cup.

Radiation Shields

Support Tube

Fin

Heat Transfer Surface

Loading Ring

Clamping Ring
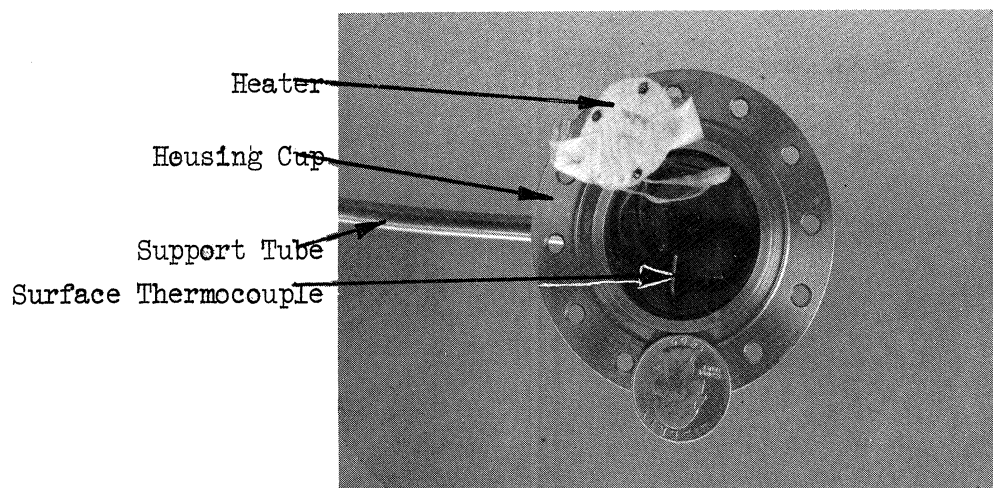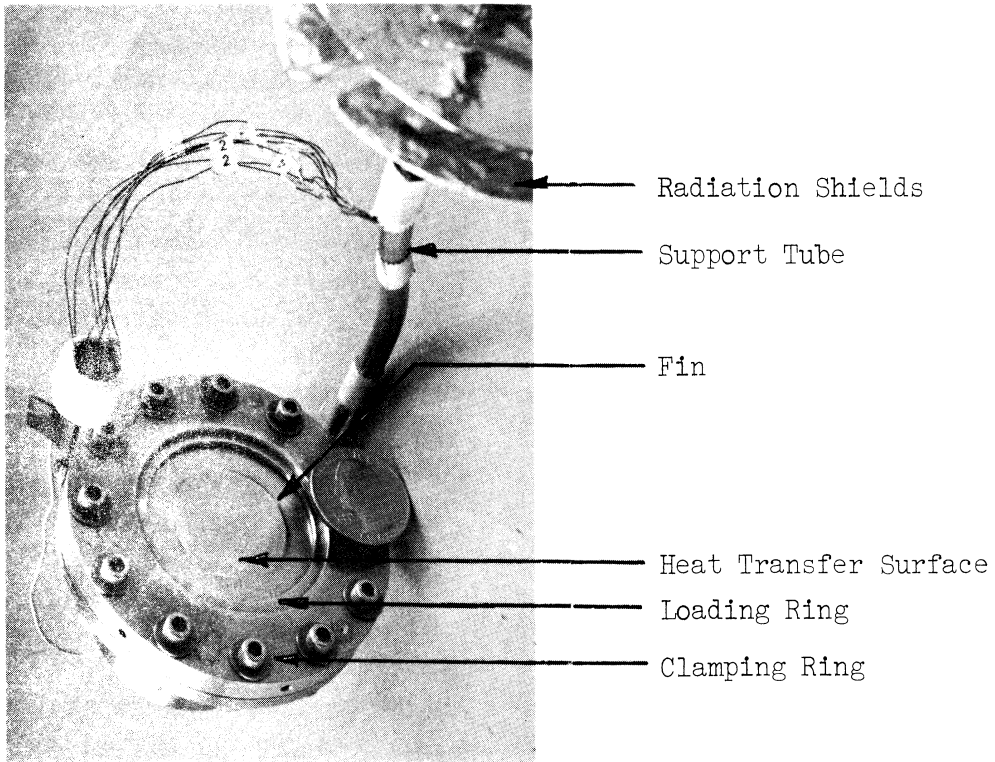
Fig. 8a.   Mounted surface without convection shield.

Thermocouple Lead Wires

Reference Cylinder

Convection Shield

Surface Thermocouple
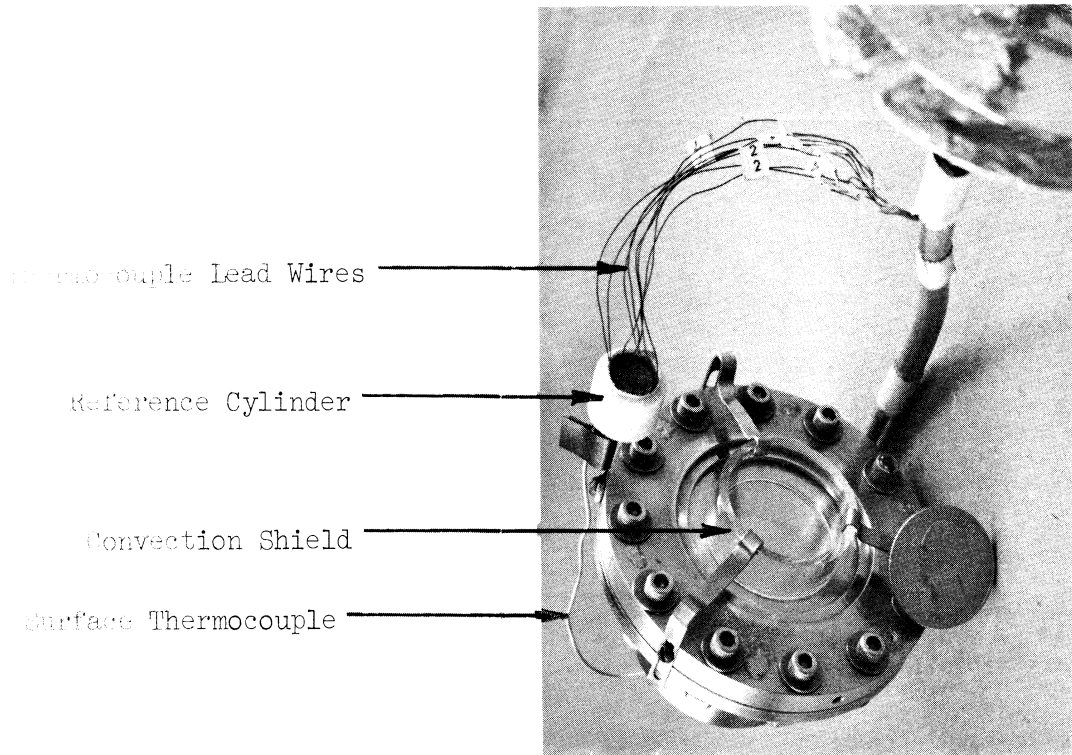
Fig. 8b.   Mounted surface with convection shield.

The loading ring was necessary to maintain the seal in liquid hydrogen. Teflon has a larger thermal coefficient of expansion than the other materials and thus the Teflon ring contracted more than the clamping members when cooled from room temperature to the test temperature. The seal was tight in liquid nitrogen, but at about 40°K the differential contraction was sufficient to completely relax the elastic deformation in all the parts. The joint then opened and allowed liquid hydrogen to flow into the housing cup. The loading ring acted as a stiff spring during clamping and absorbed most of the differential contraction during cool down.

The housing cup provided a location for connecting the heater leads to heavy copper leads.

D. SUPPORT TUBE

The housing cup was fastened to a support tube. Heavy copper leads for the heater passed through the inside of the tube and into the housing cup. The support tube was bent to position the test surface in the desired orientation and also served as a vacuum line to the housing cup. The support tube passed through the cover plate to the outside of the dewar.

E. COVER PLATE

The cover plate was mounted on the manifold ring and sealed the top of the dewar. A sealing gland passed the support tube and allowed it to be raised and lowered as desired. Thermocouple leads entered the test dewar through sealing glands mounted in the cover plate. A port for the insertion of the liquid hydrogen transfer line was also provided.

F. HEATER

The heater consisted of 7 mil resistance wire coiled between two layers of glass tape to form a disc 1 in. in diameter. The resistance at the test temperatures was approximately 4 ohms. The leads were 30 gage wire 12 cm long, chosen to approximately balance the I^2R heat generation and the heat conduction in the wires. Iron and copper wires were used with liquid hydrogen and liquid nitrogen, respectively.

The heater was mounted on the back face of the heater block. It was covered by 1/8 in. of transite insulation and a stainless steel backing disc. Screws passing through the backing disc into the heater block were used to hold the heater and insulation firmly against the heater block.

G. POWER SUPPLY

The power leads were connected to a circuit designed to give a continously variably voltage of from 0.3 to 36 v. The power was supplied by storage batteries. The maximum power was limited by the heater leads and the amount of liquid vaporized during a test run.

H. RADIATION SHIELDS

When the surface was mounted to heat in the upward orientation, two radiation shields were mounted on the support tube, in the liquid above the heating surface. These were considered to be necessary as in this orientation the surface faced the cover plate which was at room temperature. When the surface was mounted in the other orientations, it faced the 4 silvered surfaces of the two dewars and no radiation shields were used.

I. CONVECTION SHIELD

The convection shield shown in Fig. 8b was used during some of the tests. This is a 1/2 in. length of pyrex tubing mounted in the liquid around the circumference of the test surface. If fluid motion produced by bouyancy forces can be eliminated, a "o-g" environment can be simulated in a "1-g" environment. When heating downwards, the buoyancy forces hold the warm liquid against the surface and if gross convection currents are prevented from sweeping across the surface, a "o-g" environment should be simulated. The convection shield was used to shield the surface from the gross convection currents in the liquid. In the downwards orientation, the mechanism of heat transfer in the liquid should approach pure conduction if convection currents are eliminated. The growth of a vapor nucleus should then require a minimum surface superheat, as the temperature gradient in the liquid is a minimum. The convection shield was always used when a surface was heating downwards. When a surface was heating in an upwards direction, the direction of the buoyancy forces, relative to the surface were reversed. In this orientation, the convection shield was used during some of the tests to prevent the gross convection currents in the bulk liquid from sweeping across the surface. The convection shield was never used with a surface heating in the vertical direction because here it was desired not to interrupt the normal convection pattern.

III. INSTRUMENTATION

The measurements recorded were thermocouple EMFs, vapor pressure of the test liquid, voltage drop across the heater and voltage drop across a shunt used to determine the heater current. The measuring instruments are shown in Figs. 9 and 10. Readings not recorded include the reference cylinder pressure and the pressure (vacuum) in the housing cup.

A. THERMOCOUPLES

The surface temperature was indicated relative to the liquid temperature by a calibrated (see Appendix A) sheathed thermocouple. The 36 gage copper-constantan measuring junction was ungrounded from its 0.040 in. O.D. sheath. The sheath was inserted approximately 1/2 in. into a 0.042 in. hole in the copper heater block. Aluminum dust mixed in a grease binder insured good thermal contact between the heater block and the sheath. The sheath passed through the housing cup and into the liquid through a small hole drilled in the cup.

The thermocouple hole in the heater block bottomed at a maximum of 0.032 in. from the surface. The precise location of the thermocouple junction is not important, as at the test temperatures the thermal conductivity of the copper is very large. This, and the relatively small heat fluxes used, results in very small temperature gradients in the copper.

The early experiments were conducted with three differential thermocouples located in the liquid thermal boundary layer at various distances
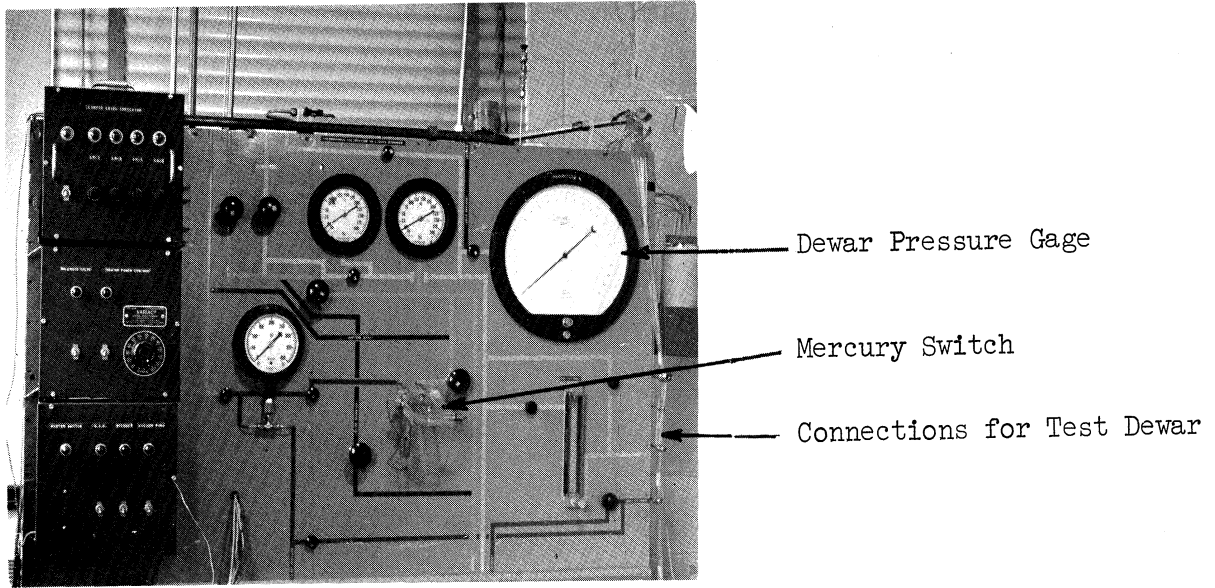
Fig. 9. Control panel.
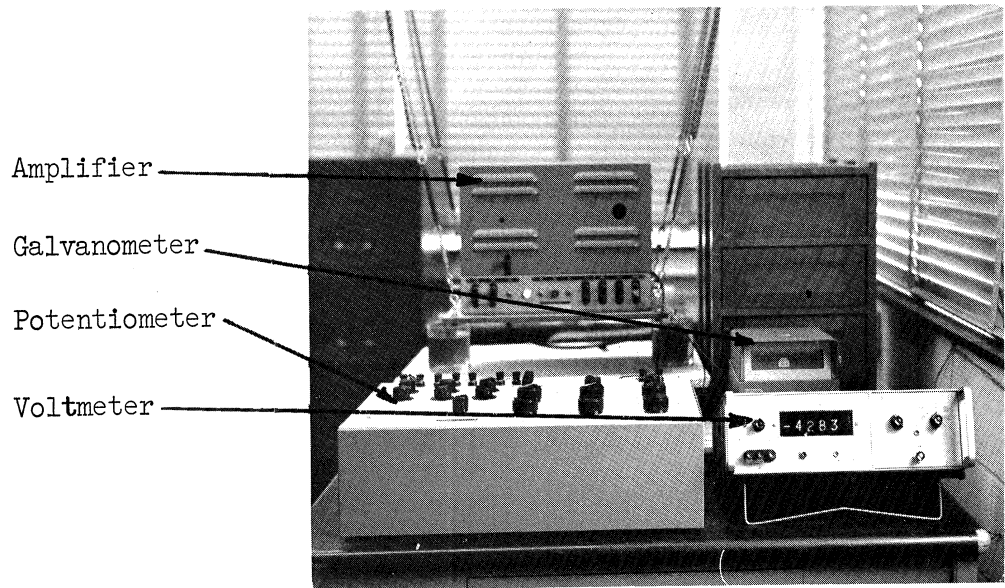
Fig. 10. Measuring instruments.

from the heater surface. They were made from calibrated 2 mil copper-
constantan wire and were mounted in a holder which was seated against the
heat transfer surface at opposite ends of a diameter. The measuring junc-
tions were in the approximate center of the surface with the leads running
parallel to the surface. The distances from the surface to the junctions
were assumed to be the same as the distances measure from a flat surface to
the center of the approximation 4 mil diameter beads. The distances were
measured at room temperature with a calibrated microscope eyepiece scale.
The holder was removed when it was determined that the initial vapor was
being formed where the holder seated against the surface.

The differential thermocouples were referenced to a small copper cyl-
inder located in the liquid at the level of the test surface. The junctions
were insulated from the cylinder by finger nail polish on the junctions and
a single layer of 7 mil thick glass cloth tape covering the cylinder. The
junctions were held in place by several layers of tape and a Teflon ring
snapped over the tape. The differential contraction between the Teflon and
copper produced a large pressure to hold the junctions against the cylinder
in the test liquid. This was evidenced by deep impressions in the tape at
the edge of the Teflon ring. The ends of the cylinder were exposed to the
liquid.

Also mounted on the reference cylinder was a 30 gage copper-constantan
thermocouple, made from calibrated wire and referenced to distilled water
ice, and the midpoints of loops of copper and constantan thermocouple wire.
The thermocouple wire loops ran outside the dewar to a potentiometer. As

the thermocouple lead wires were slightly cold worked each time a surface

was inserted into or removed from the test dewar, the parasitic EMFs in

the lead wires increased with use. The thermocouple loops were used to

determine the approximate size of the parasitic EMFs and determine when new

lead wires should be installed. See Section IV.H for a discussion on the

parasitic EMFs.

The copper thermocouple lead wires passed through the cover plate to a

series of all copper knife switches. These were used to select the input

into the potentiometer.

B. POTENTIOMETER

The thermocouple EMFs were read on a Honeywell Model 2768 6 dial micro-

volt potentiometer. This instrument has a digital readout in steps of 0.01

μv. The accuracy in the range of interest is $\pm(0.01\%$ of Reading + 0.02 $\mu v)$.

C. NULL DETECTION

The unbalance from the potentiometer was amplified with a Rubicon Model

3550 photoelectric galvanometer and amplifier system. Building vibrations

made it necessary to locate this on a platform suspended from the ceiling.

Soft springs in the supports helped to isolate the platform and paddles in

oil supplied viscous damping.

A Honeywell series 3100 spotlight galvanometer was used to indicate the

unbalance. For the surface thermocouple the galvanometer deflection was ap-

proximately 100 mm/μv. Even with the amplifier suspended from the ceiling,

daytime building vibrations resulted in a noise in the galvanometer of about

± 3 mm.

D. PRESSURE

A calibrated 12 in. Heise bourdon tube gage was used to measure the vapor pressure of the test liquid. The 25 psig range was divided into 0.1 psi steps. The calibrated accuracy of the gage over the entire range was ±0.025 psi. Barometric pressure was measured with a mercury barometer.

A well type mercury manometer was located in parallel with the Heise gage to measure vacuums during purging operations.

E. HEATER VOLTAGE

The voltage drop across the heater was measured by a Hewlett Packard Model 3440A digital voltmeter with a model 3444A plug-in unit. For readings under 10 v the accuracy is ±(0.05% of reading + 0.001 v) and for readings over 10 v the accuracy is ±(0.05% of reading + 0.01 v).

The voltage measurements were made at the power supply. The voltage drop in the copper leads (16 gage) running to the heater is negligible.

F. HEATER CURRENT

The heater current was determined by measuring the voltage drop across a resistor in series with the heater. The resistor was a Leeds and Northrup 0.01 ohm precision shunt with an accuracy of ±0.04%. The voltage was measured with the same circuit used for the thermocouple measurements.

IV. PROCEDURE

Most of the tests were conducted in the same manner. A prepared surface with heater and surface thermocouple in place was clamped in its mounting. The surface was then cleaned and the thermocouple connections completed. The mounted surface was placed in the test dewar which was then purged. The test liquid was transferred into the dewar and equilibrium conditions were established. After a voltage was applied to the heater, sufficient time was allowed to establish steady state conditions. Visual observations were made and the heater voltage, the heater current and the thermocouple EMFs were measured and recorded. When the surface was heating upwards or vertically, the visual observations were to determine if vapor was being formed at the surface, and if so, the pattern of the boiling. When the surface was heating downwards, the observations were to determine if vapor had already been formed at the surface and filled the convection shield. The heater voltage was then changed and new reading made.

A. SURFACE PREPARATION

The original design for the heat transfer surface (see Fig. 4), was a round disc of the test surface material mounted in a Teflon housing cup. Teflon was used because of its low thermal conductivity and its large coefficient of thermal expansion. As the surface was cooled down, the Teflon contracted more than the metal and sealed around the surface. This allowed a vacuum to be drawn inside the housing cup to reduce the heat losses. When

this design was tested, the initial boiling was at the edge of the surface.

The vapor appeared to be forming at the discontinuity between the polished

metal surface and the Teflon holder. This prompted an effort to cover up

the discontinuity. Data obtained later, with surfaces of the final design,

show that vapor forms at a lower superheat on a Teflon surface than on a

polished metal surface. It is likely that the vapor formed at the surface's

edge was from the Teflon holder, where it was being heated by the metal

surface.

A thin layer of vacuum grease was used to cover the discontinuity be-

tween the surface and the Teflon holder. This eliminated the boiling at the

edge when using liquid nitrogen, but when using liquid hydrogen the grease

developed hairline cracks which served as nucleation sites. About a dozen

materials were used to cover the discontinuity, without finding one that

would prevent boiling from the edge in liquid hydrogen. A major redesign

of the test surface and its holder was made to allow a fin to be attached

to the edge of the surface in order to eliminate the discontinuity there.

The details of these surfaces are discussed below.

The first tests of incipient boiling of cryogenic liquids were tests

to study the conditions at which the first vapor would form, while increasing

the heat, at an artificial site placed in a polished metal surface. Two

90° conical diamond indentors, one with a nose radius of 0.0007 in. and one

with a nose radius of 0.0001 in., were used to make artificial sites in

metal surfaces. These artificial sites did not serve as locations for the

initial vapor formation from the surface. If vapor did form from them,

there were usually so many other active sites on the surface that it could

not be observed. The sizes of the artificial sites tested, the surface

material and the liquid in which they were tested are tabulated in Table II

(Section VI.E).

When the investigation of the initial vapor formation from artificial

sites proved to be impractical, the conditions under which the initial vapor

formed from a uniform surface were studied. The surfaces investigated are:

CSF-1	Polished stainless steel
CSF-3	280 grit lapped stainless steel
CSF-4 and CSF-4a	600 grit lapped stainless steel
CF-2 and CSF-2a	Polished copper
CF-4	600 grit lapped copper
CTF-1	TFE Teflon
NASA	Glass fiber web with an epoxy cement coating

The preparation of the heat transfer surface is extremely important in

any study of boiling heat transfer. Seemingly unimportant changes in the

preparation can produce large changes in the data. For this reason, the

preparation of the surface will be discussed in detail.

The basic components of a surface were a disc of electrolytic tough

pitch copper 1 in. in diameter and 1/2 in. thick and a piece of 347 stain-

less steel foil 1 mil thick. Threaded screw holes were provided on the back

face of the copper disc to mount the heater and a thermocouple hole was

drilled from the side to within 0.032 in. of the front face. The disc

served as a heater block to smooth out spacial temperature variations pres-

ent at the resistance heater.

The front face of the copper disc was soldered to the foil. The solder-

ing was performed on a lapped surface heated by an electric heater to pro-

vide control of the temperature and a flat surface on which to work. Care

was taken to achieve a bond over the entire face of the disc and to remove

excess solder.

The stainless steel heat transfer surfaces were made by either polishing

or lapping the face of the foil. The polishing was performed with the copper

disc mounted in a slowly rotating lathe. The rotating surface was polished

with a diametrical motion with cheese cloth dampened by a solution of red

rouge dissolved in kerosene. Very little material was removed during polish-

ing and the surface remained slightly wavy from the soldering process. The

lapping was performed in a figure eight motion on window glass covered with

Clover lapping compound. The lapping was continued only until the foil

covering the disc was uniformly lapped. As the foil was not lapped com-

pletely through at any point, there was no discontinuity on, or at the edge

of, the heat transfer surface.

When making a copper surface, a small chamfer was placed on the edge of

the copper disc before it was soldered to the foil. The foil and solder on

the face of the disc were completely removed by lapping. The solder filling

the chamfer held the fin in place. The lapped copper was either tested in

the lapped condition or polished smooth in the same manner that the stainless

steel was polished.

The Teflon surface was made by coating one side of a piece of foil with

1-1/2 mils of TFE Teflon before soldering it to a copper disc. Micrometer

measurements of the coated and uncoated foil were used to determine the thick-

ness of the Teflon coat.

The epoxy coated glass fiber web that was tested is the interior lining of the Saturn IV B liquid hydrogen tank. It was carefully removed from its foam insulation backing and glued over a copper surface.

When lapping the foil it was possible to observe any spots that were not bonded to the copper disc because these spots pulled away from the disc and lapped faster than the rest of the foil. With practice it was possible to consistently make surfaces which had only 1 or 2% of the surface area unattached.

Of the surfaces prepared, approximately one out of every ten was acceptable for use. The main reason that stainless steel surfaces were unacceptable is that the foil at the unbonded locations would lap completely through before the rest of the foil was uniformly lapped. When making a copper surface, the joint between the copper and fin was often broken when the solder was being lapped from the face of the copper. Visual observations of apparently good copper surfaces sometimes revealed pin holes in the soldered joint that could possibly act as nucleation sites. When a copper surface was tested, if the initial vapor consistently formed at or very near the edge of the copper, the data was rejected and a new surface made.

B. ASSEMBLY

The assembly began by mounting the heater on the back of the heater block. Then the sheath thermocouple was coated with the aluminum and grease mixture and inserted into the heater block. The surface was positioned, sliding the excess length of the thermocouple through a hole in the housing

cup and placing the heater leads inside the cup. After the clamping assembly was loosely fastened, the thermocouple sheath was sealed to the housing cup with Woods metal. Final tightening of the assembly forced the thermocouple against the bottom of the hole in the heater block.

The surface was cleaned with a tissue wetted with methylene chloride. When desired, the convection shield and/or liquid thermocouples were positioned. Lead wires were soldered to the thermocouple wires and the junctions, together with the reference cylinder thermocouple and thermocouple wire loops, were mounted on the reference cylinder. A final cleaning of the surface was performed with a cotton swab wetted with reagent grade methylene chloride.

The surface was placed inside the test dewar and the cover plate sealed. The thermocouple leads were connected to the all copper knife switches leading to the measuring circuit and the copper leads to the heater were connected to the power source.

C. PURGING

The system was now ready to be purged. One purge cycle consisted of drawing a vacuum of at least 1/2 cm Hg absolute and then pressurizing with the purge gas to 2 psig. If nitrogen was to be the test liquid, 3 purge cycles were run with nitrogen gas. If hydrogen was to be the test liquid, 2 purge cycles were run with nitrogen gas and then 3 with hydrogen gas. One exception is noted. If nitrogen tests were run with more than one surface, the liquid nitrogen was not emptied from the test dewar while changing the the surfaces. The new surface was held in the vapor space above the liquid for 1 hr so the vapor being vented would provide a purge.

If liquid nitrogen remained in the shield dewar from a previous set of tests, it was necessary to keep the surface in the upper portion of the dewar while purging. If the surface was placed in the lower portion of the dewar, the liquid nitrogen would cool the surface and a light frost would then form on the surface from the water vapor in the unpurged air. This made the data unreproducible.

D. FILLING

The test dewar was filled from portable storage dewars. The liquid nitrogen was purchased locally and supplied in 50 liter flask type dewars. It was transferred into the test dewar through the dump line. The liquid hydrogen was purchased from commercial sources and supplied in 150 liter, superinsulated dewars. It was transferred into the test dewar through a vacuum insulated transfer line inserted through the cover plate. The dip tube extended into the double walled portion of the test dewar.

A positive pressure of the purging or boil off gas was maintained in the test dewar at all times. This insured that the purge would not be contaminated when connections were being made or during filling. The connections for filling were made from the test dewar towards the supply dewar. A flow of the purging gas through the transfer line purged it as the connection was being made at the supply dewar.

The liquid nitrogen in the shield dewar was adjusted to the desired level before filling the test dewar. During testing it was desired to have a flow of heat into the test liquid to maintain it at saturation conditions. When

testing with liquid hydrogen the outer dewar was filled with liquid nitrogen but when testing with liquid nitrogen it was filled only about 1/3 full. This gave an inward flow of heat even though the liquid nitrogen in the test dewar was warmer than that in the outer dewar.

E. ESTABLISHING TEST CONDITIONS

After the test dewar was filled, the pressure control was set to maintain a vapor pressure in the test dewar of 2.5 to 3.0 psig. This pressure was held 1 hr before a test run was begun. Tests showed that 10 min was sufficient for heat transfer from the surroundings to heat the test liquid from its saturation temperature at atmospheric pressure to its saturation temperature at the test pressure.

Stratification in the test liquid was not a serious problem. The test dewar had a small volume to area ratio and heat was transferred to the test liquid over most of the surface area. In both liquid nitrogen and liquid hydrogen, a travelling thermocouple probe was used to determine the amount of stratification present. In both cases there appeared to be a slight amount of stratification, but the changes in temperature were within the accuracy of the temperature measurement.

After equilibrium conditions were established, the system was pressurized to 5 psig (2 to 2.5 psi over pressure) for 1 min. This was done when a surface was in the downward orientation to condense the vapor that had been trapped in the convection shield. This procedure was followed when surface was in another orientation in order to maintain a consistent pro-

cedure. With a surface in the upward orientation no change in any data could be detected if the system was not pressurized or if it was pressurized to 10 psig for 2 min. After pressurization, 10 min were allowed before a heat flux was applied to the surface.

Originally a small vacuum line was placed on the surface to remove the vapor from the convection shield when a surface was facing downwards. After the vapor was removed from the surface, liquid would fill the vacuum line and this liquid was slowly vaporized by heat transferred to it from the surroundings. As the valve on the vacuum line was closed, the vapor eventually backed up onto the surface. At first this was recorded as very inconsistent data for the initial vapor formation point.

F. TESTING

A test run consisted of a series of steady state heat flux and temperature measurements along with visual observations. The heat flux was the independent variable and controlled by setting the voltage drop across the heater.

The test procedure was to set a voltage drop across the heater and then to allow sufficient time to establish steady state conditions. The heater voltage, shunt voltage, and thermocouple EMFs were then measured and recorded along with comments on the visual observations. Periodically the slowly varying pressure and EMFs from the reference cylinder thermocouple and thermocouple wire loops were also recorded. After all measurements were completed, the heater voltage was changed and the measurements repeated.

The time needed to establish steady state conditions was determined by stepping the heat flux and recording the surface temperature as a function of time. The criterion for steady state was that no change in surface temperature could be detected over a 5 min period. The time needed varied from a few seconds for a metal surface heating upward in liquid hydrogen to 1/2 hr for a metal surface heating downward in liquid nitrogen. The Teflon surface was a special case and is discussed in Section VI.C.

An electric light was used to provide indirect lighting for observing the test surface when testing with liquid nitrogen. When testing with liquid hydrogen, especially with a copper surface, it was observed that the light could initiate boiling. Observations were made in liquid hydrogen by shining a flashlight into the dewar but not directly on the surface. This provided sufficient light at the surface to make observations but did not appear to initiate boiling. The tests were conducted with the unsilvered strips in the outer and inner dewars aligned.

The heat flux was generally begun in the natural convection range and increased in steps through the incipient point. When heating downward, the test had to be terminated at the incipient point, as once the first vapor formed, the entire convection shield filled up with vapor. In the other orientations, if boiling heat transfer data were desired, the heat flux was increased in steps to a maximum and then decreased in steps until the surface superheat became so small it could not be measured accurately. Natural convection conditions were established on some surfaces when the heat flux was decreased but vigorous boiling remained on other surfaces until the test was

terminated. The size of the step in heat flux depended on the portion of the heat transfer curve being investigated. Near the incipient point, the step size was approximately 10% of the heat flux level.

Several runs were made consecutively with the same surface and liquid charge. If the heat flux was increased immediately after a test was terminated, the last active sites while decreasing the heat flux became active, while increasing the heat flux, at a lower heat flux than would have been necessary if the surface had been maintained for a period of time with no vapor formation. The time necessary to fully deactivate all the surface sites varied from 5 min for the 280 grit stainless steel surface to over 2 hr for the Teflon surface. It was found that pressurizing the system to 5 psig also deactivated the surface sites. After a test was terminated, 15 min were allowed before the system was pressurized to 5 psig and a new test begun.

After a series of hydrogen tests with a particular surface was completed, the test dewar was pressurized with hydrogen gas and the liquid hydrogen forced through the dump tube. It was vaporized in a heat exchanger and exhausted into the atmosphere. Sufficient time was allowed for the test dewar to warm up to the nitrogen temperature and then it was purged with nitrogen gas. The test surface was then removed from the dewar and a new one installed. When testing with liquid nitrogen, the liquid was not removed from the test dewar when changing surfaces. The entire system was warmed up to room temperature and cleaned with methylene chloride after two surface changes.

G. VIBRATION TESTS

A series of tests were conducted to determine if random building vibrations had an affect on the initial vapor point. A polished stainless steel surface with liquid thermocouples was mounted in the downward orientation in liquid nitrogen and a vibrometer was mounted on the dewar stand. The outputs from the vibrometer and a liquid thermocouple were placed on adjacent channels of a strip recorder. The heater voltage was stepped from zero to a value that would give a steady state heat flux approximately 20% above that expected to produce nucleation. The slow temperature transient in the liquid and the output from the vibrometer were recorded. When the initial vapor formed, it produced a blimp in the thermocouple trace. This served as a time mark for determining if vibrations might have caused the nucleation.

H. REPLACING THERMOCOUPLE LEADS

Care was taken to avoid unnecessary cold working of the thermocouple leads, but some cold working of the leads was unavoidable as a test surface was inserted into, or removed from, the test dewar. This cold working resulted in an increase in the size of the maximum parisitic EMF generated in the wire loops. An effort was made to replace all of the thermocouple lead wires when the EMF generated in the copper loop exceeded 0.4 μv. A few tests were run after an EMF this large was observed in the copper loop, as it was desired to complete a series of tests.

When testing in liquid nitrogen, the average, of the absolute value, of the parisitic EMF in the wire loops was 0.06 μv for 25 readings on the

copper loop and 0.64 μv for 11 readings on the constantan loop. When testing

in liquid hydrogen, the values were 0.21 μv for 50 readings on the copper

loop and 0.84 μv for 29 readings on the constantan loop.

I. SURFACE MEASUREMENTS

After the heat transfer studies were completed, measurements were made

on the surfaces. These included photomicrographs and measurements of sur-

face roughnesses The roughnesses were measured first on an instrument that

produced a trace of the surface profile and then on an instrument that gave

an RMS reading. The RMS values reported in Section V.F are the average of

4 readings taken in 2 perpendicular directions. Both of the roughness in-

struments used a conical diamond tracer with a nose radius of 0.0005 in. and

a cone angle of 90°.

J. DATA REDUCTION

An IBM 7090 computer was used to reduce the heat transfer data. From

the test data, the computer calculated the power into the heater, the sur-

face thermocouple superheat, the heat losses, the net heat flux, a tempera-

ture correction for the temperature drop from the thermocouple to the sur-

face and the surface superheat. A discussion on the heat losses and tem-

perature correction is given in Appendix B. The calibration data for each

surface thermocouple was fitted with a second order equation over a limited

liquid hydrogen temperature range and with another one over a limited liquid

nitrogen temperature range. These equations were used to calculate the

thermocouple superheat from the differential EMF measurement, using the

saturation temperature of the test liquid, corresponding to the test dewar

pressure, as a base. The reference cylinder thermocouple was used only to

make sure that the liquid was saturated when data was being recorded.

V. RESULTS

A. NATURAL CONVECTION

Natural convection heat transfer data were obtained while determining

the initial vapor point. Data from the natural convection measurements are

shown in Figs. 11-13.

The solid lines in Fig. 11 are reasonable fits to the temperatures meas-

ured in liquid nitrogen with fine wire thermocouples, with a polished stain-

less steel surface heating downwards. The dashed lines represent calculated

temperature distributions, based on the measured surface temperatures and

heat fluxes, assuming that conduction is the only mode of heat transfer in

the liquid. When a surface was heating downwards in liquid nitrogen, all of

the steady state temperatures were very stable with no appreciable oscilla-

tions. It was stated in Section III.I that the purpose of heating down-

wards was to eliminate the fluid motion produced by bouyancy forces and thus

to simulate a "o-g" environment in a "1-g" environment. If all of the fluid

motion could be eliminated, the only significant mode of heat transfer in the

liquid would be conduction. The two sets of curves in Fig. 11 match reason-

ably well near the vertical axis, indicating that when a surface is heating

downwards with the convection shield, the mechanism of heat transfer in the

liquid does approach pure conduction in a appreciable region near the surface.

The liquid thermocouples were also used with a surface heating upwards

with the convection shield in liquid nitrogen. During natural convection,

the superheat of the liquid 0.010 in. from the surface randomly varied from
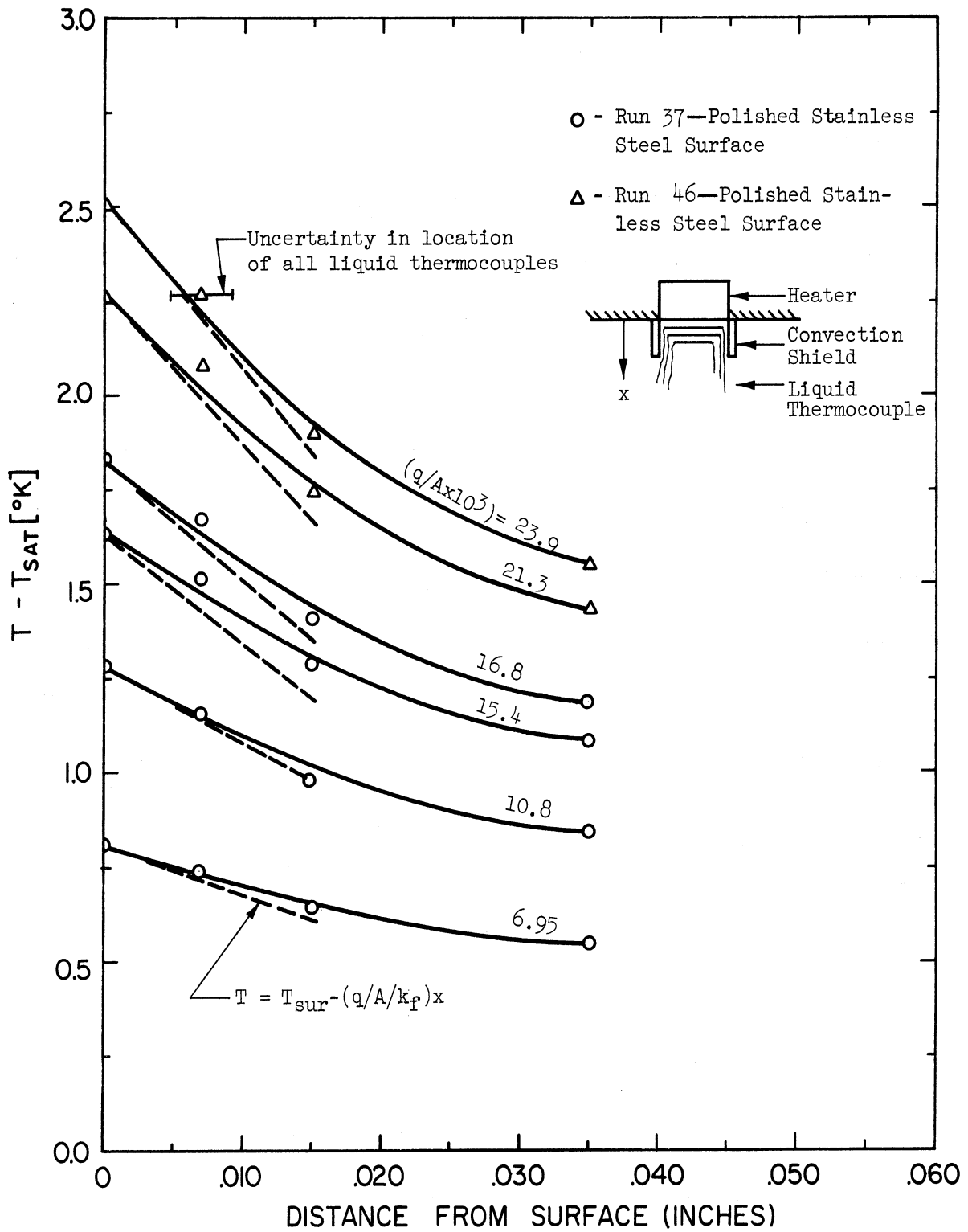
Fig. 11. Temperature distribution in liquid nitrogen when heat downwards.
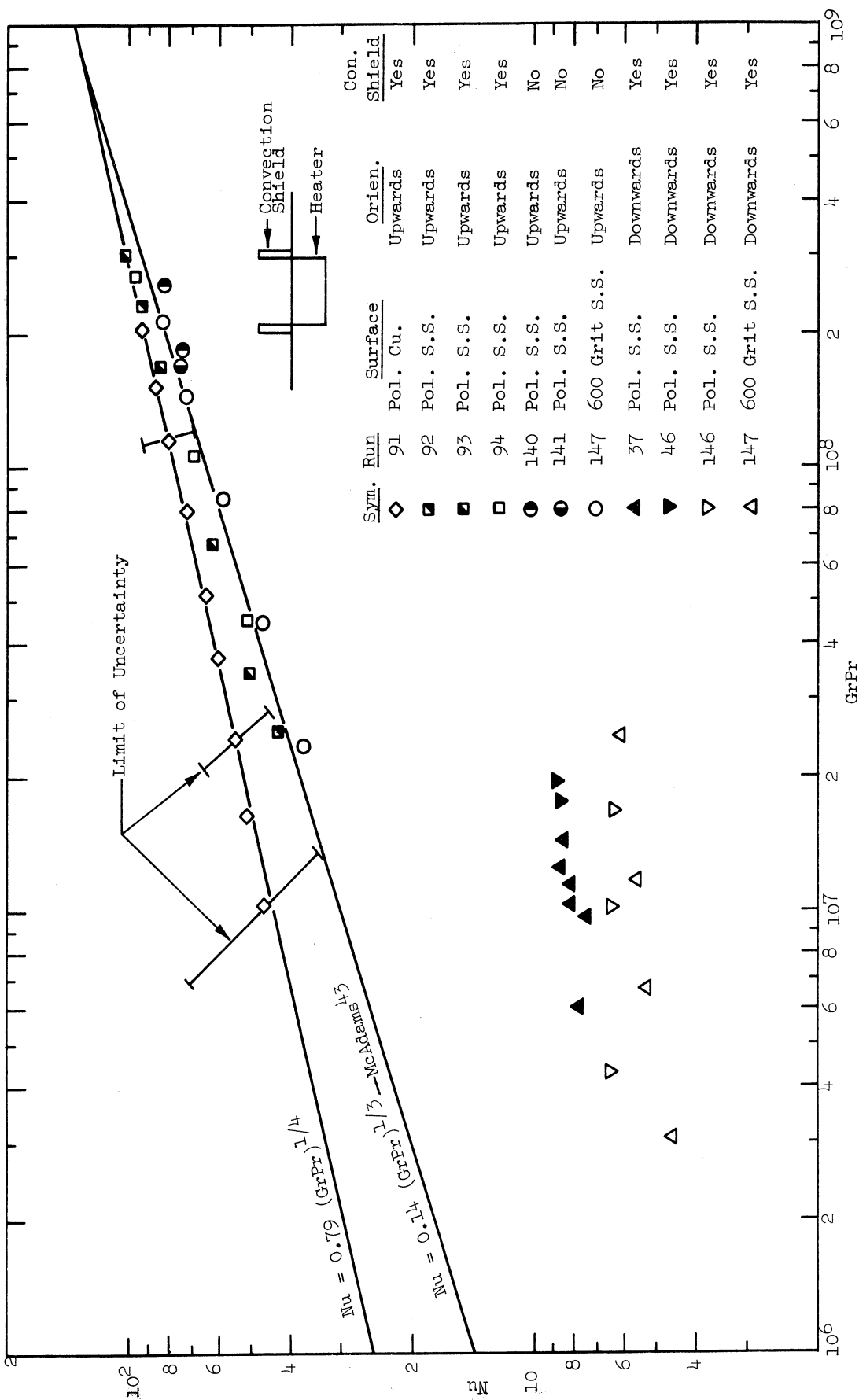
Fig. 12. Natural convection heat transfer to liquid nitrogen.
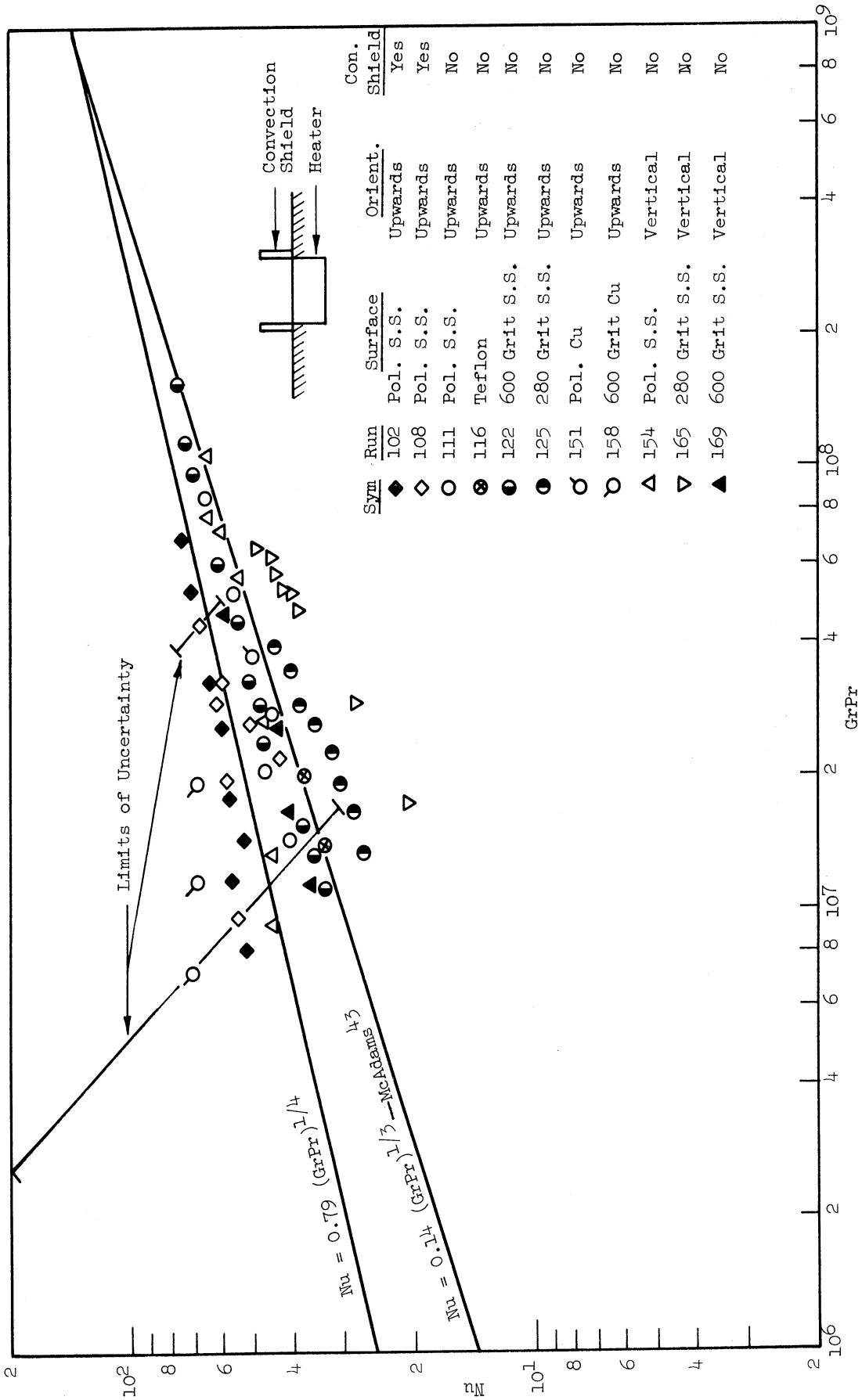
Fig. 13. Natural convection heat transfer to liquid hydrogen.

10 to 35% of the surface superheat. As the readings were being made with a potentiometer, it was impossible to obtain any accurate measurements of the average liquid temperatures or oscillations.

Data for natural convection heat transfer are presented in the form of Nu vs. (GrPr) in Figs. 12 and 13 for liquid nitrogen and liquid hydrogen, respectively. When heating upwards or vertically, the surface temperature oscillated during natural convection about ±4% of the surface superheat, with an unsteady period of 10-30 sec. Each temperature reported under such conditions is near the mean of its observed range. When calculating Nu and (GrPr), the physical properties were obtained from[44,47,49,52] and evaluated at the arithmetic mean of the surface and bulk fluid temperatures. Except when heating downwards, the characteristic length was taken as 0.9D as recommended by Krieth[51] for a horizontal disc. When heating downwards, the depth of the convection shield was taken as the characteristic length, as this is representative of the thermal boundary layer thickness if there is no fluid motion inside the convection shield and complete mixing outside of it. When one-dimensional conduction is the only significant mode of heat transfer, Nu is unity for all values of (GrPr) if the thermal boundary layer thickness is taken as the characteristic length.

The symbols in Fig. 12 represent three sets of data conditions: the diamonds and squares a surface heating upwards with the convection shield, the circles a surface heating upwards without the convection shield and the triangles a surface heating downwards with the convection shield. Although the diamonds and the squares represent data obtained with the same geo-

metrical arrangement, the data appear to be different and were treated as two different sets. The uncertainties in the diamonds and the squares overlap, but at the smaller values of (GrPr) the differences between the surface and liquid temperatures are small and the main contribution to the uncertainties is the uncertainty in the thermocouple calibration. The same surface thermocouple and calibration curve was used for all of the upward data shown in Fig. 12, so all of the upwards data at the smaller values of (GrPr) should be in error by about the same amount and in the same direction. At the larger values of (GrPr) the main contribution to the uncertainties is the uncertainty in the heat transfer area. This is $\pm 12\%$ for the copper surface and $\pm 4\%$ for the stainless steel surfaces. The same polished stainless steel surface was used both with and without the convection shield, so the data for both conditions at the larger values of (GrPr) should again be in error by about the same amount and in the same direction. In addition to the above uncertainties, there is the uncertainty due to the oscillations of the surface temperatures during natural convection heat transfer.

The diamonds and the squares in Fig. 12 were each correlated by a least squares fit to a straight line, giving

$$Nu = 1.05 \ (GrPr)^{.239} \tag{3}$$

and

$$Nu = 0.146 \ (GrPr)^{.335} \tag{4}$$

respectively. The exponents in Eqs. (3) and (4) indicates that the fluid motion was most likely laminar during Run 91 and turbulent during Runs 92, 93,

and 94. The transition point given by McAdams[43] is (GrPr) = 2 x 10⁷. Background vibrations, as witnessed by the "noise" in the galvanometer used to detect the potentiometer unbalance (see Section IV.C), varied considerably according to the time of day. In view of the facts that the data are in the transition range and that the background vibrations varied, it is not surprising that there is a possible change in flow regimes. A 1/4 slope line was fitted to the diamonds and a 1/3 slope line was fitted to the squares, giving

$$\text{Nu} \;=\; 0.79 \, (\text{GrPr})^{1/4} \tag{5}$$

and

$$\text{Nu} \;=\; 0.15 \, (\text{GrPr})^{1/3} \tag{6}$$

respectively. The equations recommended by McAdams[43] for a flat plate heating upwards are

$$\text{Nu} \;=\; 0.54 \, (\text{GrPr})^{1/4} \tag{7}$$

when the fluid motion is laminar and

$$\text{Nu} \;=\; 0.14 \, (\text{GrPr})^{1/3} \tag{8}$$

when the fluid motion is turbulent. Equation (5) predicts heat transfer rates 46% larger than predicted by Eq. (7) and Eq. (6) predicts heat transfer rates 7% larger than predicted by Eq. (8). Equations (5) and (8) are shown in Fig. 12.

A comparison of the circles and squares in Fig. 12 indicates that the use of the convection shield increases Nu at a given (GrPr), i.e., there is an increase in the heat transfer rate at a given ΔT_s. This is most likely because the convection shield disrupts the normal fluid flow pattern. When using the convection shield, the fluid cannot flow towards the heat transfer surface along the fin and therefore a large velocity boundary layer does not build up. As the slow moving fluid in the velocity boundary layer can thermally insulate the surface, the use of the convection shield increases the heat transferred at a given ΔT_s. There are no data available for comparison to Run 91 in Fig. 12, but the effect of the convection shield would seem to be especially large when the fluid motion is laminar, as the data for Run 91 has approximately 46% more heat transfer than is predicted by Eq. (7). Merte and Clark[17] used a similar shield while boiling water in an accelerating system. For values of (GrPr) around 10^{10}, they found that the shield increased the heat transfer rate during natural convection about 50%.

The Nu at a given (GrPr) varies considerably between the runs in which the surface was heating downwards. It is noted that Runs 37 and 46 were made with the liquid thermocouples in place. The liquid thermocouple wires and the thermocouple holder, which was seated against the surface, provided conduction paths for the transfer of heat away from the superheated liquid near the surface. This serves to increase the Nu at a given (GrPr) over runs during which the conduction paths are not present. Some of the variation between runs may also be because the convection shield did not seat exactly the same each time. If superheated fluid could leak past the convection shield,

the Nu at a given (GrPr) would again be increased.

The symbols in Fig. 13 represent three sets of data conditions: the diamonds a surface heating upwards with the convection shield, the circles a surface heating upwards without the convection shield and the triangles a surface heating vertically without the convection shield. The uncertainty in the data points shown in Fig. 13 is due mainly to the uncertainty in the temperature measurements. For the points with the smaller values of (GrPr), the difference between the surface and liquid temperatures is about 0.10°K, not much larger than the uncertainty of ±0.08°K caused by paristic EMFs in the thermocouple lead wires. The uncertainties in the temperature measurements remain about the same in magnitude but decrease as a percentage of the surface superheat as the ΔT_s increases. This results in a much smaller uncertainty in the data points at the larger values of (GrPr). A more complete discussion of the uncertainties is given in Appendix B. The very large uncertainty, especially at the smaller values of (GrPr), results in the spread of the data shown in Fig. 13. The same correlations shown in Fig. 12 are shown in Fig. 13 for comparison purposes. The correlation given by McAdams[43] for turbulent natural convection heat transfer from a vertical plate is

$$Nu = 0.13 \ (GrPr)^{1/3} . \tag{9}$$

This equation predicts about 7% less heat transfer than Eq. (8), recommended by McAdams for a horizontal plate under the same conditions. The uncertainties in the data prevent precise calculations, but the data in Fig. 12 show only minor difference between the vertical and horizontal surfaces.

No data were taken with a surface heating downwards in liquid hydrogen, although a number of attempts were made. Vapor continuously formed at the end of the dump tube and on machine screws used in mounting the surface. It proved to be impossible to prevent some of these vapor bubbles from becoming trapped in the convection shield. As power was applied to the heater, the trapped bubbles grew until vapor completely filled the convection shield.

B. NUCLEATE BOILING

Nucleate boiling heat transfer data were obtained for a number of surfaces heating upwards and vertically in liquid hydrogen and upwards in liquid nitrogen. No boiling data could be obtained when a surface was heating downwards, as once the initial vapor formed the convection shield filled up with vapor. The surface temperatures during nucleate boiling were much steadier than those during natural convection, oscillating about ±0.5% of the surface superheat. Each temperature reported is near the mean of its observed range.

1. Hysteresis

The hysteresis in the surface temperature, which was observed by first increasing the heat flux and then decreasing it, depended upon the surface and orientation. Data for typical runs are shown in Figs. 14-17.

The data shown in Fig. 14 are for the polished stainless steel surface heating upwards in liquid hydrogen. This almost complete lack of hysteresis is characteristic of all the runs made with this surface heating upwards. Visual observations indicate that, when increasing the heat flux, a few individual sites distributed rather uniformly over the surface become active
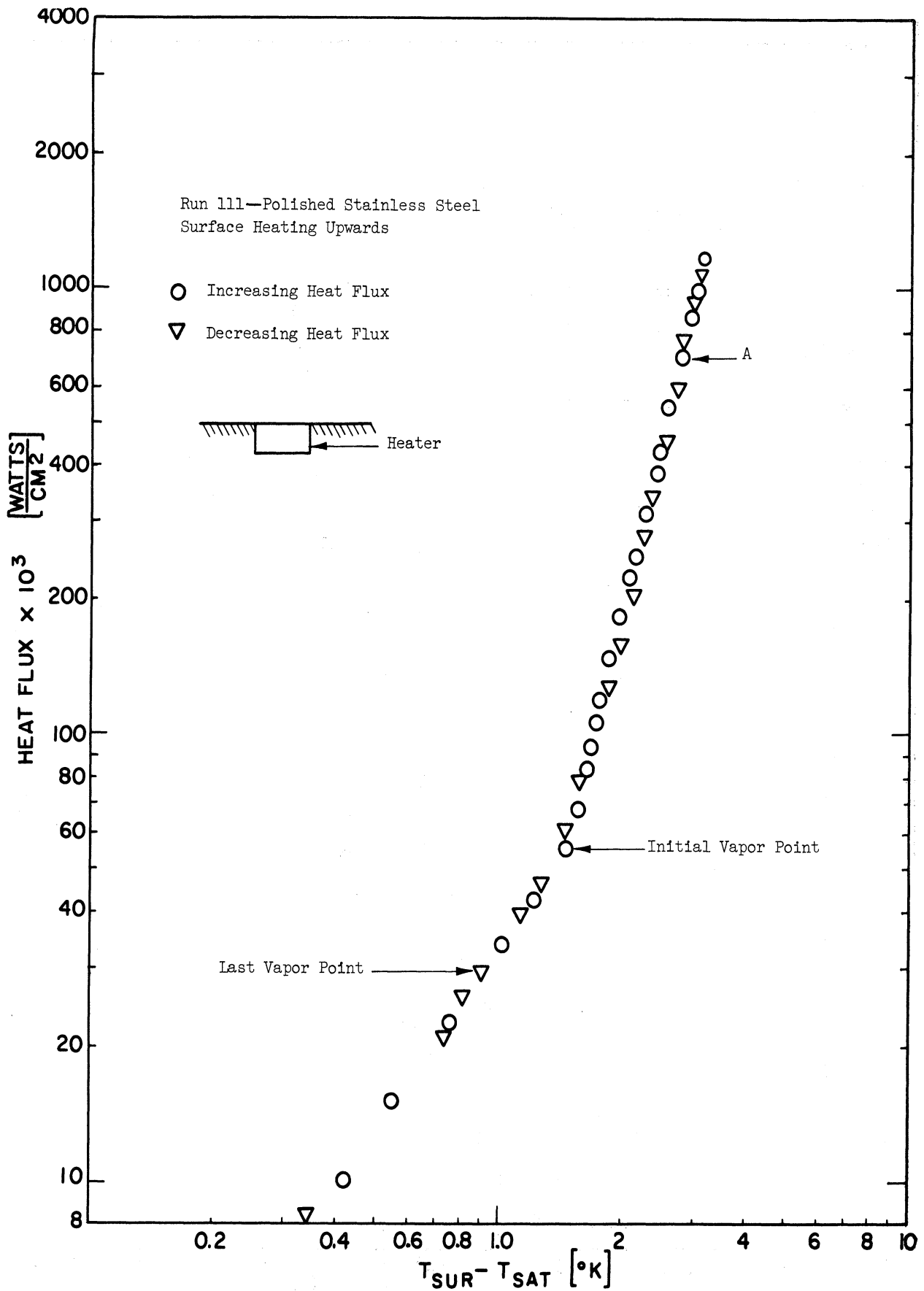
Fig. 14. Hysteresis of polished stainless steel surface
heating upwards in liquid hydrogen.
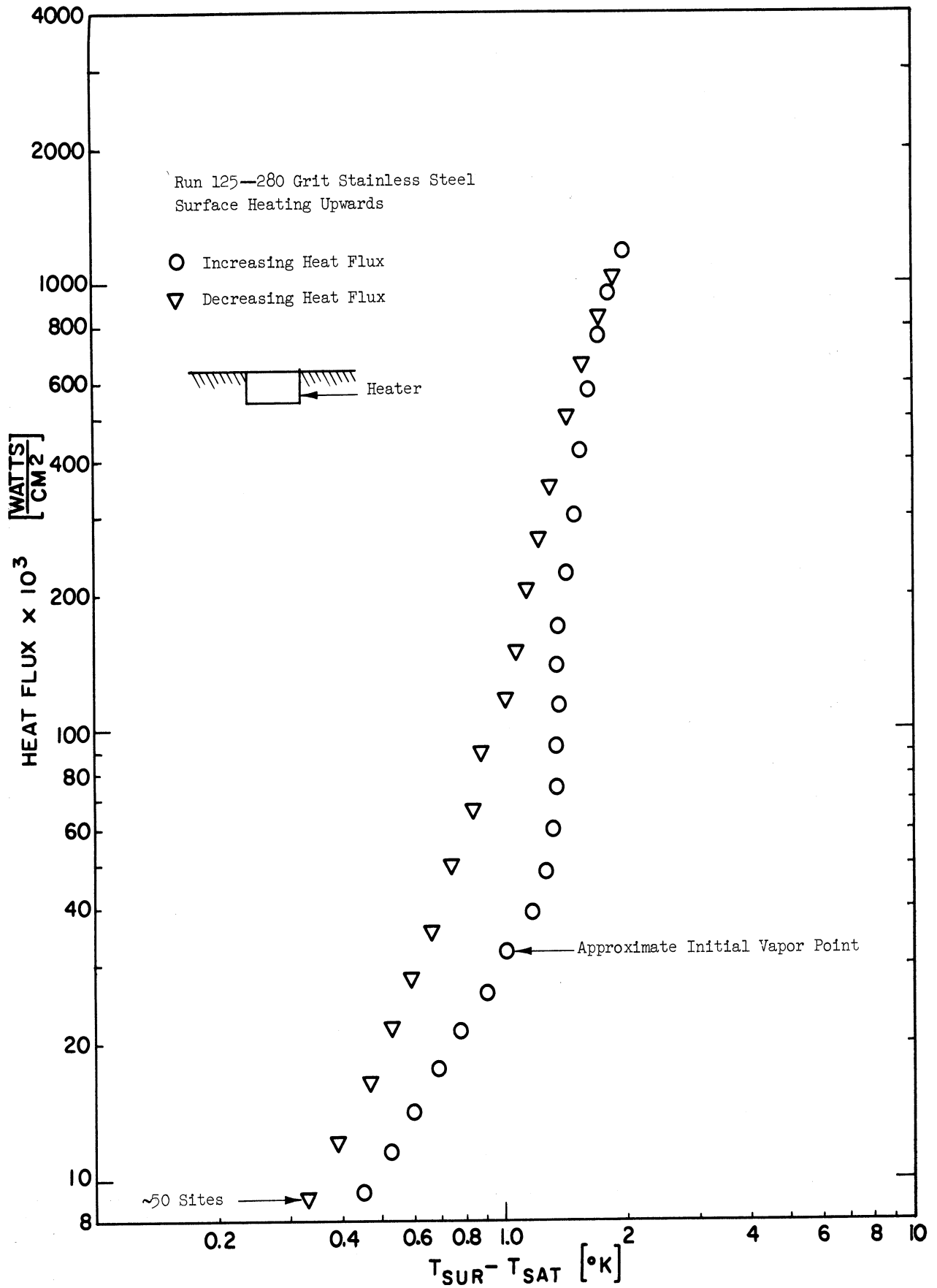
Fig. 15. Hysteresis of 280 grit stainless steel surface
heating upwards in liquid hydrogen.
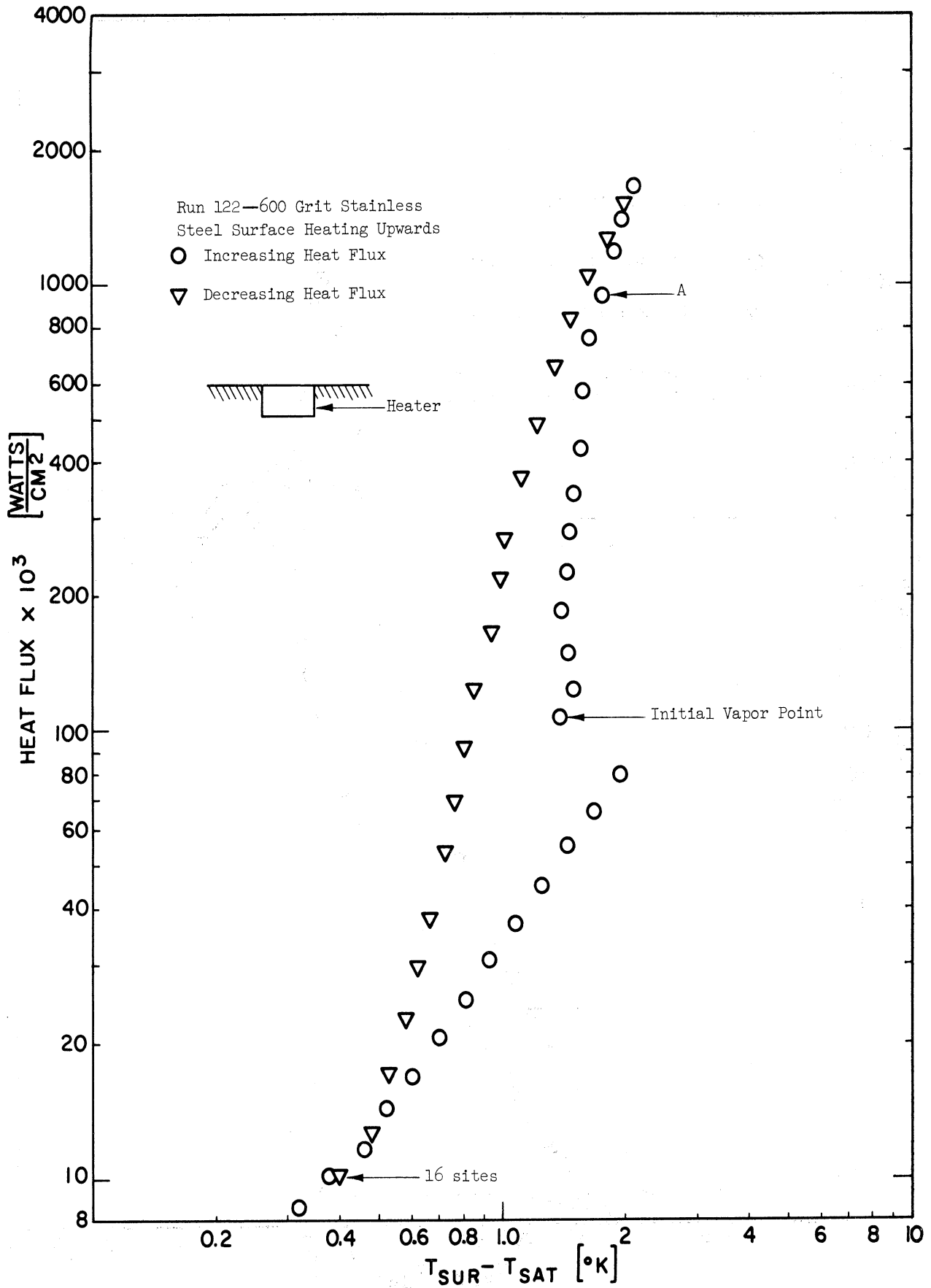
Fig. 16. Hysteresis of 600 grit stainless steel surface heating upwards in liquid hydrogen.
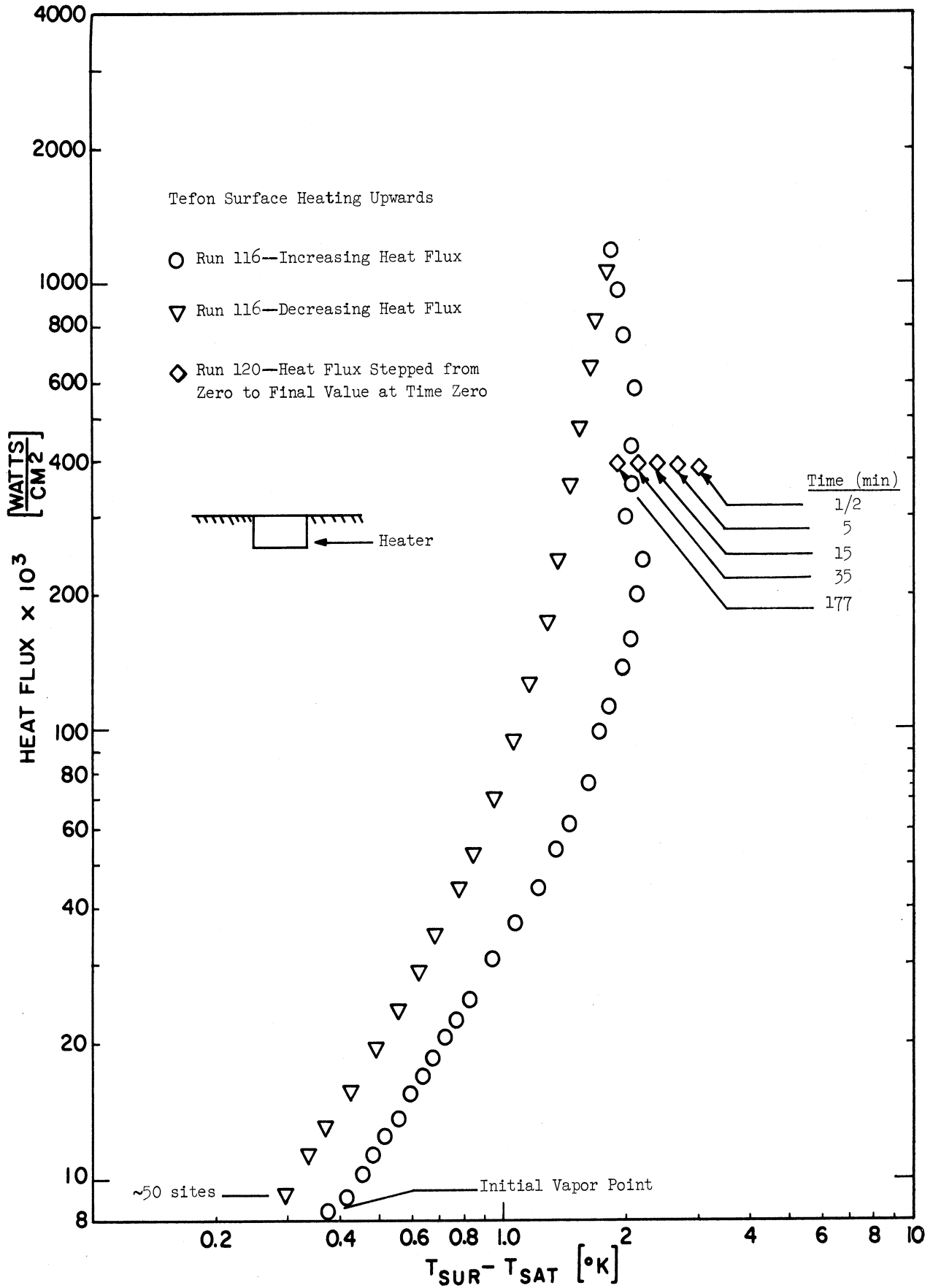
Fig. 17. Hysteresis of Teflon surface heating upwards in liquid hydrogen.

first. As the heat flux was increased more, some of the individual sites formed small clusters of 2 or 3 sites which eventually grew larger, joined together and formed patches of active boiling. Other portions of the surface were almost void of active sites with only a few individual sites and clusters. As the heat flux continued to be increased, the patches grew until they completely covered the surface, corresponding to point A in Fig. 14. The site density in the patches was not large and did not increase appreciably until after the patches covered the entire surface. When decreasing the heat flux, the site density decreased fairly uniformly over the surface. At very low values of boiling heat fluxes, a steady site would sometimes have one or two intermittent sites adjacent to it. The fact that the boiling pattern was different when increasing the heat flux and when decreasing the heat flux lead to the expectation that the surface temperature, at a given heat flux, would be different in the two cases and that a hysteresis would be observed.

The hysteresis in surface temperature observed with the 280 grit stainless steel surface heating upwards in liquid hydrogen is shown in Fig. 15. When increasing the heat flux, the active sites again formed first as individual sites distributed rather uniformly over the surface and then as small clusters of as many as 4 and 5 active sites. The clusters did not grow and join up to form patches of active sites as with the polished stainless steel surface. The individual sites and clusters increased in number as the heat flux was increased. Near the maximum heat flux used, the entire surface appeared to be covered with active sites. The site density decreased

fairly uniformly over the surface as the heat flux was decreased. As the pattern of boiling was somewhat similar when the heat flux was being increased and when it was being decreased, only a small amount of hysteresis was anticipated.

Shown in Fig. 16 are data illustrating the hysteresis in surface temperature observed with the 600 grit stainless steel surface heating upwards in liquid hydrogen. The first vapor came from a patch of active sites which formed suddenly and covered approximately 5% of the surface area. The active site density appeared to be very large in the patch and a drop in surface temperature accompanied the formation of the patch. When the heater power was increased by a step change, the surface temperature was observed to rise slightly for 1 or 2 sec and then to drop as the patch spread. After each increase in heater power, a steady state condition was soon reached in which the patch did not spread further and the surface temperature remained constant. The steady state temperature was approximately constant until the patch of active sites appeared to cover the surface, corresponding to point A in Fig. 16. When decreasing the heat flux, the site density appeared to decrease uniformly over the surface.

The heat flux during patchwise boiling appears to be very non-uniform By assuming that the estimate of the fraction of the surface covered by the patch is accurate, that the portion of the surface covered by the patch transfers heat at the rate measured at the same surface temperature when decreasing the heat flux, and that the remaining portion of the surface transfers heat at the rate measured at the same surface temperature during natural con-

vection, it is possible to calculate the average heat transfer rate during

patchwise boiling to within 15% of the measured rate.

The data shown in Fig. 16 and the description of the vapor formation

pattern from the 600 grit stainless steel surface also describe the vapor

formation pattern from the 600 grit copper surface, heating upwards in liquid

hydrogen.

The polished copper surface, heating upwards in either liquid hydrogen

or liquid nitrogen, first developed a few individual active sites and then

suddenly developed a small patch of active sites, similar to the 600 grit

surfaces. The site density in this patch was not as large as with the 600

grit surfaces and did not increase appreciably until after the patch had

covered the entire surface. Again the site density appeared to decrease uni-

formly over the surface as the heat flux was decreased. There was a rela-

tively small amount of hysteresis in the data from the polished copper sur-

face.

When testing the stainless steel surfaces in the vertical position, bub-

bles rising from an active site were moved back and forth across the surface

by convective currents in the liquid. It was common for potential sites in

the path of the rising bubbles to be active for 1 or 2 sec after the bubbles

passed them, and then to become inactive again. When a site on the lower

portion of the surface produced vapor steadily, sites in a triangle of surface

area above the steady site also became active. This produced a hysteresis,

which is somewhat similar to that shown in Fig. 16, in the boiling curve of

all the surfaces tested in the vertical position. There was not a single large

shift to a lower ΔT_s as the initial vapor formed, but rather a series of smaller shifts as sites on the lower portion of the surface became active and influenced the potential sites located above them. This made the increasing portion of the heat transfer curve rather inconsistent. Visual observations indicated that in the vertical orientation, most of the sites that became active at the lower heat fluxes were on the top half of the surface. This was most likely because one active site on the lower half of the surface influenced many potential sites on the top half. When decreasing the heat flux in the vertical orientation, the density of active sites was more uniform over the surface then when increasing the heat flux, but was still much greater near the top of the surface than near the bottom.

The Teflon surface exhibited the hysteresis in surface temperature shown by the data for Run 116 in Fig. 17. The sites formed individually with no observed clusters of active sites. All of the sites active at the lower boiling heat fluxes seemed to have difficulty in remaining active. After several seconds or minutes of steady vapor formation at a given site, it was often noted that the site became inactive. The time between successive data points during the increasing heat flux portion of Run 116 averaged about 10 min. The hysteresis shown was noted with each run made with the Teflon surface, even after it had been in the liquid hydrogen for 24 hr. Upon decreasing the heat flux, the sites were still individual sites and the bubbles produced became very small at low heat fluxes.

Also shown in Fig. 17 are the data from Run 120. For this run the power input into the heater was stepped from zero, to its final value, at time

zero. The surface temperature was then measured at various times, holding

the heater power constant. There were a large number of active sites spread

uniformly over the surface area. The surface temperature was decreasing

very slowly when the last measurement was made almost 3 hr after the test

began. As shown by the data in Appendix C, the surface temperature had de-

creased only 0.04°K during the last 47 min of Run 120. It is felt that if

Run 120 had been continued, the surface temperature would have eventually ap-

proached the value measured at the same decreasing heat flux during Run 116.

The behavior of the surface temperature during Run 120 is felt to be caused

by additional sites becoming active with time. This could not be confirmed

by visual observations as it was impossible to accurately compare the site

density over the duration of the test. This effect seems to be cumulative

and causes the surface temperature to decrease while the heat flux is in-

creased during Run 116.

Comparison of boiling heat transfer data from various runs is made only

for the data points obtained while decreasing the heat flux as the decreasing

heat flux data is more reproducible and consistent than the increasing heat

flux data.

Both the increasing and decreasing heat flux data obtained during the

boiling runs are tabulated, along with comments from the visual observations,

in Appendix C. The data points with very small surface superheats are in-

cluded in Appendix C, but are not plotted in the figures showing boiling heat

transfer data because of the large percentage uncertainty pointed out in

Section V.A. Also tabulated in Appendix C, but not plotted because of ex-

tremely large uncertainties in the surface temperatures, are the data from Run 89, made with the epoxy coated glass fiber web surface heating upwards in liquid hydrogen. In general, the data from runs made only to determine the initial vapor point are not included in Appendix C.

2. Reproducibility

In order to make the visual observations it was necessary to have the unsilvered strips in the inner and outer dewars aligned. The possibility that radiation through these strips affected the heat transfer data was investigated. Data are shown in Fig. 18 which were obtained with the polished stainless steel surface heating upwards in liquid hydrogen. Run 112 was made immediately following Run 111. The only difference between the two runs is that during Run 111 the unsilvered strips were aligned and during Run 112 the outer dewar was rotated 90°. There is no appreciable difference between the data obtained during Runs 111 and 112. All of the data presented in the other figures were taken with the unsilvered strips aligned.

Typical of the excellent reproducibility between runs is that shown in Figs. 18 and 19. The two runs shown in Fig. 19 were made 24 hr apart. The Teflon surface was immersed in the liquid during the entire period between the runs. No data were obtained during Run 121 while increasing the heat flux. The heat flux was stepped to the maximum value for Run 121 at the conclusion of Run 120, shown in Fig. 17, and data taking began immediately on the decreasing heat flux curve. The excellent agreement between the two runs indicates that the Teflon surface temperatures were close to their steady state values.
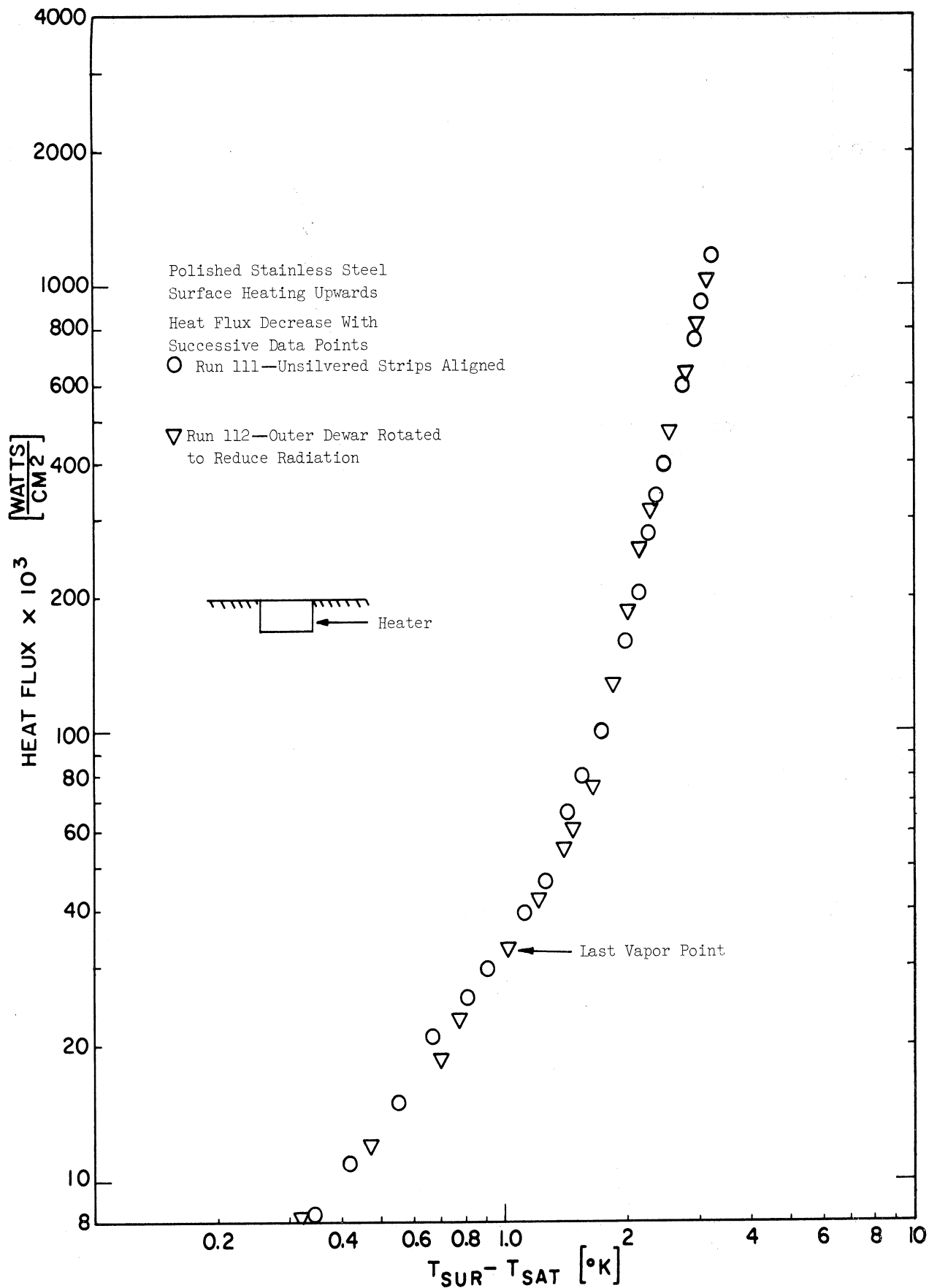
Fig. 18. Effect of rotating outer dewar on
heat transfer to liquid hydrogen.
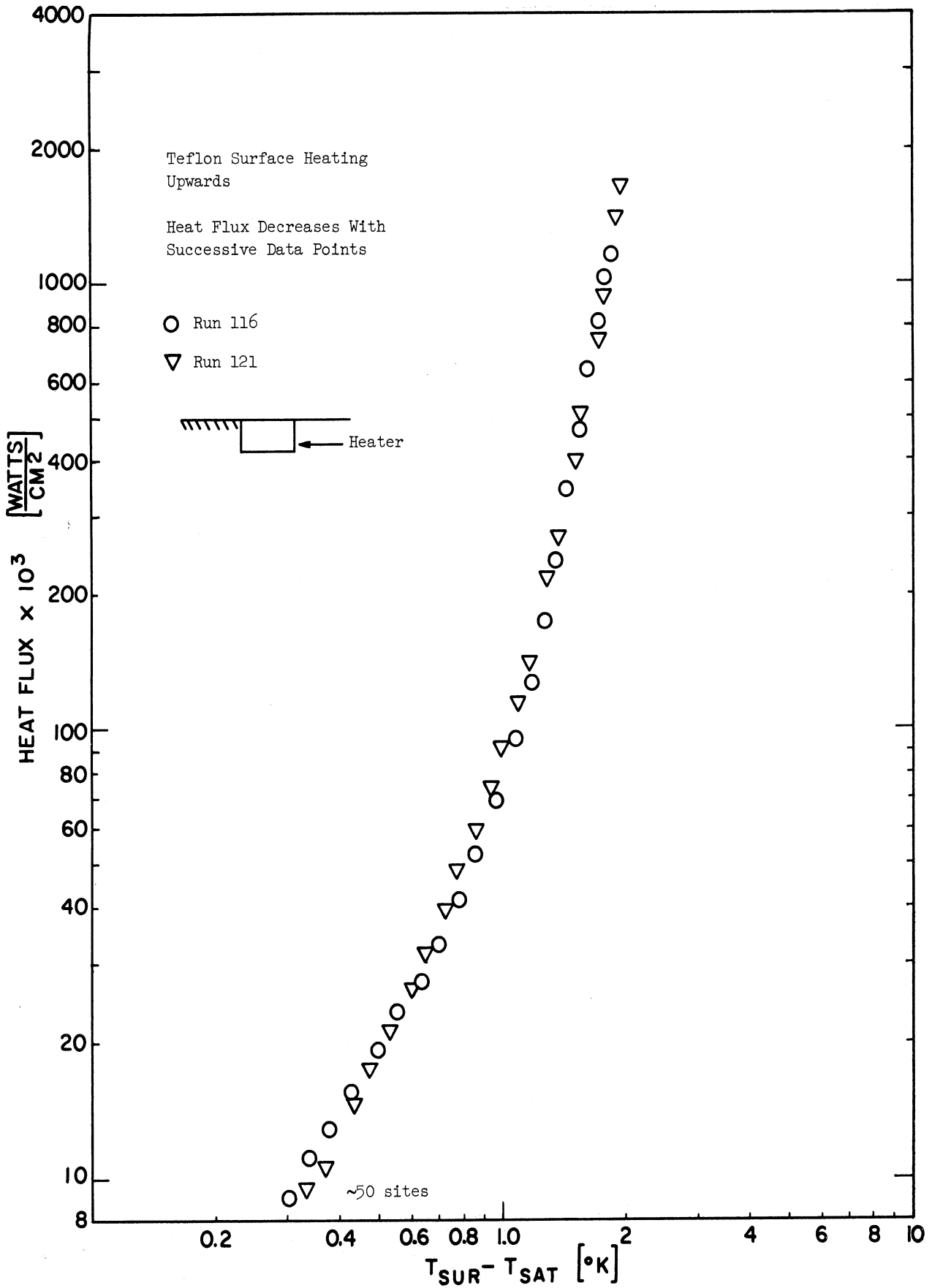
Fig. 19. Reproducibility of heat transfer to liquid hydrogen from a Teflon surface.

3. Effect of the Convection Shield

The effect of the convection shield upon the heat transfer curve is shown by the data in Fig. 20, obtained with the polished stainless steel surface heating upwards in liquid hydrogen. It can be seen that the use of the convection shield increases the heat transferred at a given ΔT_S, during both nucleate boiling and natural convection. The disruption of the normal liquid flow pattern was given in Section V.A as a possible explanation for the natural convection portion of the curve. This same argument can be extended to the boiling portion of the curve. Without the convection shield, the liquid flows towards the heat transfer surface along the fin. This relatively cool liquid can slightly suppress the boiling near the surface edge. This results in a non-uniform heat flux and a decrease in the average heat flux at a given ΔT_S.

Another possible explanation is also considered for the nucleate boiling portion of the curve. There is a considerable flow both towards the surface and away from it during boiling. When the convection shield is not used, liquid can flow towards the surface from the sides and vapor away from the surface through the area above it. When the convection shield is used, the flows toward the surface and away from it both must pass through the area above the surface. This increases the velocities and mixing and perhaps also the heat transfer coefficient. The difference in the final vapor points shown in Fig. 20 is considered normal for two runs made either with or without the convection shield.
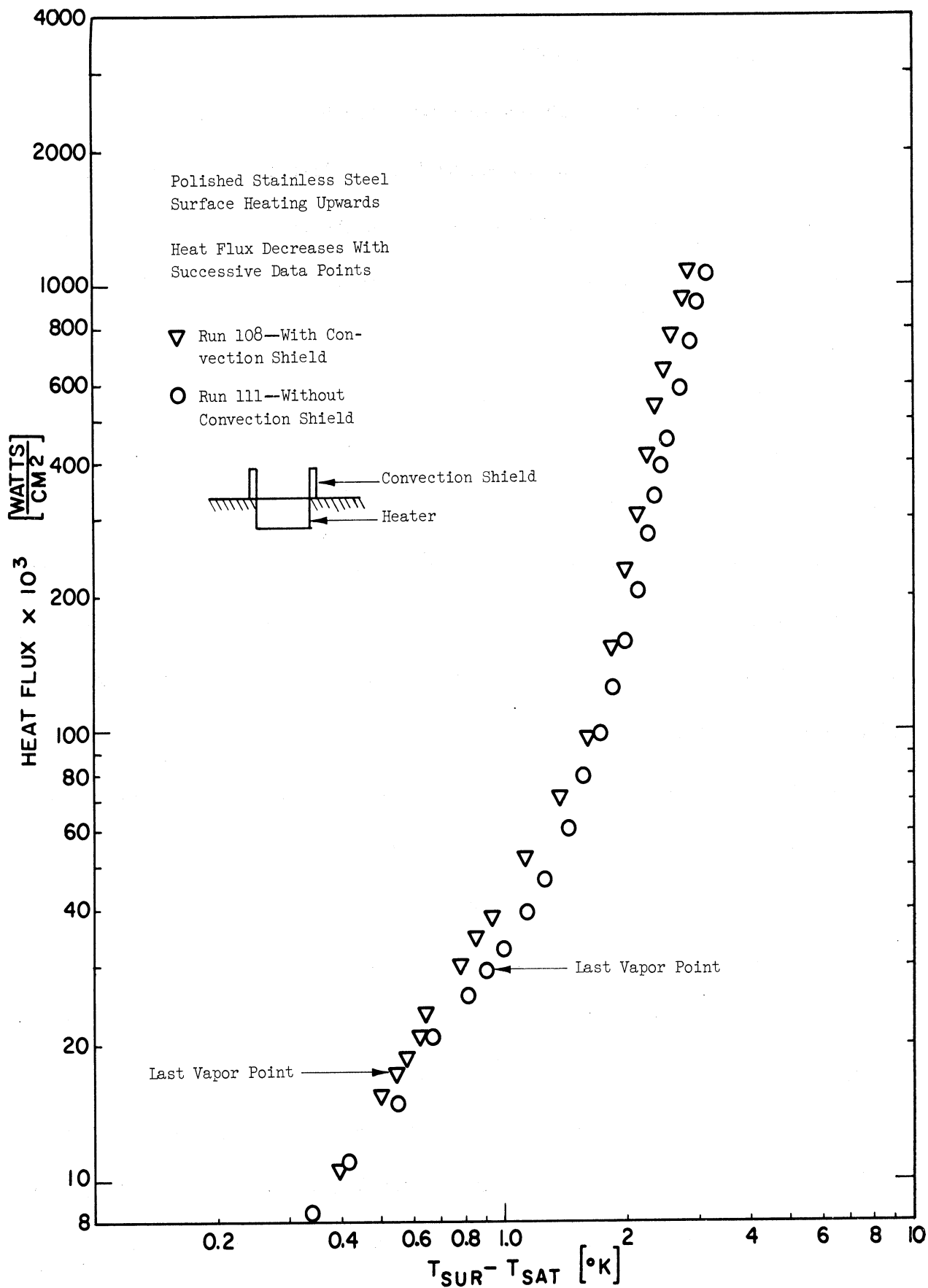
Fig. 20. Effect of convection shield on heat transfer to liquid hydrogen.

4. Effect of Roughness

The effect of surface roughness on the boiling heat transfer to liquid hydrogen is shown by the data in Figs. 21-23.

The data shown in Fig. 21 were obtained from three horizontal stainless steel surfaces with different surface finishes: polished, lapped with 600 grit lapping compound and lapped with 280 grit lapping compound. It is seen that the lapped surfaces are more efficient boiling surfaces, i.e., require a smaller surface superheat to transfer a given heat flux, than the polished surface. It is interesting to note that, except for very low heat fluxes, the 600 grit surface is more efficient than the rougher 280 grit surface. The surface superheat necessary to transfer a given heat flux does not decrease monotonically as the surface roughness is increased. A possible explanation for this is discussed in Section VI.B.

It is also noted from Fig. 21 that the boiling curves, i.e., the loci of the surface superheat vs. heat flux points, of both lapped surfaces bend towards larger surface superheats at the higher heat fluxes, while the boiling curve of the polished surface does not. This is especially true of the boiling curve of the 600 grit surface. The maximum heat fluxes used were limited by the size of the heater leads and the amount of liquid in the test dewar that could be vaporized during a run. The burnout heat flux was not determined for any of the surfaces, but the magnitude of it can be obtained from values found in the literature. For a horizontal flat surface, Class, et al.,[27] report a burnout heat flux of around (4000) x 10^{-3} watts/ cm^2. The data of Mulford and Nigon[26] show that the burnout heat flux for a
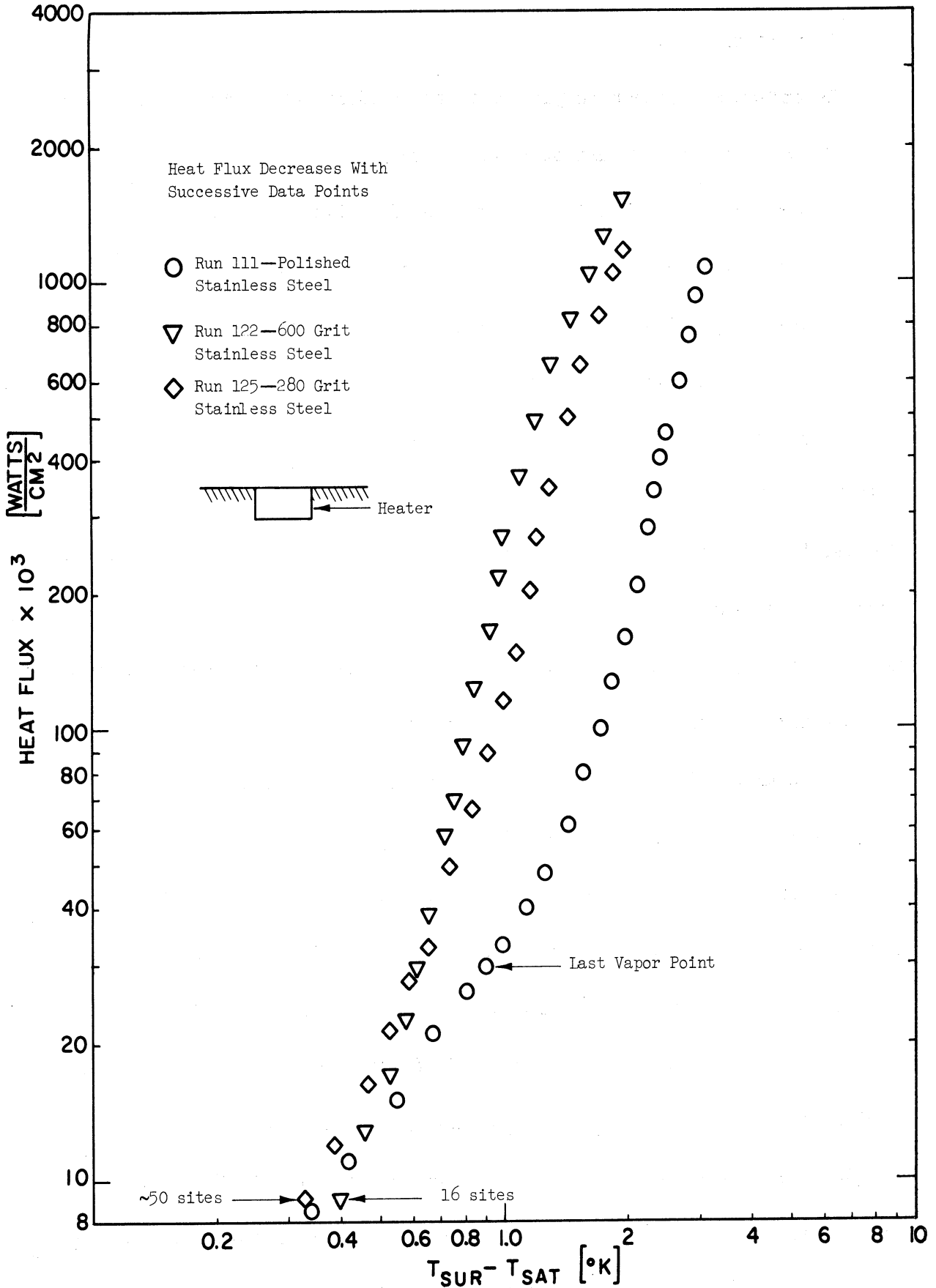
Fig. 21. Effect of roughness on heat transfer to liquid
hydrogen from horizontal stainless steel surfaces.
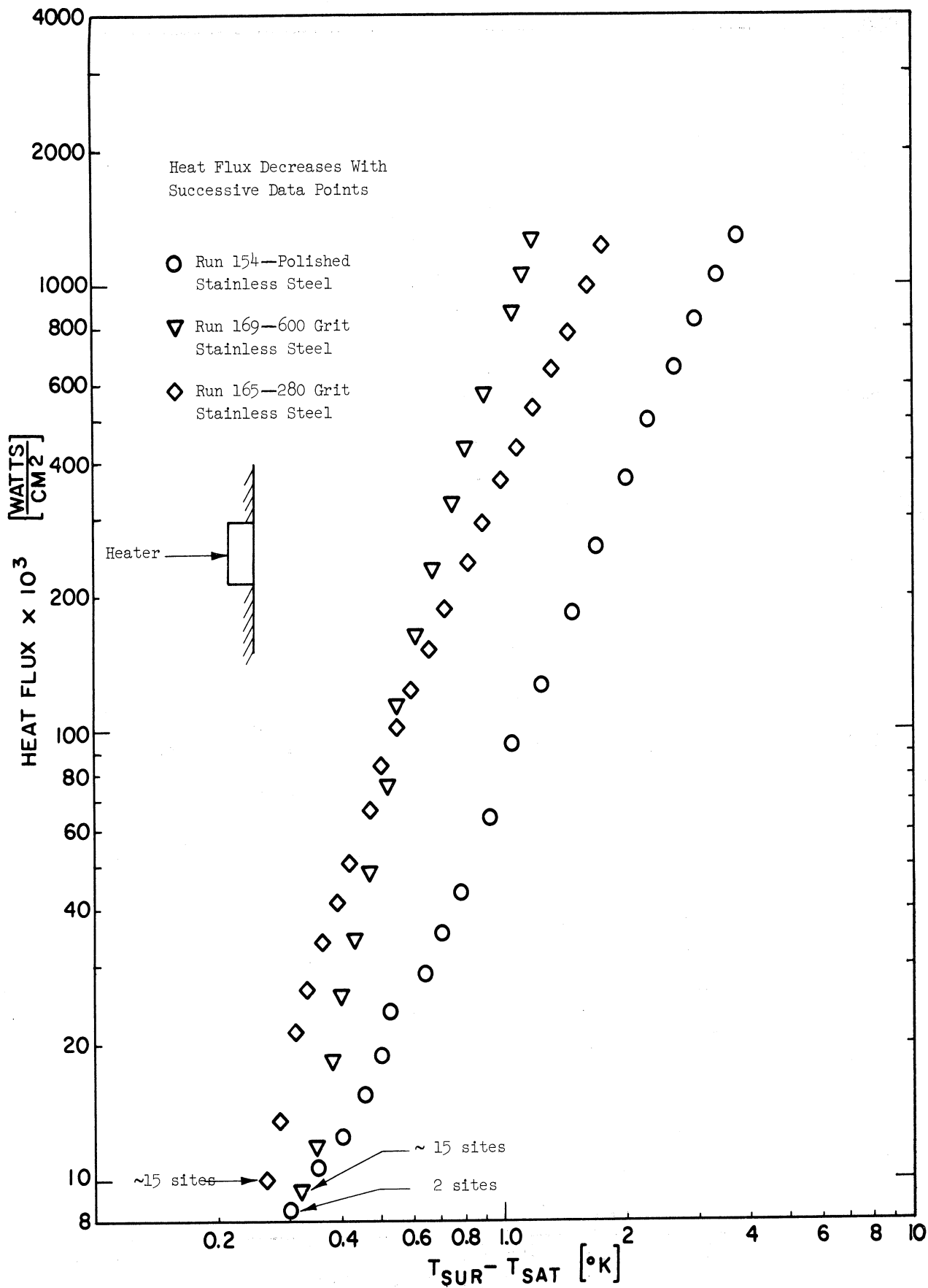
Fig. 22. Effect of roughness on heat transfer to liquid hydrogen from vertical stainless steel surfaces.
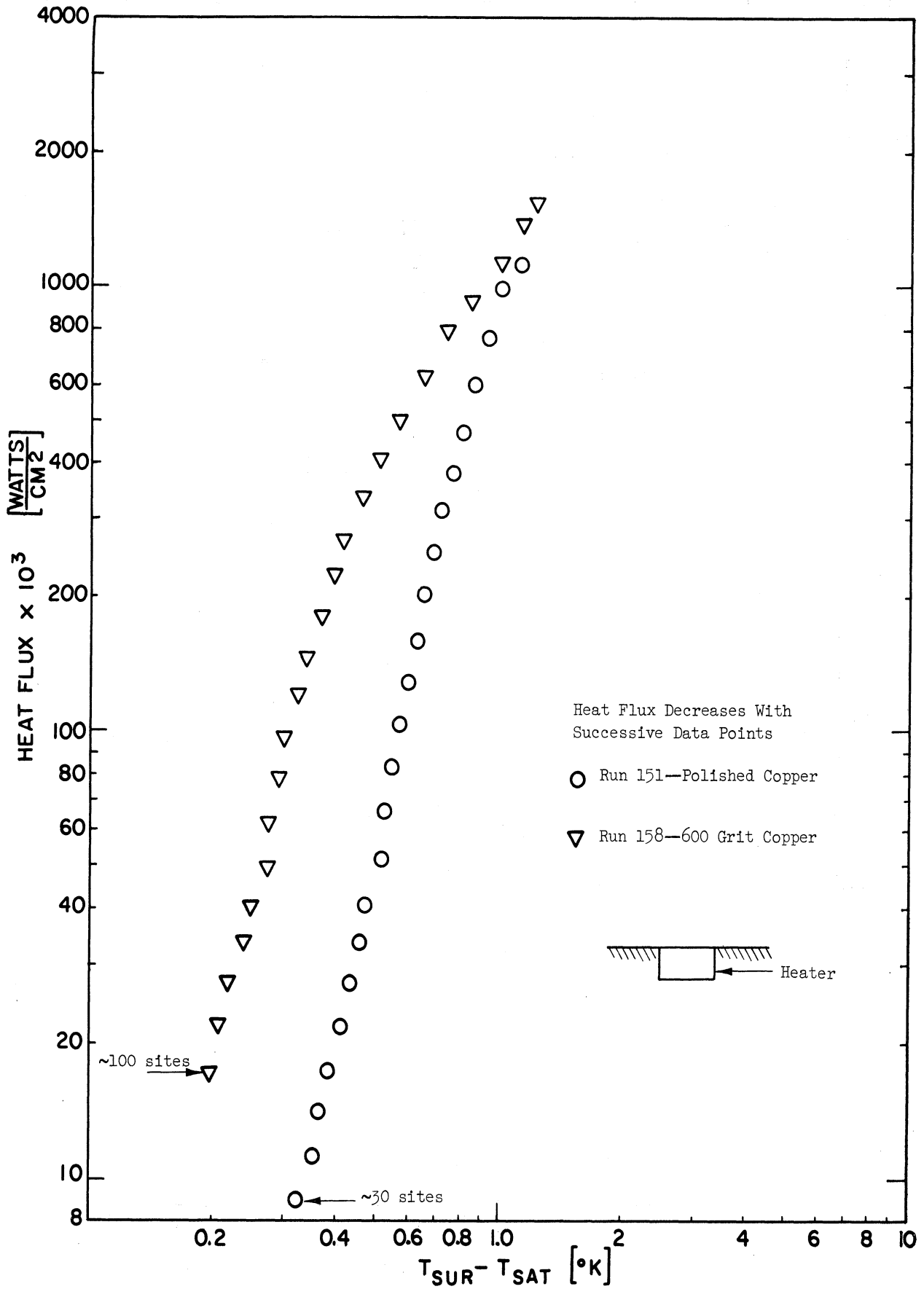
Fig. 23. Effect of roughness on heat transfer to liquid hydrogen from horizontal copper surfaces.

horizontal cylinder ranged from (1500) x 10^{-3} to (6500) x 10^{-3} watts/cm^2.

The bending of the boiling curves of the lapped surfaces at the higher heat

fluxes is attributed to interference between adjacent sites. The lapped

surfaces are saturated with surface cavities and the "area of influence" of

an active site will overlap potential sites adjacent to it. When two ac-

tive sites have overlapping "areas of influence," the effectiveness of each

individual site is reduced. The density of active sites is larger on the

lapped surfaces than on the polished surfaces, and many of the sites that

become active at the larger heat fluxes most likely are located within the

"area of influence" of sites already active. Therefore, a relatively large

increase in surface temperature is needed to produce a given increase in

the heat transfer rate.

Shown in Fig. 22 are data obtained from three stainless steel surfaces

heating vertically in liquid hydrogen. The surface finishes were the same

as those used in the horizontal orientation: polished, lapped with 600 grit

lapping compound and lapped with 280 grit lapping compound. The polished

and 280 grit surfaces used in the vertical orientation were the same ones

used in the horizontal orientation. The 600 grit surface used in the hori-

zontal orientation was damaged before it could be tested vertically, so a

new 600 grit stainless steel surface was made and used only for the vertical

tests in liquid hydrogen. Again it is noted that except for the low heat

fluxes, the 600 grit surface is a more efficient boiling surface than the

rougher 280 grit surface. The shape of the boiling curve of the 280 grit

surface resembles that of the polished surface more than the boiling curve

of the 600 grit surface does. The boiling curves of the lapped surfaces

bend slightly towards higher surface temperatures at a much lower heat flux

than where the bending took place in the horizontal boiling curves. This

might be expected from the observation made earlier that, even at very low

heat fluxes, active sites on the bottom portion of the surface have an in-

fluence on potential sites located above them. The effective "areas of in-

fluence" of the sites on the bottom portion of the surface are very large

and overlap even at low heat fluxes.

The data in Fig. 23 show the effect of roughness on the heat transfer

from horizontal copper surfaces. The 600 grit surface is again more effic-

ient than the polished surface. The bending of the heat transfer curve of

the lapped surface to higher temperatures at the higher heat fluxes is

especially noticable in Fig. 23.

5. Effect of Orientation

The data shown in Figs. 21 and 22 are replotted in Figs. 24-26 to

show the effect of orientation on the heat transfer from a stainless steel

surface to liquid hydrogen. It is again pointed out that two different 600

grit surfaces were used, one in the horizontal orientation and another one

in the vertical orientation. It is seen from Figs. 24-26 that, except for

the highest heat fluxes, all of the surfaces have a larger boiling efficiency

in the vertical orientation than in the horizontal orientation. This is ex-

pected from the observation that when a surface was mounted vertically, po-

tential sites in the path of bubbles rising from an active site became active.
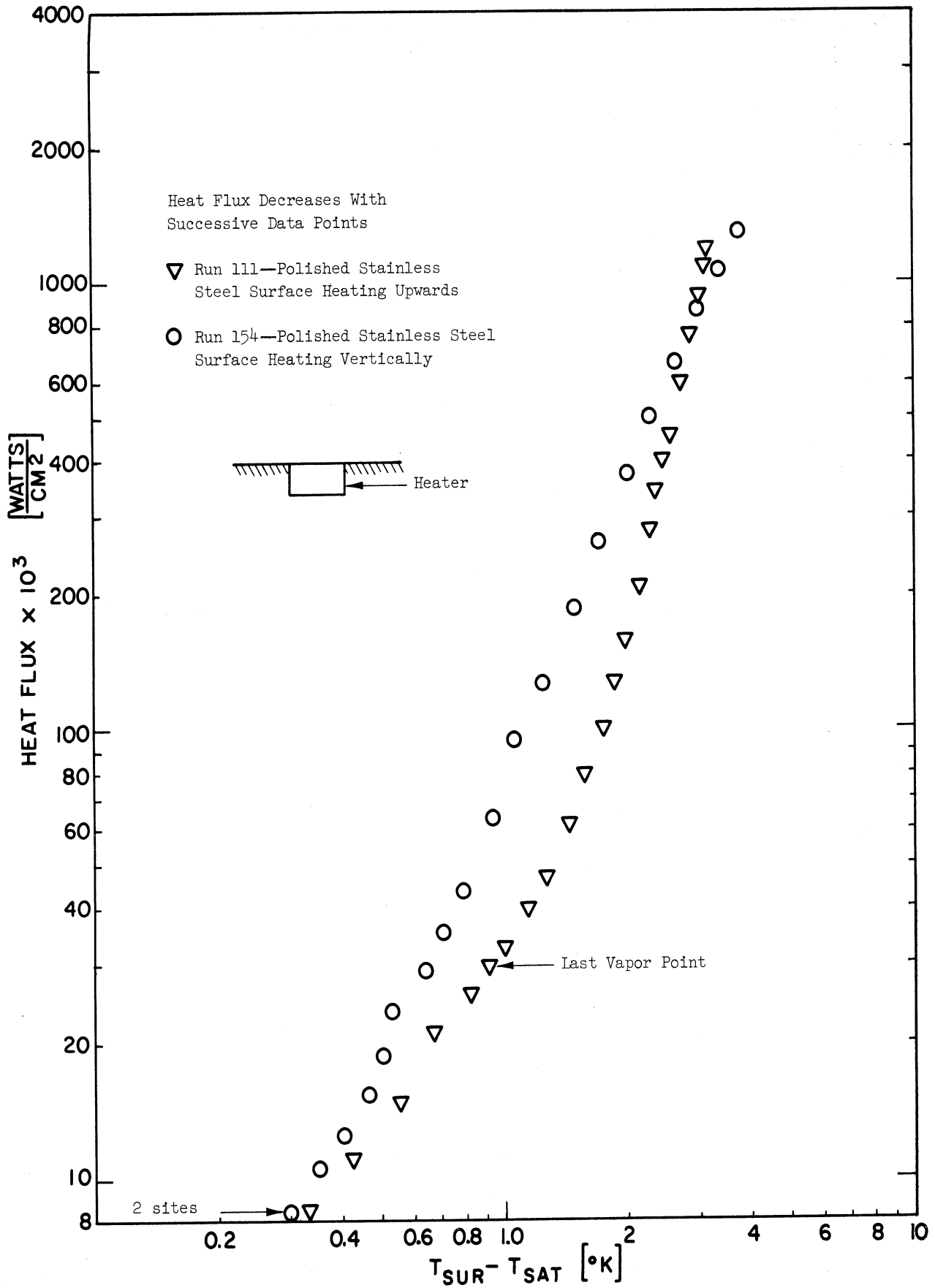
Fig. 24. Effect of orientation on heat transfer to liquid hydrogen from a polished stainless steel surface.
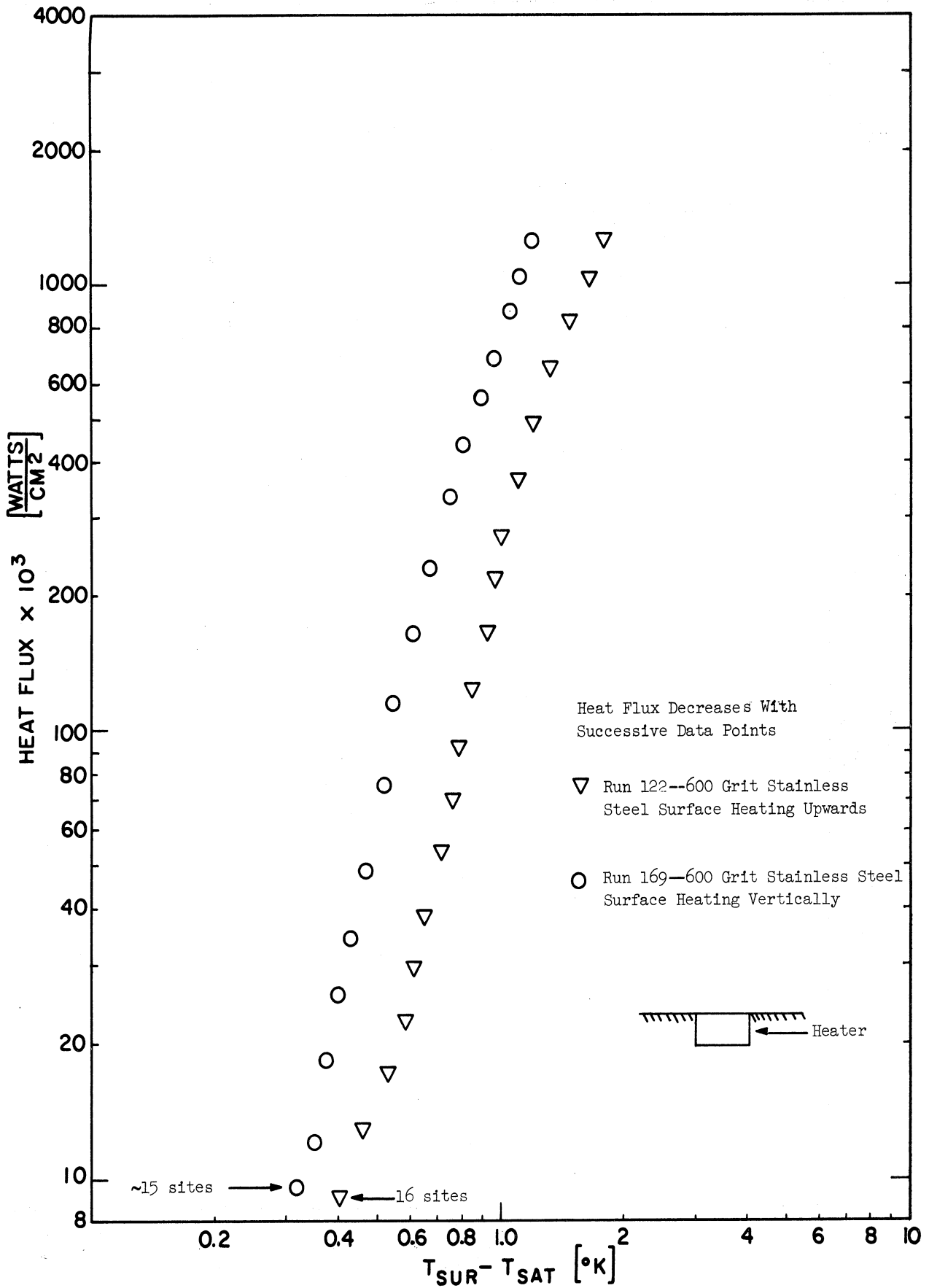
Fig. 25. Effect of orientation on heat transfer to liquid
hydrogen from 600 grit stainless steel surfaces.
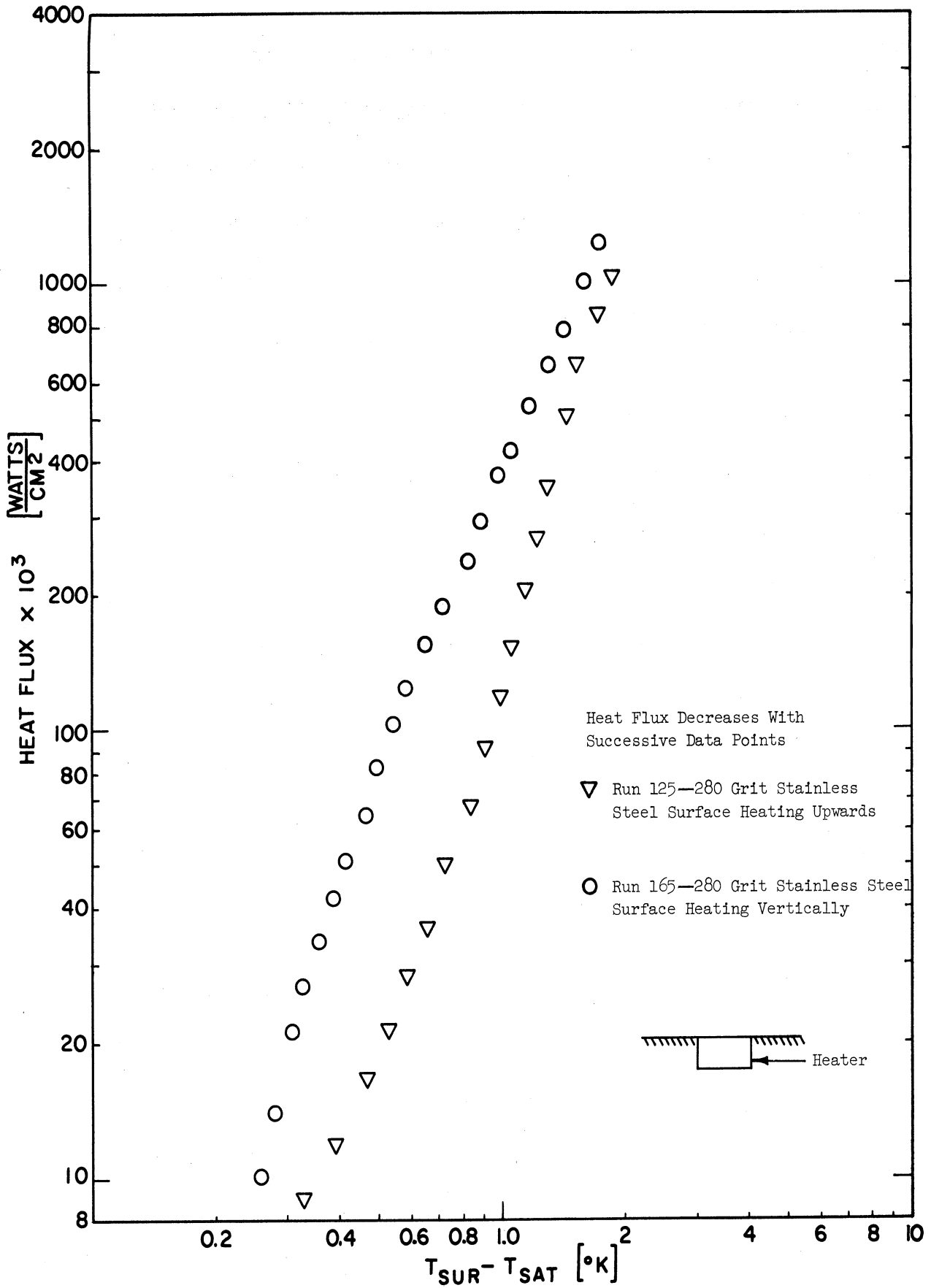
Fig. 26. Effect of orientation on heat transfer to liquid hydrogen from a 280 grit stainless steel surface.

At the largest heat fluxes used, the polished surface was more efficient at boiling when heating upwards than when heating vertically. It appears that if a slightly larger heat flux was used, the same statement could be made for the 280 grit surface but not for the 600 grit surface. The bending of the boiling curves of the lapped surfaces toward higher surface temperatures is more noticable in Figs. 25 and 26 than in Figs. 21 and 22.

6. Effect of Surface Material

The effect of surface material on the heat transfer from a horizontal surface to liquid hydrogen is shown by the data in Figs. 27 and 28. The same effect is shown in Fig. 29 for heat transfer to liquid nitrogen.

In Fig. 27, the boiling heat transfer data obtained with "smooth" surfaces are compared. The Teflon was applied by a plating or spraying process and, although it is smooth, there is no reason to expect it to have the same boiling characteristics as the metal surfaces mechanically polished. Copper is relatively soft and stainless steel is relatively tough, so a consistent manner of surface preparation will produce a different number and size distribution of pits and scratches on copper and stainless steel surfaces. However, it was anticipated that the boiling characteristics of the two different metal surfaces prepared in the same manner would be somewhat similar.

Surface roughness measurements, presented in Section V.E, show that the gross roughness of the two polished surfaces was about the same, but photomicrographs, also presented in Section V.E, show more and larger fine surface imperfections on the polished copper surface than on the polished stainless
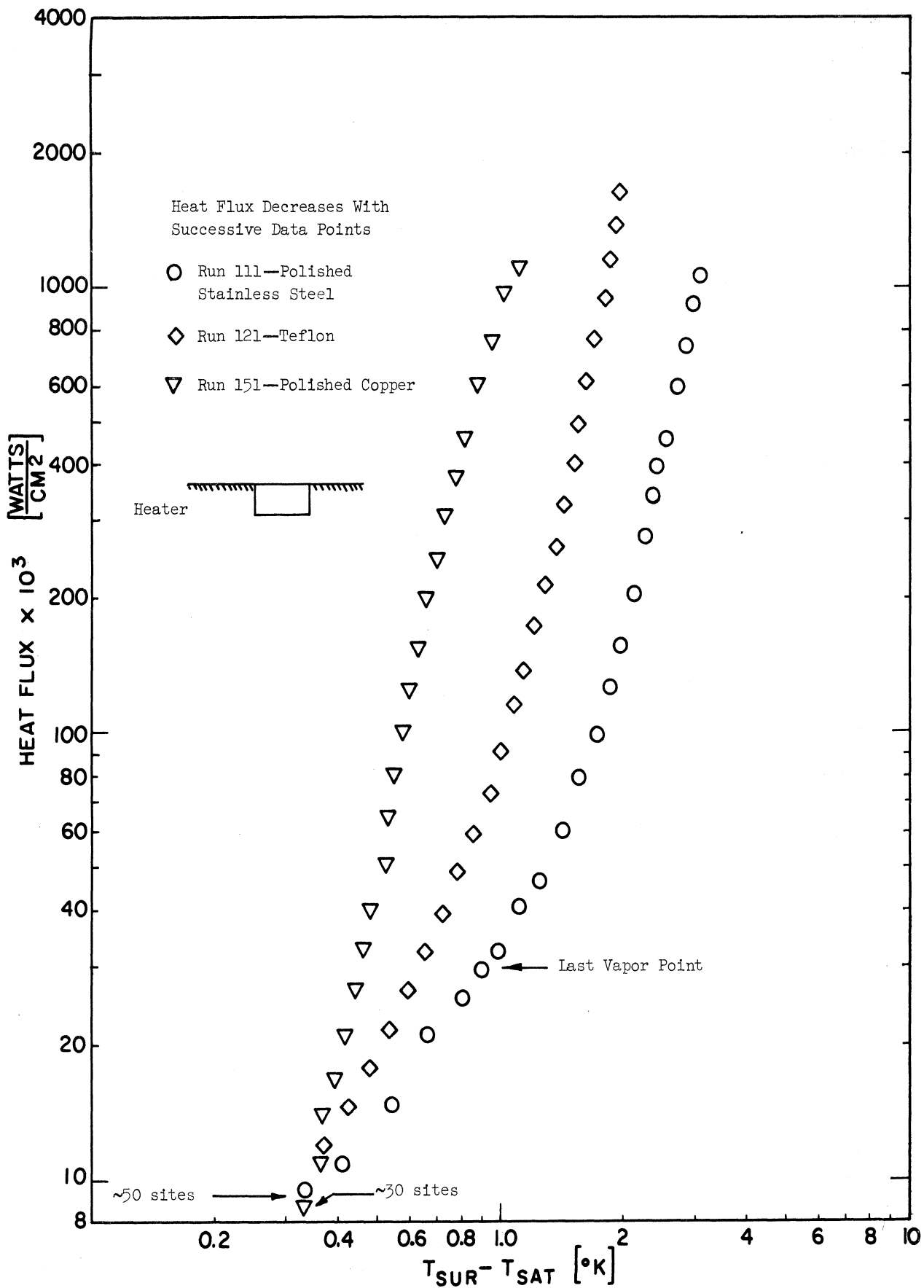
Fig. 27. Effect of surface material on heat transfer to liquid
hydrogen from smooth horizontal surfaces.
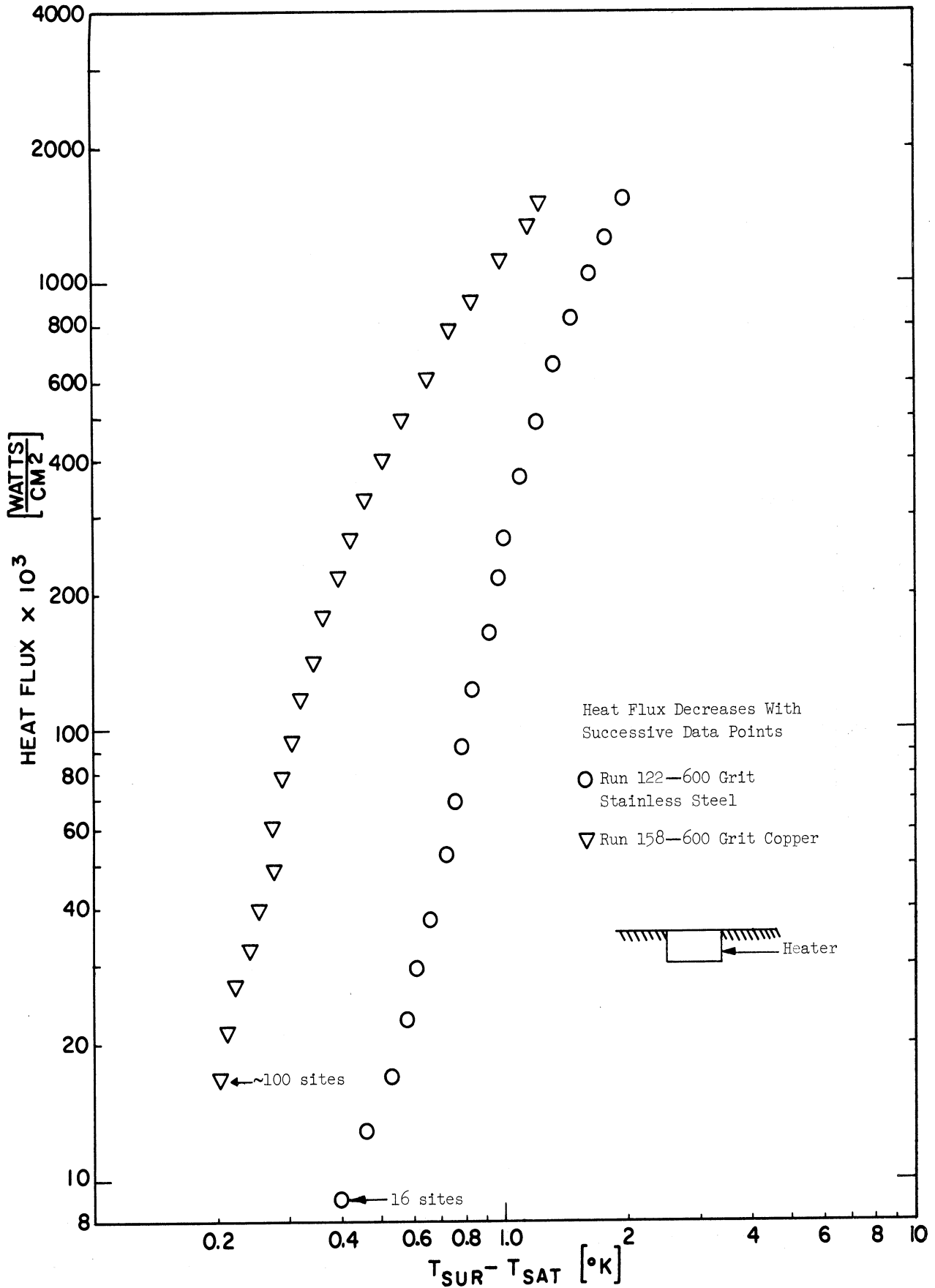
Fig. 28. Effect of surface material on heat transfer to liquid hydrogen from rough horizontal surfaces.
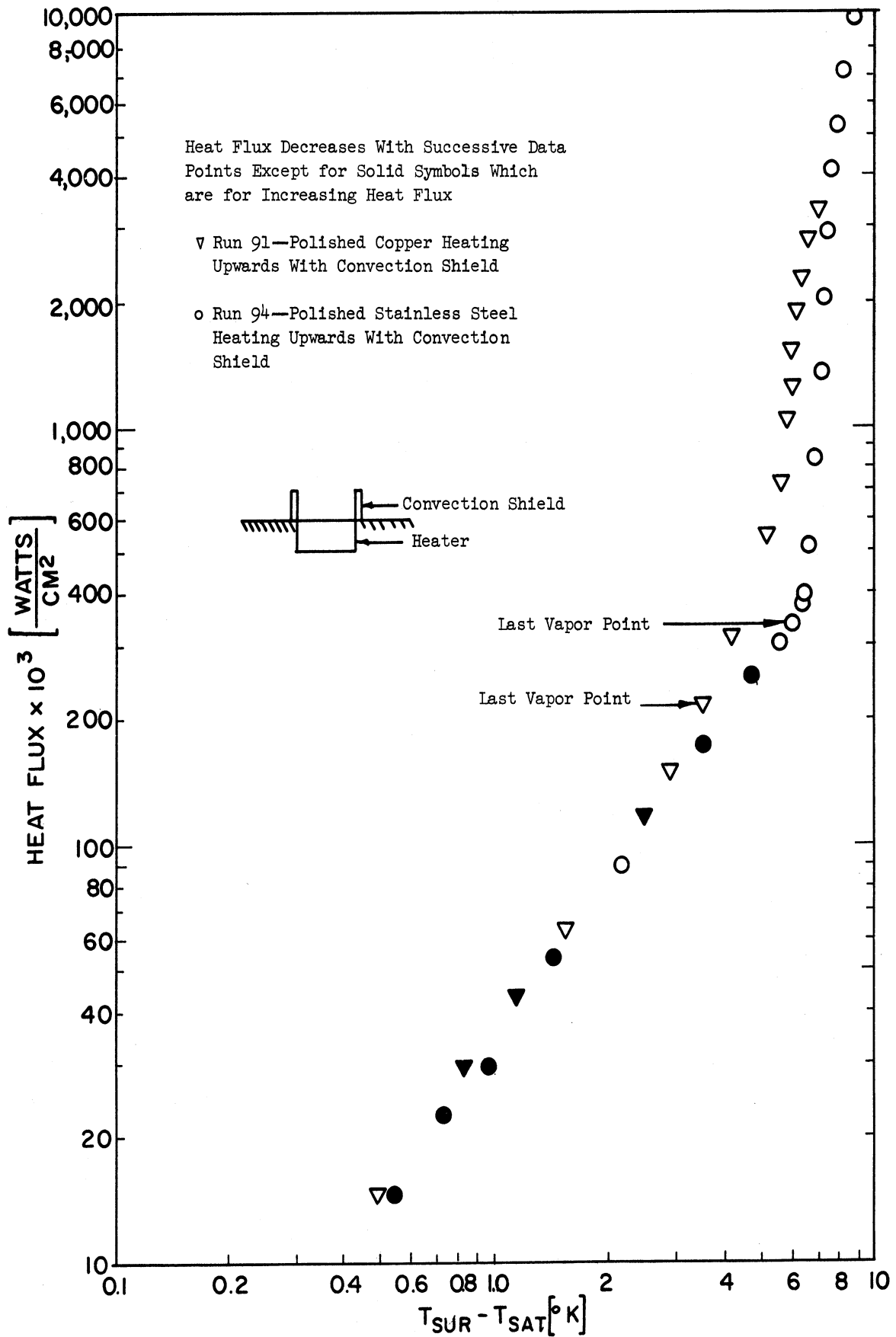
Fig. 29. Effect of surface material on heat transfer to liquid nitrogen from smooth horizontal surfaces.

steel surface. At a given surface superheat, the heat transfer rate from the polished copper surface was as much as 25 times larger then the heat transfer rate from the polished stainless steel surface. Differences in the fine surface finish of the two surfaces may account for part of this difference, but it is difficult to explain the entire difference on this basis.

In Fig. 28, data from a 600 grit copper surface and a 600 grit stainless steel surface are compared. Again the surface roughness measurements show that the gross roughness of the two surfaces was about the same. In the lapped condition, as in the polished condition, the copper makes a more efficient boiling surface than the stainless steel. At a given surface superheat, the heat transfer rates from the two surfaces differ by as much as a factor of 20.

The data shown in Fig. 29 are for a polished copper surface and a polished stainless steel surface heating upwards with the convection shield in liquid nitrogen. As the copper surface was polished just before each series of tests, the polished copper surfaces tested in liquid hydrogen and liquid nitrogen were not the same surface. In liquid nitrogen, the polished copper surface was again a more efficient boiling surface than the polished stainless steel surface. The difference in surface temperature between the two surfaces was about the same in magnitude when boiling either hydrogen or nitrogen, but was much smaller as a percentage of the surface superheat when boiling nitrogen.

7. Effect of Liquid

Shown in Fig. 30 are data from a polished stainless steel surface heat-
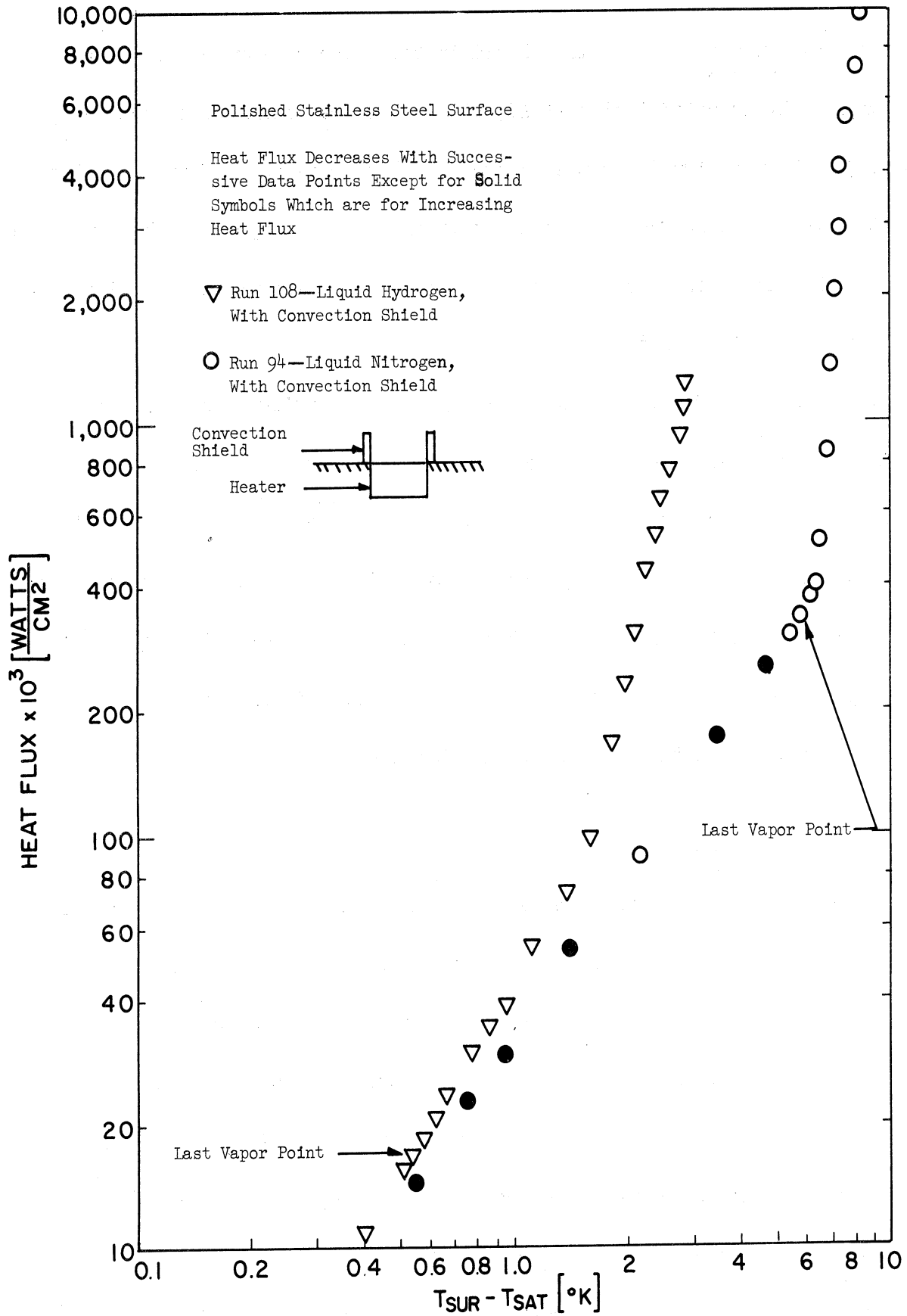
Fig. 30. Effect of liquid on heat transfer from a horizontal polished stainless steel surface.

ing upwards with the convection shield in both liquid nitrogen and liquid

hydrogen. It is noted that that ΔT_s at a given heat flux agree reasonably

well for the two liquids in the natural convection region. There is a large

difference in the surface superheat at which the last vapor was observed with

the two liquids. The slope of the boiling curve is larger with liquid nitro-

gen than with liquid hydrogen.

Data for a 600 grit stainless steel surface heating upwards in both

liquid hydrogen and liquid nitrogen are shown in Fig. 31. The boiling curve

bends towards larger surface superheats at the larger heat fluxes in both

liquids. This occurs at a larger heat flux in liquid nitrogen than in liquid

hydrogen. Again the slope of the boiling curve is larger with liquid nitro-

gen than with liquid hydrogen and there is a large difference in the sur-

face superheat when the last vapor was observed.

C. INCIPIENT BOILING

The values of heat flux and surface superheat when the initial vapor

was observed were measured for 15 combinations of liquids, orientations and

surfaces. The results of the measurements from 14 of the combinations are

shown in Fig. 32. The one not shown is the surface consisting of a glass fiber

web coated with an epoxy cement, heating upwards in liquid hydrogen. One

site on this surface could be activated without any heater power by shining

a flashlight on the surface. A second site on the surface became active at

approximately 1/4°K surface superheat. The symbols in Fig. 32 represent the

average of the initial vapor point heat fluxes and surface superheats ob-

served when conducting the tests for the particular point. The lines show

600 Grit Stainless Steel
Surface Heating Upwards

Heat Flux Decreases With Succes-
sive Data Points Except for Solid
Symbols which are for Increasing
Heat Flux

▽ Run 122—Liquid Hydrogen

◯ Run 147—Liquid Nitrogen

Heater ⟶

~25 sites ⟶ ▽●

Last Vapor Point

HEAT FLUX × 10³ [WATTS / CM2]

$T_{sur} - T_{sat}$ [°K]
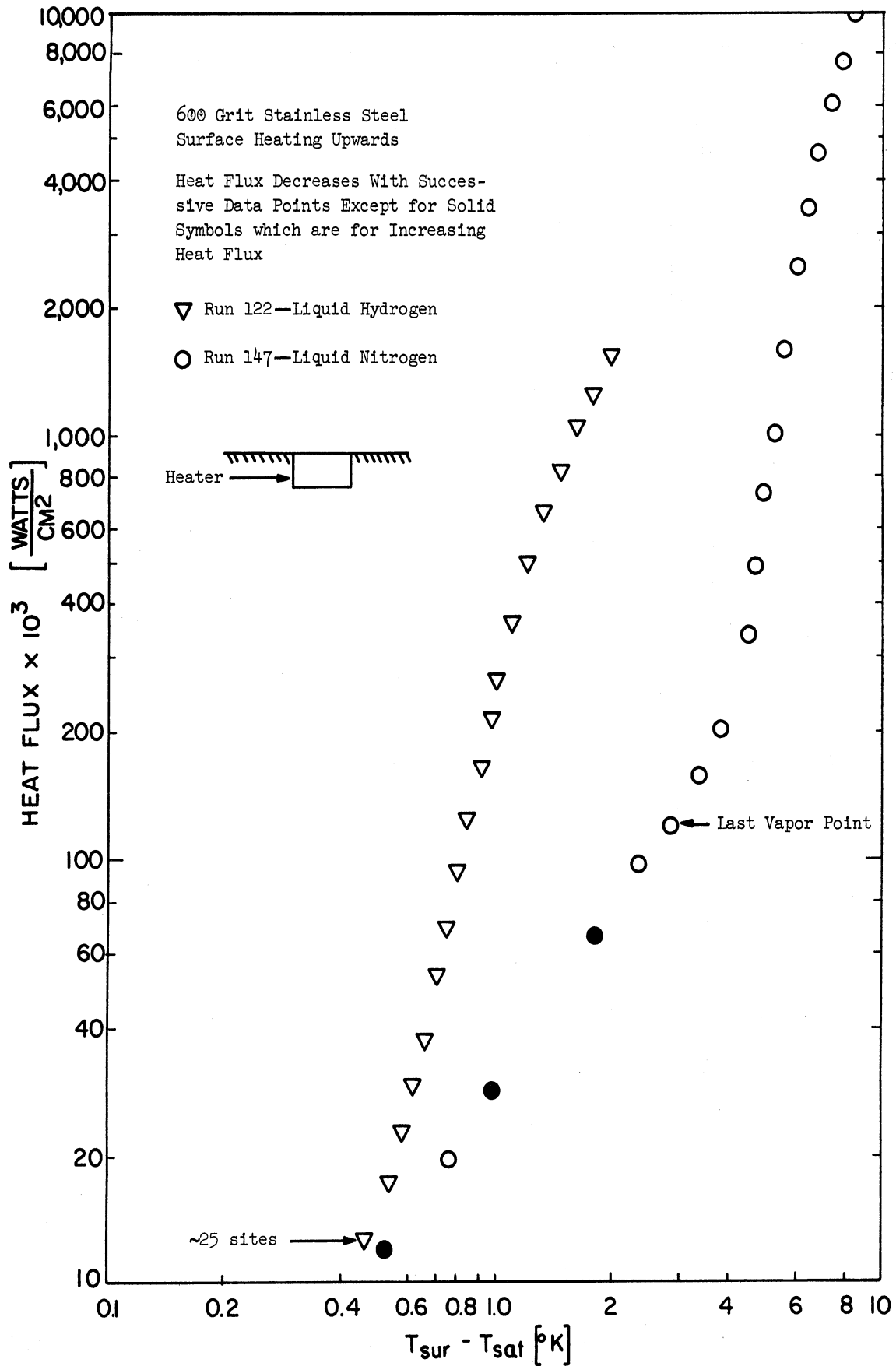
Fig. 31. Effect of liquid on heat transfer from a horizontal
600 grit stainless steel surface.

88

HEAT FLUX × 10³ [WATTS/CM2]

No.	Surface	Orientation	Observations
1	Polished S.S.	Upward	6
2	Polished S.S.	Downward	4
3	600 Grit S.S.	Upward	3
4	600 Grit S.S.	Downward	5
5	Polished Cu	Upward	1
6	600 Grit S.S.	Upward	3
7	Polished S.S.	Upward	7
8	Polshed S.S.	Vertical	4
9	280 Grit S.S.	Upward	3
10	280 Grit S.S.	Vertical	3
11	Teflon	Upward	4
12	Polished Cu	Upward	4
13*	600 Grit S.S.	Vertical	3
14	600 Grit Cu	Upward	5

*Different surface than 3, 4, and 6

Average q/A and ΔT_s

← Range of ΔT_s →

Individual Observations Fell Along the Natural Convection Correlation Shown. The range of Heat Fluxes Observed is not Shown.

$Nu = 0.14(GrPr)^{1/3}$

Liquid Hydrogen | Liquid Nitrogen

$T_{SUR} - T_{SAT}$ [°K]

Fig. 32. Initial vapor formation conditions.

the range of surface superheats observed. There was a corresponding range

of heat fluxes which are not shown. The heat flux and surface superheat of

each individual observation was generally located along the natural convec-

tion correlations shown. Each symbol in Fig. 32 represents a particular

surface and the solid symbols are points obtained with the surface heating

vertically.

As was pointed out above, the 600 grit stainless steel surface tested

in liquid hydrogen in the vertical orientation was a different surface than

used for the other 600 grit stainless steel tests. Also, the polished copper

surfaces tested in liquid hydrogen and liquid nitrogen were different sur-

faces.

There were considerable background vibrations so a series of 5 tests

were run to determine if vibrations were influencing the formation of the

initial vapor. As described in Section IV.G, the moment of vapor formation

on a polished stainless steel surface, heating transiently downwards in

liquid nitrogen, was compared with peaks in background vibrations. The aver-

age time span between the last vibration of approximately 10% or more above

the steady background level and the moment of vapor formation was 29 sec.

The smallest time span was 2 sec. This indicates that the background vibra-

tions were not a significant factor in the formation of the initial vapor.

When determining the initial vapor point, the heat flux was increased

in steps of approximately 10% of its value and steady state conditions estab-

lished at each level. For some orientations and surfaces, the last condi-

tions without vapor is reported in Fig. 32 as the initial vapor point and

for other orientation and surfaces the first conditions with vapor is reported
as the initial vapor point. The differences and the reasons will be dis-
cussed one at a time.

When testing with a surface heating downwards, a relatively large amount
of superheated liquid was present on the surface. Once the initial vapor
formed, the superheated liquid flashed into vapor and filled the convection
shield. In liquid nitrogen, the surface temperature was observed to drop
slightly as the superheated liquid flashed into vapor, and then to increase.
For points 2 and 4 in Fig. 32, it was thus necessary to report the last con-
ditions observed with no vapor present as the initial vapor point. When heat-
ing downwards in liquid nitrogen, the superheated liquid was very stable. It
was possible to maintain the liquid superheat at about 75% of the initial
vapor point superheat for several hours without forming vapor. No data were
obtained heating downwards in liquid hydrogen. As was discussed in Section
V.A, vapor was formed in the bulk liquid away from the surface and some of
this vapor became trapped in the convection shield, preventing data from being
obtained.

When conducting the tests included in points 1, 3, 7, and 11 in Fig. 32,
the initial vapor was observed to form at individual sites. Often a site
would produce a steady stream of vapor bubbles for 3 or 4 sec and then be-
come inactive for several minutes. In an effort to be as consistent as pos-
sible with the downwards data, this is reported as the initial vapor point.
On the polished surfaces the first vapor was sometimes in the form of in-
dividual bubbles that grew very slowly for 2 or 3 sec. The bubbles assumed

an almost perfect spherical shape and remained on the surface for 5-10 sec before departing. After a bubble left the surface, a new bubble would form at the same site several seconds later.

When conducting the tests for the remaining points in Fig. 32, there was a tendency for active sites to form in small clusters rather than as individual sites. The formation of these clusters of active sites was often accompanied by a drop in the surface temperature, such as shown in Fig. 16. For these points, the highest surface temperature observed without vapor formation is reported in Fig. 32 as the surface temperature when the initial vapor formed.

The initial vapor on any particular surface formed at a different site almost every test, indicating that the surface area of each surface was reasonably uniform as far as the initial vapor formation is concerned.

In one test with a polished copper surface heating upwards in liquid nitrogen, a felt tipped pen was used to mark on the surface. Numerous sites became active along the ink marks at a value of surface temperature and heat flux lower than that necessary to form vapor from the polished surface.

The data for points 2, 4, and 5 in Fig. 32 were taken with the convection shield and the data for points 1 and 7 were taken partly with it and partly without it. Comparing the initial vapor points obtained for a particular surface with and without the convection shield, no significant difference could be found. The data for the remaining points in Fig. 32 were taken without the convection shield.

The observations composing points 1 and 7 were made over a period of time while the observations composing the rest of the points were made in a series of consecutive tests. Four series of tests ran over a one week period are included in point 1. The surface was warmed to room temperature and cleaned between each series. The observations for point 7 were made in two series of tests separated in time by three months. The two observations in the second set of tests were both in the middle of the range of the surface superheats and heat fluxes observed during the first set of tests. This indicates that the nucleation characteristics, with respect to the initial vapor formation, of the polished stainless steel surface did not change with time and usage.

Comparing points 7 and 9 in Fig. 32 with points 8 and 10, respectively, it is seen that the surface superheat and heat flux, when the initial vapor was observed on a given surface, were about the same when the surface was heating either upwards or vertically in liquid hydrogen. Point 6 and 13 are not directly comparable as two different surfaces were used to obtain them. As shown in Fig. 16, the surface superheat represented by point 6 in Fig. 32 is considerably larger than the surface superheat necessary to form addition active sites on the 600 grit stainless steel surface. If only one site is made when preparing the surface that becomes active at a lower surface superheat, the entire surface will be covered with active sites before the superheat of point 6 is reached. For this reason it is felt that the data for point 13 is more characteristic of what can be expected from a 600 grit stainless steel surface than those for point 6.

A comparison of points 1 and 3 with points 2 and 4, respectively, provides a comparison of the heat flux and surface superheat at the reported initial vapor point for a given surface heating upwards and downwards in liquid nitrogen. The heat flux is an order of magnitude less in the downward position but the surface superheat is almost the same. It is again pointed out that when conducting the tests heating upwards, the first point at which vapor was observed is reported as the initial vapor point and that sites were sometimes observed to be active for a few seconds and then to be inactive for minutes. When conducting the tests heating downwards, the last point without vapor is reported as the initial vapor point. Once a vapor bubble formed when heating downwards, the superheated liquid near the surface flashed into vapor and filled the convection shield. The vapor was held on the surface and could be observed at any later time. The actual surface superheats when the first vapor formed while a surface was heating downwards and upwards were closer than those reported in Fig. 32.

The initial vapor formation on a given surface heating in liquid nitrogen or liquid hydrogen is primarily a function of surface superheat and is not a strong function of orientation or heat flux. For a given surface heating in a given orientation, the surface superheat and heat flux when the initial vapor forms are reproducible to within ±25% of their average values.

If point 13 in Fig. 32 is taken as being characteristic of the 600 grit stainless steel surface, except for the Teflon surface, the order of the surfaces determined by the order of increasing surface superheats at the initial vapor point is the same as the order of the surfaces determined by the order

of increasing surface superheats at a given boiling heat flux in the upwards

orientation. To make the correspondence complete, point 11 in Fig. 32 should

coincide with point 10. There appears to be a direct relationship between

the ease of forming the initial vapor from a surface and the boiling efficiency

of the surface.

D. THEORETICAL ANALYSIS

A theoretical analysis for the growth of a vapor nucleus in a saturated

pool of liquid will be developed following the analysis of Bergles and Rohse-

now.[11] As shown in Fig. 33, a vapor nucleus is assumed to completely fill

a surface cavity and to extend into the liquid as a hemisphere with a radius

equal to that of the surface cavity. The pressure differential between the

vapor and the liquid is given by Gibbs equation for the static equilibrium of

a vapor bubble

$$P_v - P_l = \frac{2\sigma}{r_c} \quad . \tag{1a}$$

The Claperon relation in finite difference form,

$$\frac{\Delta P}{\Delta T} = \frac{h_{fg}}{T_{sat} v_{fg}} \approx \frac{h_{fg} \rho_g}{T_{sat}} , \tag{2a}$$

relates the slope of the vapor pressure curve to the physical properties.

Equations (1a) and (2a) are combined to give

$$\Delta T = \frac{2\sigma T_{sat}}{r_c h_{fg} \rho_g} = T_{vap} - T_{sat} \tag{10}$$
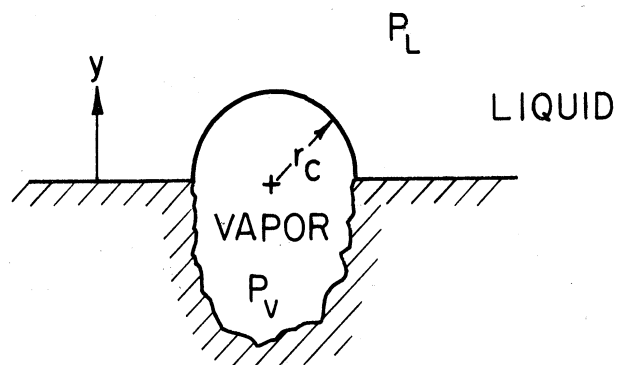
Fig. 33. Model for analysis of the growth of a vapor nucleus.

where T_{vap} is the saturation temperature of the vapor at P_v and T_{sat} is the saturation temperature of the vapor at P_1.

It is assumed that the temperature in the liquid, near the surface, is represented by

$$T = T_{sur} - \frac{q''}{k_f} y \tag{11}$$

and that the vapor nucleus grows whenever the liquid temperature at $y = r_c$ is equal to or greater than the saturation temperature of the vapor inside the nucleus, obtained from Eq. (10). Combing Eqs. (10) and (11), the range of active cavity sizes at a given surface superheat is

$$r_{max,min} = \frac{(T_{sur}-T_{sat}) \pm (T_{sur}-T_{sat}) \left[1-4\left(\frac{q''}{k_f}\right) \left(\frac{2\sigma T_{sat}}{h_{fg}\rho_g}\right) \left(\frac{1}{T_{sur}-T_{sat}}\right)^2 \right]^{1/2}}{2 \frac{q''}{k_f}} \tag{12}$$

Using property values of liquid hydrogen at 21°K from[44,47,48] and of liquid nitrogen at 80K from,[44,49,50] the value of $2\sigma T_{sat}/h_{fg}\rho_g$ is 1.30×10^{-5} °K cm and 1.59×10^{-4} °K cm for hydrogen and nitrogen, respectively. The maximum value of q''/k_f when the initial vapor formed on a surface is approximately 70°K cm and 260°K cm for hydrogen and nitrogen, respectively. At the initial vapor point $4(q''/k_f)(2\sigma T_{sat}/h_{fg}\rho_g)(1/T_{sur}-T_{sat})^2$ will always be much less than unity. The square root in Eq. (12) can then be accurately represented by the first two terms of its series representation, giving

$$r_{max} = \frac{T_{sur}-T_{sat}}{q''/k_f} \tag{13}$$

and

$$r_{min} = \left(\frac{2\sigma T_{sat}}{h_{fg}\rho_g}\right)\left(\frac{1}{T_{sur}-T_{sat}}\right). \tag{14}$$

The radius of the largest cavity theoretically active at a given $(T_{sur}-T_{sat})$ is the thickness of the thermal boundary layer, defined by conduction in the liquid. For a given orientation, this is approximately constant and independent of the heat flux level. Changes in r_{max} cannot account for additional sites becoming active as the surface superheat is increased.

The radius of the smallest cavity theoretically active at a given $(T_{sur}-T_{sat})$ is independent of the heat flux, i.e., the temperature distribution in the liquid. Because of the physical properties of liquid hydrogen and liquid nitrogen, the vapor nucleus that is theoretically just on the verge of growing, at the initial vapor point conditions observed, is so small that there is no appreciable temperature drop in the liquid between the surface and the outer edge of the nucleus. Thus the vapor growth theories discussed in Section I.B all give the same result for the size of the marginally active cavity for the same assumed equilibrium shape. If the vapor nucleus is assumed to extend into the liquid in some form other than a hemisphere, the radius of the liquid-vapor interface can be geometrically related to the cavity radius. The nucleus will theoretically grow when the vapor-liquid interface has a radius of curvature within the range limited by Eqs. (13) and (14).

The cavity size that will theoretically become active at the average initial vapor point conditions and at the knee of the heat transfer curve,

observed when heating upwards, was calculated for the various surfaces. The knee of the heat transfer curve is defined as the intersection of the extensions of the fully developed boiling curve and the natural convection curve. The results of these calculations are presented in Table I.

From Table I it is noted that the size of the surface cavities that are theoretically marginally active is extremely small. There is fair agreement between the size calculated for a given surface from the knee data and the initial vapor point data in the same liquid. There is little agreement between the sizes calculated for a given surface from the nitrogen data and the hydrogen data. In every case, the sizes calculated from the hydrogen data are smaller than the sizes calculated from the nitrogen data.

Experimentally, the surface superheat at the initial vapor point was almost independent of orientation. The vapor growth analysis predicts that the growth of a vapor nucleus at the initial vapor conditions will be a function of only the surface superheat. For liquids with considerably different physical properties, the analysis depends upon the orientation. Extreme care should be used in extending the results of the initial vapor tests to liquids that have considerably different physical properties than those here.

E. ARTIFICIAL SITES

Surface cavities were placed in polished copper and stainless steel surfaces with two different 90° conical diamond indentors. The one indentor had a nose radius of 0.0007 in. and the other one a nose radius of 0.0001 in. The potential sites formed with these indentors were not the first active

TABLE I

THEORETICAL MARGINALLY ACTIVE CAVITIES

Surface	Liquid	Orientation	$(q/A \times 10^3)_{IVP}$ (watts/cm²)	$(\overline{\Delta T_s})_{IVP}$ (°K)	$(d_{act} \times 10^6)_{IVP}$ (in.)	$(q/A \times 10^3)_{knee}$ (watts/cm²)	$(\Delta T_s)_{knee}$ (°K)	$(d_{act} \times 10^6)_{knee}$ (in.)
Polished Stainless Steel	Nitrogen	Upwards	347	6.04	20.7	400	6.60	19.0
	Nitrogen	Downwards	35.6	4.22	29.6			
	Hydrogen	Upwards	55.7	1.35	7.8	62.0	1.62	6.3
	Hydrogen	Downwards	48.7	1.39	7.4			
600 Grit Stainless Steel	Nitrogen	Upwards	269	4.59	27.3	200	4.10	30.5
	Nitrogen	Downwards	28.5	3.80	33.0			
	Hydrogen	Upwards	82.9	2.01	5.1	1.43	.53	19.3
	Hydrogen	Vertical	24.6	.74	13.8			
280 Grit Stainless Steel	Hydrogen	Upwards	29.2	.92	11.1	17.0	.66	13.6
	Hydrogen	Vertical	23.2	.86	11.9			
Polished Copper	Nitrogen	Upwards	295	5.02	24.9	305	4.90	25.6
	Hydrogen	Upwards	13.2	.56	18.3			
600 Grit Copper	Hydrogen	Upwards	17.4	.52	20.5			
Teflon	Hydrogen	Upwards	17.4	.63	16.2	30.0	.92	9.7

sites on the surface. If they became active at all, there were so many

other active sites on the surface that it was impossible to observe when

vapor was first produced at them. Two of the sites appeared to be active

while decreasing the heat flux, but it is possible that the cavities were

placed on top of naturally active sites already on the surface. The vapor

formed at the natural site would then appear to be formed at the cavity.

The sizes of the artificial sites tested, the liquid in which they were

tested and the results are tabulated in Table II.

TABLE II

ARTIFICIAL SITES

Surface Material	Liquid	Indentor Nose Radius (in.)	Cavity Diameter (in.)	Results
Stainless Steel	Hydrogen	.0007	.0013	Inactive
Stainless Steel	Hydrogen	.0007	.0041	Active when decreasing heat flux to 0.25°K
Stainless Steel	Hydrogen	.0001	.0046	Active when decreasing heat flux to < 0.15°K
Stainless Steel	Nitrogen	.0001	.0046	Inactive
Copper	Nitrogen	.0001	.0042	Inactive
Copper	Nitrogen	.0001	.0058	Inactive
Copper	Nitrogen	.0001	.0064	Inactive
Copper	Nitrogen	.0001	.0069	Inactive
Copper	Nitrogen	.0001	.0110	Inactive
Copper	Nitrogen	.0001	.0185	Inactive

F. SURFACE MEASUREMENTS

Photomicrographs were made of the various surfaces to obtain information

about the microscopic surface finishes. The photomicrographs are shown in

Figs. 34-39.
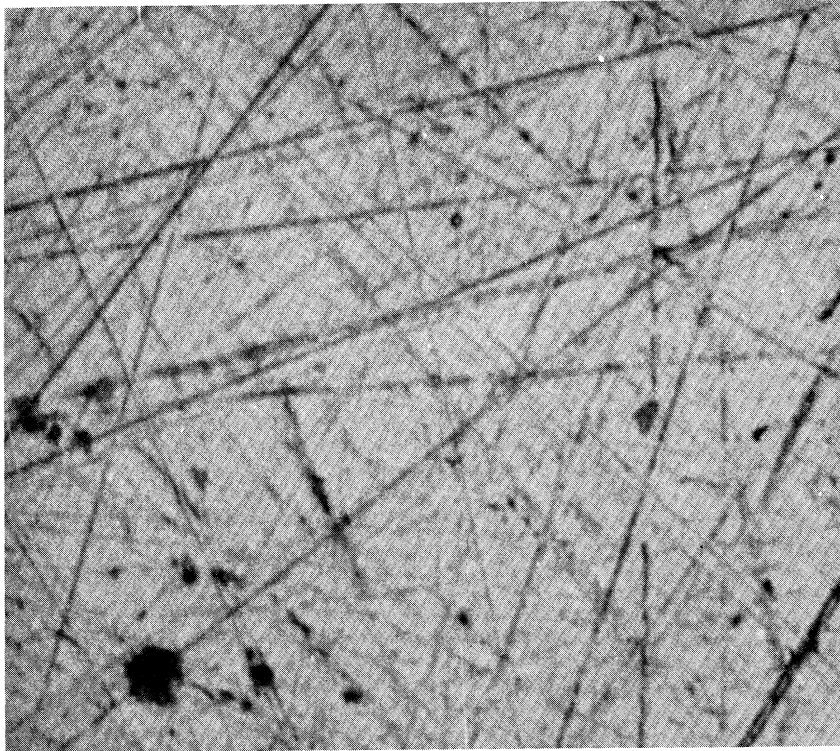
500 μin.

Fig. 34. Photomicrograph of polished copper surface.
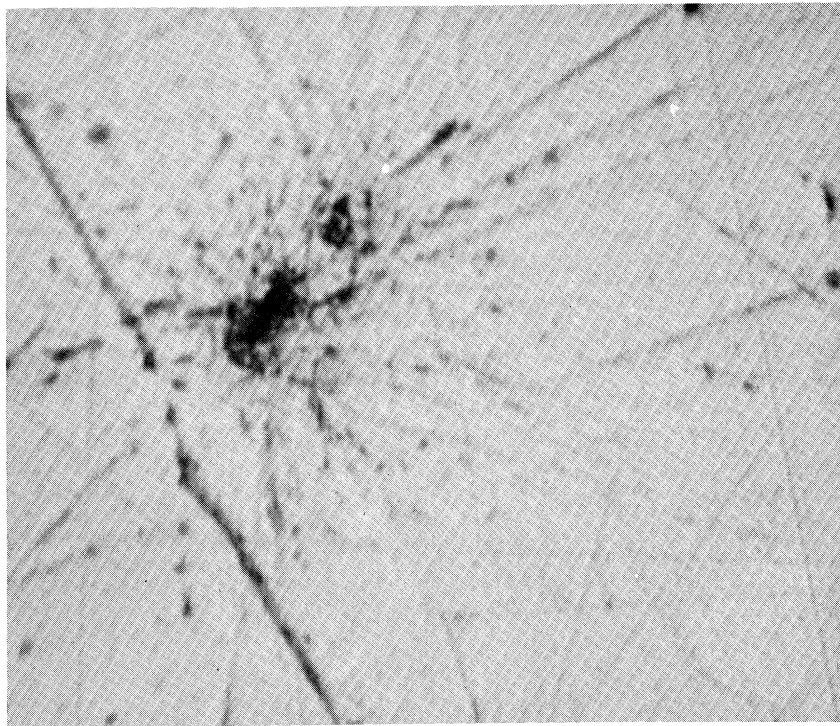
500 μin.

Fig. 35. Photomicrograph of polished stainless steel surface.
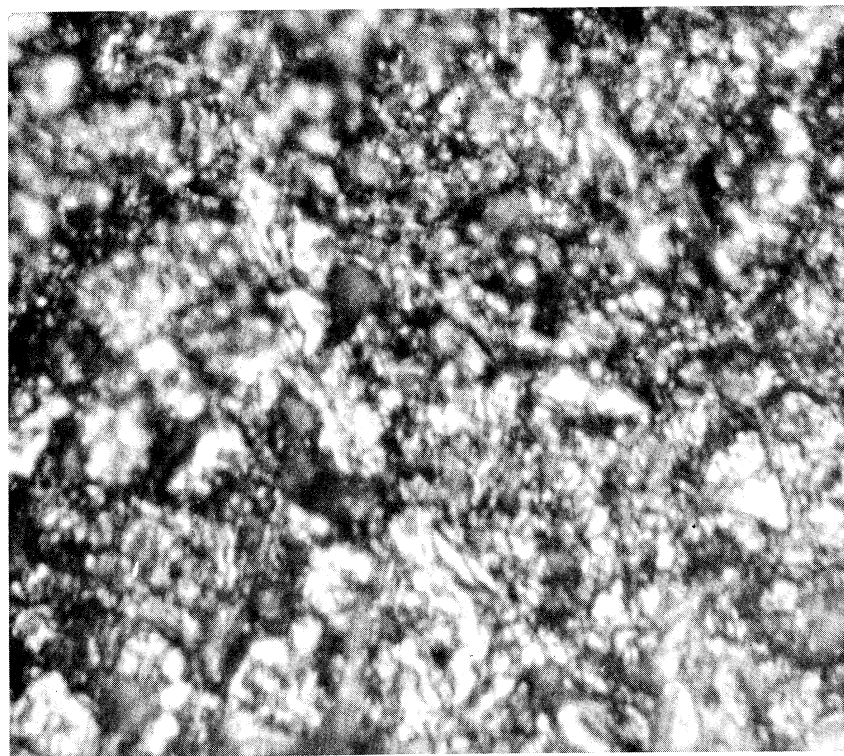
500 μin.

Fig. 36. Photomicrograph of 600 grit copper surface.
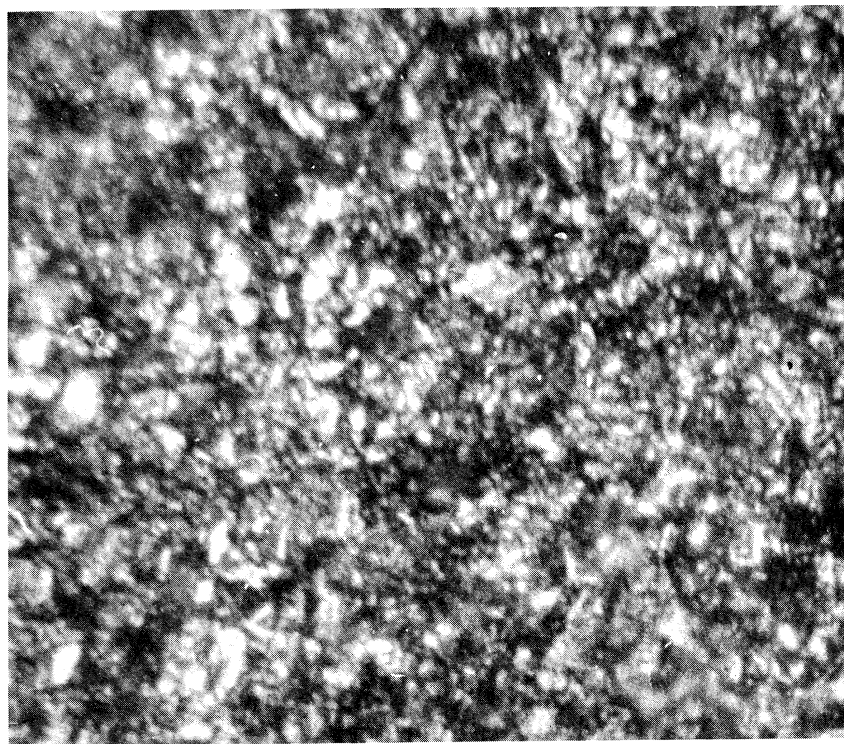
500 μin.

Fig. 37. Photomicrograph of 600 grit stainless steel surface.
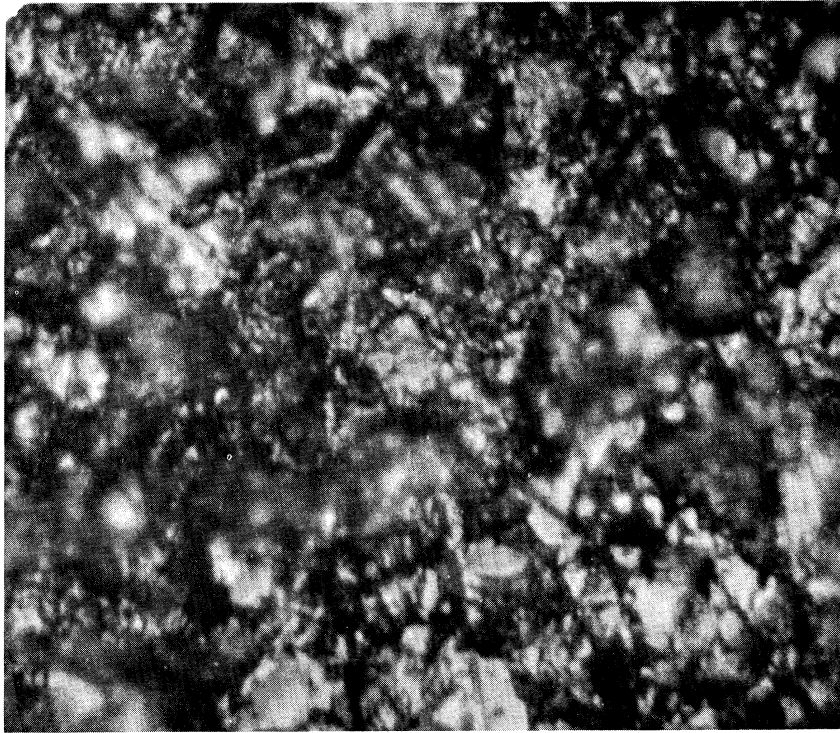
500 μin.

Fig. 38. Photomicrograph of 280 grit stainless steel surface.

Bare Metal
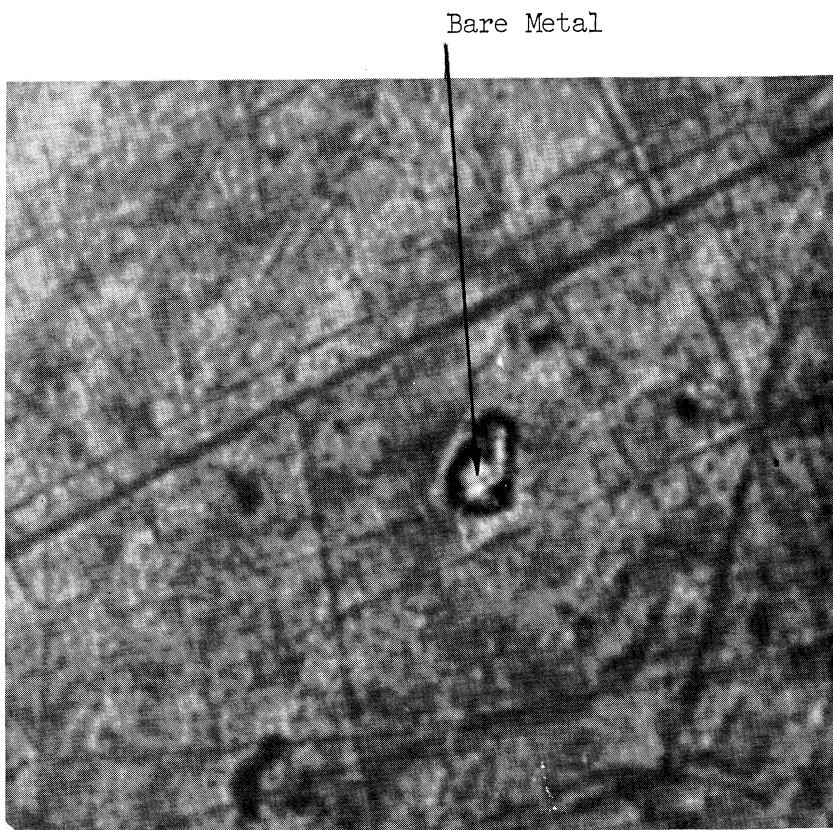
1000 μin.

Fig. 39. Photomicrograph of Teflon surface.

It was noted in Section V.B that the photomicrograph of the polished copper surface, Fig. 34, shows more scratches than the photomicrograph of the polished stainless steel surface, Fig. 35. The largest scratches on the copper surface are about 45 μin. wide and the smallest ones visible are 3-4 μin. wide. Several pits that are from 40 to 200 μin. in diameter are also visible on the copper surface. The stainless steel surface has scratches in the same size range as observed on the copper surface, but fewer in number and a larger percentage are of the smaller sizes. There are numerous pits on the polished stainless steel surface, ranging in diameter up to 400 μin. Surface imperfections of the size calculated to be active in Section V.D are present on the polished surfaces. There are also larger cavities, that should theoretically be active at a smaller surface superheat.

When viewing the lapped surfaces with a stereomicroscope, it was determined that they were saturated with overlapping surface cavities of approximately uniform size. From the photomicrographs of the lapped surfaces, Figs. 36-38, it is difficult to make any quantitative statements about the size or distribution of the surface cavities because the overlapping cavities are not readily distinguishable in the two-dimensional photomicrographs. Qualitatively it can be said that the 600 grit copper surface, Fig. 36, and the 600 grit stainless steel surface, Fig. 37, have about the same surface roughness. The 280 grit stainless steel surface, Fig. 38, has larger but fewer surface cavities than the 600 grit surfaces. Some portions of the photomicrographs are out of focus because the surface roughness exceeded the depth of focus of the optical system.

The photomicrograph of the Teflon surface, Fig. 39, was made at a low magnification because the lack of contrast on the surface did not permit any detail to be observed at a higher magnification. A spot where the Teflon does not cover the base metal is noted. Examination of the surface under the microscope revealed 3 or 4 such spots.

Table III contains the results of the surface roughness measurements. Listed for each surface are the average of 4 RMS measurements made with a Profilometer and the average of 15 consecutive peak-to-peak distances measured from a trace of the surface profile made with a Proficorder. Both the Profilometer and the Proficorder were manufactured by Micrometrical Division of Bendix Corporation. The surface traces showed small ripples within the surface cavities, but the tracing instrument was limited by the diamond tracer described in Section IV.I and the readout. The 600 grit surfaces were only slightly rougher than the polished surfaces. The 280 grit surface was considerably rougher than the other surfaces tested. The copper and stainless steel surfaces prepared in identical manners had about the same gross surface roughness.

TABLE III

SURFACE ROUGHNESS

Surface	RMS (μin.)	Average Peak-to-Peak Distance x 10^4 (in.)
Polished Stainless Steel	5	1.4
600 Grit Stainless Steel	8	2.4
280 Grit Stainless Steel	31	3.2
Polished Copper	4	1.4
600 Grit Copper	9	2.3

VI. CONCLUSIONS

A. NATURAL CONVECTION

From the data shown in Figs. 12 and 13, it is concluded that for a surface heating upwards in either liquid hydrogen or liquid nitrogen without the convection shield, turbulent natural convection heat transfer is correlated well by Eq. (7-8) in McAdams,[43]

$$Nu = 0.14 \, (GrPr)^{1/3} . \tag{8a}$$

The use of the convection shield with a small surface increases the natural convection heat transfer slightly when the fluid motion is turbulent and most likely considerably, as demonstrated by Run 91 in Fig. 12, when the fluid motion is laminar. The data from Run 91 is correlated by

$$Nu = 0.79 \, (GrPr)^{1/4} . \tag{5a}$$

B. NUCLEATE BOILING

The visual observations of the boiling while increasing the heat flux showed that on most of the surfaces there were patches of active sites while other areas of the surface were void of active sites. It is felt that a mechanism described by Corty and Foust[7] for the development of the patches is reasonably accurate. According to this mechanism, the larger surface sites lose their vapor nucleus, either because it is displaced as a unit by the liquid or because the vapor diffuses into the liquid. To form the initial vapor, the surface temperature has to be increased until a smaller site,

which still contains a vapor nucleus, becomes active. The vapor generated

at the active site spills over into the larger adjacent sites and seeds

them with a vapor nucleus. The seeded sites then become active and seed

additional sites, forming a patch of active sites. The local heat flux in

the patch area increases considerably as the patch forms, so in order to

maintain a constant average heat flux the surface temperature must drop.

The patch will stop growing when there are no potential sites within the

seeding range of the active sites that will become active at the surface

temperature. When the average heat flux is increased, the surface tempera-

ture rises momentarily and then the patch begins to grow again.

For the proposed mechanism to work, it is necessary for potential sites

to be located close together. The lapped surfaces are saturated with sur-

face cavities and satisfy this requirement while the photomicrographs of the

polished surfaces show numerous scratches that could be used to spread a

patch. Three surfaces did not develop patch boiling, the Teflon surface,

the epoxy coated glass fiber surface and the 280 grit stainless steel surface.

The Teflon and epoxy were applied by spraying or plating and most likely

have the sites well separated. The 280 grit stainless steel surface will be

discussed in detail below.

Good and Ferry[41] report that liquid hydrogen had a zero contact angle

on all the materials that they investigated, including stainless steel and

Teflon. The theory of Bankoff,[14] predicts that liquid will replace vapor

in all the surface cavities when the liquid completely wets the surface. It

is postulated that, due to the extreme wettability of liquid hydrogen, the

liquid replaces any vapor that may be introduced into the larger surface cavities. This is especially important with the 280 grit stainless steel surface as this surface contains many cavities that are larger than most of the cavities on the other surfaces investigated. This does not exclude the possibility that secondary sites located within the surface cavities will be active.

If the liquid does wet many of the cavities on the 280 grit stainless steel surface, it might be expected not to develop patchwise boiling. After one of the smaller surface cavities or a secondary site located within a surface cavity becomes active, vapor will be introduced into adjacent surface cavities. A small cluster of active sites might form, but a lack of surface cavities adjacent to it that will retain a vapor nucleus prevents the formation of a patch. There may be secondary sites inside the inactive surface cavities that will become active at a higher surface temperature.

It was observed that on a vertical surface heating in liquid hydrogen, sites in the path of the bubbles rising from a steady site become active for a few seconds after the bubbles passed by them. It is felt that there was a tendency for these intermittent sites to be wetted by the liquid hydrogen and to lose their vapor nucleus. The seeding of these sites by the rising vapor permitted them to be active until the vapor nucleus was lost again.

If the measured surface cavity sizes in Table III are compared with the results in Table I of the site sizes calculated to be marginally active, it can be seen that secondary sites located within the surface cavities may

make a major contribution to the number of active sites on all of the surfaces.

It was noted in Section V.B that the boiling characteristics of the 280 grit stainless steel surface were consistently more like the characteristics of the polished stainless steel surface, than were those of the 600 grit stainless steel surfaces. This is likely if liquid filled many of the surface cavities on the 280 grit surface. The roughness as far as boiling is concerned would then be the roughness of the inside of the cavities. For boiling, the 280 grit surface may be smoother than the 600 grit surface. Mulford and Nigon[26] boiled liquid hydrogen from a copper cylinder and found no change in the boiling characteristics of the cylinder when it was roughened by sand blasting. It is possible that the sand blasting produced surface cavities that were wetted by the liquid hydrogen, and that the cavities serving as active sites were left unchanged.

The difficulty of making active artificial sites was noted in Section V.E. These surface cavities were relatively large because they were made by a mechanical means. If the liquid wetted them, they would not serve as active nucleation sites. This is most likely why the artificial sites were not active.

The copper surfaces were much more efficient as boiling surfaces than the stainless steel surfaces prepared in an identical manner. The reason for this not known, but it is speculated that the liquids wet the copper slightly less than the stainless steel. This means that some surface cavities on the stainless steel surfaces that are wetted by the liquid, would not be wetted

if they were on a copper surface. They would serve as active sites on the copper surface but are not active sites on the stainless steel surface because they are wetted with the liquid.

A given surface is more efficient at transferring heat when heating vertically than when heating upwards. Vapor bubbles rising from an active site tend to seed potential sites with vapor and to make them active. Some of these seeded sites remain active indefinitely and some are active only a few seconds, but in either case the result of additional sites is to increase the heat transferred at a given surface temperature.

C. INCIPIENT BOILING

The formation of the initial vapor on a surface heating in liquid hydrogen or liquid nitrogen is primarily a function of the surface superheat and is not a strong function of the heat flux or orientation. As the bouyancy forces change direction relative to the surface when the orientation of the surface is changed from upwards to downwards, the bouyancy forces do not appear to be a significant factor in the formation of the initial vapor in hydrogen or nitrogen. The surface superheat and heat flux when the initial vapor was observed on a given surface in a given orientation were reproducible within ±25% of their average values.

There is a direct relationship between the ease of forming the initial vapor on a uniform surface and the boiling efficiency of the surface when heating upwards. In general, the lower the surface superheat at the initial vapor point, the lower the surface superheat needed to transfer a given boiling heat flux.

The theoretical analysis of the growth of a vapor nucleus indicates that the nuclei that grow in liquid hydrogen and liquid nitrogen at the observed initial vapor conditions are very small. Because of the physical properties of these two liquids, the growth of vapor nuclei at the initial vapor conditions is theoretically independent of the heat flux and temperature distribution in the liquid, depending only upon the surface superheat. Extreme care should be used in extending to other liquids which have considerably different physical properties the conclusion that the initial vapor formation in liquid hydrogen and liquid nitrogen is not a strong function of orientation or heat flux.

D. RECOMMENDATIONS FOR FUTURE WORK

Perhaps the most promising area for future work is an investigation to try and determine the optimum surface preparation for obtaining an efficient boiling surface, especially for liquid hydrogen. There is not reason to believe that the 600 grit surfaces represent optimum boiling surfaces for liquid hydrogen. Surfaces lapped with a coarser lapping compound than the 280 grit compound used here should also be investigated in liquid hydrogen to see if their boiling characteristics are more like those of the polished surface than those of the 280 grit surface are.

The investigation of the effect of surface material upon boiling and the initial vapor formation should be continued. Copper surfaces are much more efficient at boiling liquid hydrogen and form the initial vapor at a lower surface superheat than stainless steel surfaces prepared in the same manner.

The data for the Teflon surface were between the data for the two polished

metal surfaces. The data from these three surfaces do not follow any con-

sistent pattern that can be related to the thermal-physical properties of

the materials, but this might be because of the physical surface finish of

the Teflon surface. More data is needed with other metal surfaces before a

pattern can be determined.

APPENDIX A

THERMOCOUPLE CALIBRATION

The accuracy desired in the temperature measurements indicated that the thermocouples should be calibrated. One of the fine wire liquid thermocouples and one of the 30 gage reference junction thermocouples were calibrated and considered to represent the calibration for all the thermocouples made with the same wire. Each of the sheathed thermocouples, used to measure the surface superheat, was calibrated separately.

A schematic of the calibration apparatus is shown in Fig. A-1. The system is similar to the test system, with the glass test dewar replaced by a stainless steel cryostat. When the cryostat was filled with a cryogenic liquid, a constant pressure was maintained in the cryostat by the pressure control described in Section II.B. The reference pressure cylinder was immersed in an ice bath to maintain a constant temperature, removing the drift in pressure that was reported for the heat transfer tests. A mechanical stirrer was used to prevent stratification in the cryogenic liquid.

The thermocouples to be calibrated were imbedded in a copper cylinder located inside the cryostat. The thermocouples were referenced to a distilled water ice bath. The EMFs generated were measured on the potentiometer circuit described in Sections III.B and III.C.

The copper cylinder contained a small equilibrium cell which could be charged with a high purity gas. The gas passed through a flow meter before
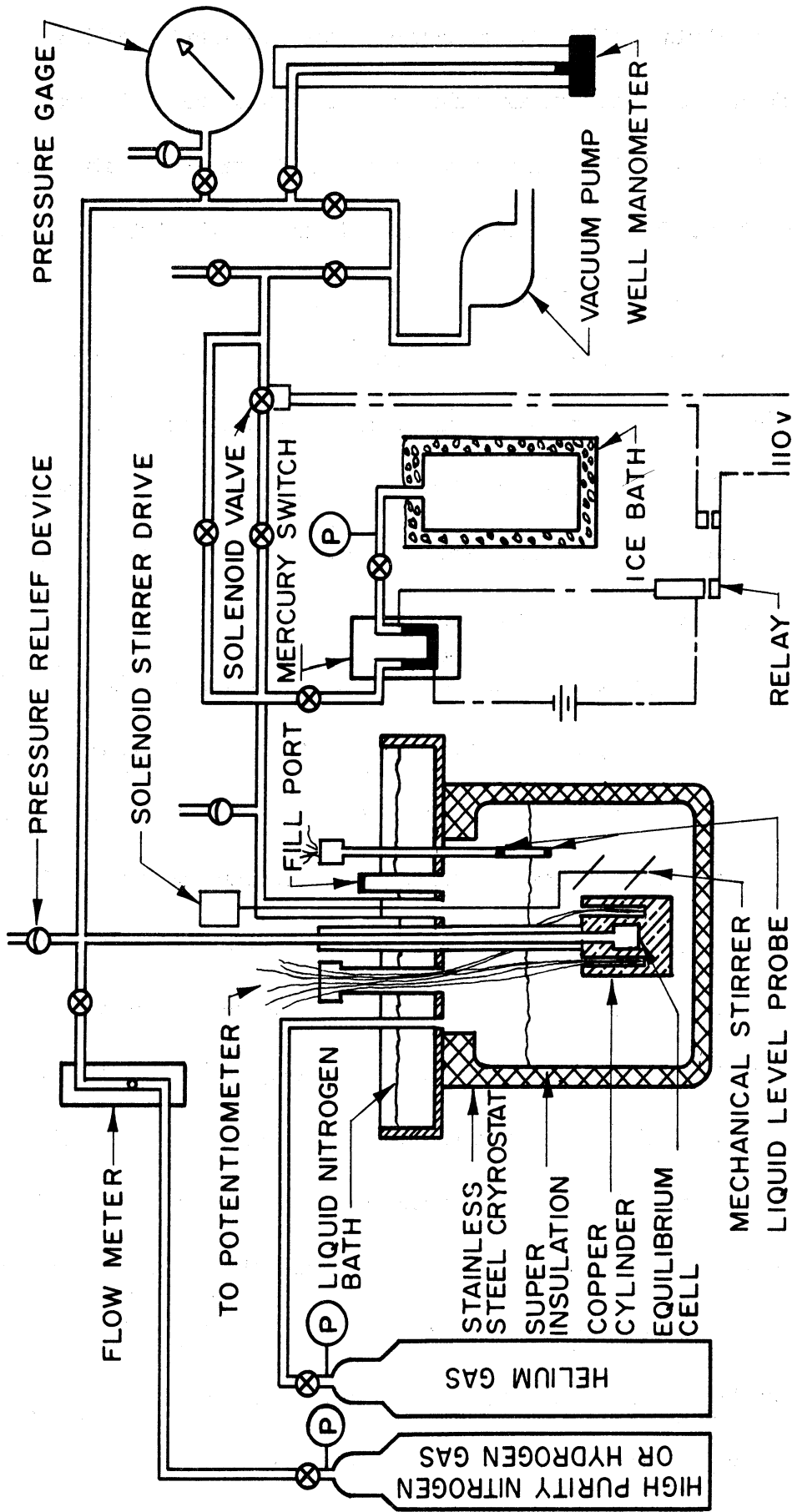
Fig. A-1. Schematic of thermocouple calibration apparatus.

entering the equilibrium cell. The pressure in the equilibrium cell was measured with a calibrated Heise bourdon tube gage if it was above atmospheric pressure, and with a well type mercury manometer if it was below atmospheric pressure. The 12 in. Heise gage had a 0-100 psi range with divisions of 0.1 psi. The calibrated accuracy over the entire range was ±0.1 psi.

The temperatures of the calibration points were limited to the temperatures between the triple point of a liquid and its saturation temperature at 100 psig. For this work, two sets of data were taken, one in the liquid nitrogen range and one in the liquid hydrogen range. They were used as separate calibrations when conducting the heat transfer tests.

The calibration began by purging the cryostat with gaseous helium and the equilibrium cell with high purity nitrogen or hydrogen gas, depending upon the temperature range of the calibration point desired. The cryostat was filled with a cryogenic liquid which was maintained at a constant pressure. The temperature of the calibration point was equal to the saturation temperature of the cryogenic liquid. When the temperature of the copper cylinder became steady, as shown by the thermocouples, the high purity gas was slowly charged into the equilibrium cell. The equilibrium cell pressure rose steadily until the saturation pressure of the gas was reached. The pressure then held steady while the flow meter showed a continuing flow, indicating that the gas was being condensed. The gas flow was shut off and 10 min allowed to dissipate the energy transferred to the copper from the gas. The equilibrium cell pressure and thermocouple EMFs were then measured and recorded.

The temperature of the copper cylinder, and the thermocouple junctions, was determined from the saturation pressure in the equilibrium cell and the vapor pressure data given by Scott.[44] For hydrogen, the normal hydrogen vapor pressure data was used.

The calibration data in the nitrogen temperature range was plotted directly as EMF vs. temperature. The sensitivity was the same for all of the thermocouples, approximately 16 $\mu v/°K$. The maximum deviations of the calibration data from the curves drawn were approximately ± 0.5 μv or $\pm 0.03°K$. The maximum uncertainty in the temperature, due to uncertainty in the pressure reading is $\pm 0.04°K$. The combined uncertainty is $\pm 0.05°K$.

The decreased sensitivity of the thermocouples in the liquid hydrogen temperature range, approximately 6 $\mu v/°K$, necessitated more care in the reduction of the calibration data. For each thermocouple, deviations of the measured EMFs from the standard values given by Powell and Bunch[45] were calculated. These deviations were plotted against the measured EMFs and a straight line was fitted to the points by a least squares method. This line was assumed to represent the exact deviation and used to construct an EMF vs. temperature curve for the thermocouple.

Except for the fine wire thermocouple, all of the deviations were within ± 0.5 μv of the fitted line. The deviations for the fine wire thermocouple were all within ± 1.0 μv of the fitted line. For the sheath thermocouple with the largest variations in the data, the mean squared variation from the fitted line was 0.032 $(\mu v)^2$. A 99% confidence interval on the slope of the line is $\pm.0057$ $\mu v/\mu v$. This is reflected in the EMF vs. temperature line as ± 0.03 $\mu v/°K$ or about $\pm 0.5\%$.

APPENDIX B

ERROR ANALYSIS

1. HEAT FLUX

The average heat fluxes reported contain errors and uncertainties from

at least four sources. The sources considered are:

1. Error in the heater current measurement.

2. Error in the heater voltage measurement.

3. Error in the heat transfer area.

4. Error in the calculated heat losses.

The heater current was determined by measuring, with a potentiometer,

the voltage drop across a precision shunt located in series with the heater.

In the range of these measurements, the accuracy of the potentiometer is

±0.01%, but the readings were made only to ±0.1%. The accuracy of the shunt

resistance is ±0.04%. Combining the uncertainties, the heater current is

known to ±0.108%.

The heater voltage was measured by a digital voltmeter with an accuracy

of ±(0.05% of reading + 0.01% of full scale). The maximum uncertainty in the

heater voltage was ±0.25%.

The uncertainty in the heat transfer area depends upon the type of sur-

face. The copper disc backing a stainless steel or Teflon surface had square

edges on the face that was soldered to the foil. A solder fillet was not re-

quired with these surfaces as the foil was soldered over the entire heat

transfer area. The fillet remaining after soldering was about 0.010 in.

This gives an uncertainty in the heat transfer area of $\pm 4\%$. A chamfer of about 0.030 in. was placed on the edge of the copper disc used to make a copper heat transfer surface. The solder fillet was required to hold the fin in place as this was the only physical bond to the fin. A fillet of about 0.030 in. was used, giving an uncertainty in the heat transfer area of $\pm 12\%$.

The total energy input into the heater was reduced by the amount of energy calculated to be conducted away from the surface by the heater leads, the thermocouple wires and the fin and its backing. The temperature of the fin decayed to the liquid temperature in about 2 mm, so the effect of curvature could be neglected. Two dimensional calculations showed that the contribution of the Teflon backing ring to the total heat loss was negligible when the stainless steel fin was between it and the liquid. A layer of solder 0.0001 in. thick was assumed to have remained on the fin when the liquid solder was wiped from it. This solder did make an important contribution to the total heat loss.

When calculating the heat losses, the heat transfer coefficient on the fin was assumed to be constant. Values of 35×10^{-3} watts/cm^2 °K and 40×10^{-4} watts/cm^2 °K were used for liquid hydrogen and liquid nitrogen, respectively, in both the upwards and vertical orientations. These values are characteristic of the natural convection data. The heat transfer coefficient on the fin, when heating downwards in liquid nitrogen, is difficult to estimate. A value of 20×10^{-3} watts/cm^2 °K was used in the heat loss calculations.

The model used to calculate the fin heat loss is shown in Fig. B-1.
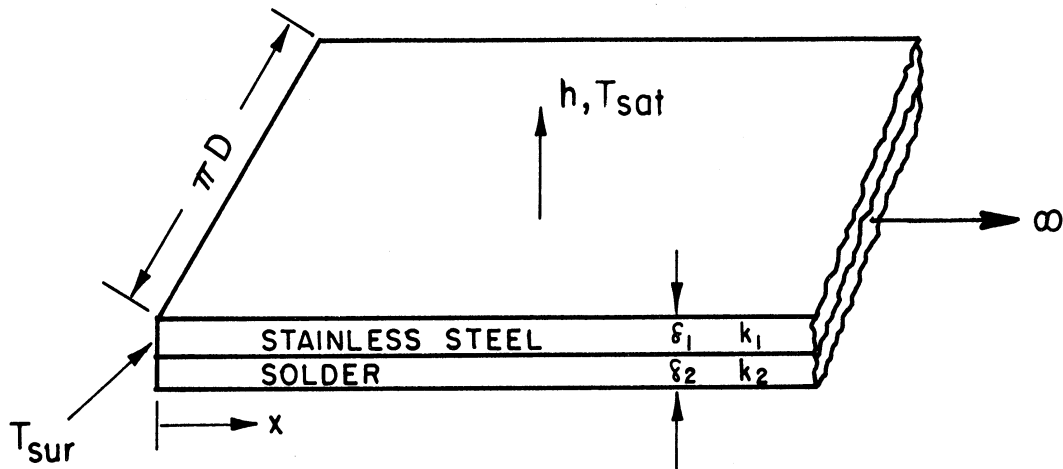
Fig. B-1. Model for fin heat loss calculations.

Lumping the temperature across the thickness of the solder and stainless steel, the temperature distribution in the fin is given by

$$(T-T_{sat}) = (T_{sur}-T_{sat})e^{-(h/k_1\delta_1+k_2\delta_2)^{1/2}x} \qquad (B-1)$$

The total heat loss from the fin is

$$(q_L)_{fin} = \pi D(T_{sur}-T_{sat})[h(k_1\delta_1+k_2\delta_2)]^{1/2} \qquad (B-2)$$

The thermocouple wires were assumed to be insulated when they were inside the housing cup and at the temperature of the liquid where they passed into the liquid. The heater leads were also assumed to be insulated and at the temperature of the liquid where they attached to the heavy copper leads. The loss in each wire is then by conduction down its length and can be written in the form

$$(q_L)_{wire} = kA(T_{sur}-T_{sat}/L) \qquad (B-3)$$

The total calculated heat losses are listed with the data in Appendix C. The percentage of the total heat input that they represent depends upon the surface superheat, the orientation and the liquid. For example, the calculated heat loss from the polished stainless steel surface, heating upwards in liquid hydrogen at the initial vapor conditions, is approximately 11% of the total heat input. This percentage increases at smaller heat fluxes and decreases to about 1% during vigorous boiling. The heat loss calculations are considered to be accurate to ±25%. For the case considered above, this represents an uncertainty in the reported heat flux of ±2.8%.

The total uncertainty in the heat flux is a combination of the separate uncertainties and depends upon the surface, heat flux, orientation and liquid. Again using the example of the polished stainless steel surface, heating upwards in liquid hydrogen at the initial vapor conditions, the total uncertainty in the heat flux is ±5.1%.

2. TEMPERATURE MEASUREMENTS

Five possible sources of error in the reported temperatures are considered. They are:

1. Error in the thermocouple calibration.

2. Error in the EMF measurement.

3. Parasitic EMFs in the thermocouple leads.

4. Error in the temperature correction.

5. Cooling of the thermocouple junction by conduction of heat in the thermocouple wires.

The thermocouple calibration was discussed in detail in Appendix A. There it is estimated that the accuracy of the calibration is within ±0.5% for the differential thermocouples in liquid hydrogen and ±0.05°K for thermocouples in liquid nitrogen, referenced to ice. For a differential thermocouple in liquid nitrogen this would be an uncertainty of ±0.07°K.

The thermocouple EMFs were measured with the potentiometer circuit described in Sections III.B and III.C. For the polished stainless steel surface, heating upwards at the initial vapor conditions, the potentiometer accuracy of ±(0.05% of reading + 0.02 μv) represents approximately ±0.25% of the surface thermocouple's EMF in liquid hydrogen, and ±0.07% of the surface thermocouple's EMF in liquid nitrogen. The percentage increases at smaller surface superheats and decreases at larger surface superheats.

The parasitic EMFs in the copper thermocouple leads add to or subtract from the thermocouple EMF. It is felt that the parasitic EMFs were almost always within the range of ±0.5 μv. This represents ±0.08°K and ±0.03°K when measuring temperatures in liquid hydrogen and nitrogen, respectively.

Except for the nonmetallic surfaces, the calculated correction to the measured temperature, to account for the temperature drop between the thermocouple and the surface, is not large. It is directly proportional to the heat flux and listed with the data in Appendix C. For the polished stainless steel surface, heating upwards at the initial vapor conditions, it represents about 1% of the surface superheat in both liquid hydrogen and liquid nitrogen. Assuming the calculated correction to be accurate within ±25%, this is an uncertainty of ±0.25% in the reported surface superheat.

An estimate has been made of the temperature difference between the thermocouple junction and the heater block, resulting from conduction in the thermocouple wires. This difference is estimated to be 0.7% of the surface superheat in liquid hydrogen and negligible in liquid nitrogen.

The total uncertainty in the surface superheat depends upon the surface, the liquid and the heat flux. For the polished stainless steel surface, heating upwards at the initial vapor conditions, the uncertainty is ±6.1% and ±1.7% in liquid hydrogen and nitrogen, respectively.

3. POSITION OF LIQUID THERMOCOUPLES

In order to determine the location of the liquid thermocouples, the thermocouple holder was seated against a flat surface and the distances from the thermocouple beads to the surface were measured at room temperature, with a calibrated microscope eyepiece scale. The thermocouple wires were 2 mils in diameter and the soldered thermocouple beads were approximately 4 mils in diameter. The distance measurements were made to the approximate center of the bead with an accuracy in the reading of ±0.001 in. This is combined with the uncertainty resulting from the relatively large size of the beads to give an uncertainty in the locations of the tremperatures measured of ±0.0022 in. The relatively small contraction of the holder when cooling from room temperature to the test temperatures is negligible.

APPENDIX C

DATA

The data from valid runs during which boiling heat transfer data were obtained, plus a few runs in which only natural convection data were obtained, are tabulated below along with comments from the visual observations. The pressure indicated is an average at the test surface over the duration of the run. This pressure changed slightly during a run because of drift in the reference pressure and a changing hydrostatic head as liquid was vaporized. The average liquid depth is the average amount of liquid above the surface. During a long run, the liquid level dropped as much as 8 in. The measured power input into the heat is q_M and the calculated heat loss is q_L. q_M is reduced by q_L and then divided by the area to obtain the net heat flux, q_{net}/A. δT_{corr} is the calculated temperature drop from the surface thermocouple to the surface. ΔT_S is corrected by δT_{corr} and is equal to the surface superheat $(T_{sur}-T_{sat})$.

Run ___37___   Date __10/18/66__   Surface _Solid Polished S.S._

Liquid ___N$_2$___   Pressure __14.0 psia__   Orientation _Downwards_

Average Depth of Liquid _____   Convection Shield _Yes_

q_M x 10^3 (watts)	q_L x 10^3 (watts)	$\frac{q_{net}}{A}$ x 10^3 ($\frac{watts}{cm^2}$)	δT_{corr} (°K)	ΔT_s (°K)	Comments
49.0	13.9	6.95	0.01	.81	Distance from surface = .000 in.
				.74	.007
				.64	.015
				.55	.035
75.6	20.6	10.8	0.01	1.28	.000
				1.16	.007
				.99	.015
				.84	.035
84.0	21.9	12.2	0.02	1.37	.000
				1.25	.007
				1.07	.015
				.90	.035
92.0	24.3	13.4	0.02	1.50	.000
				1.38	.007
				1.17	.015
				.99	.035
104	26	15.4	0.02	1.64	.000
				1.51	.007
				1.29	.015
				1.08	.035
113.5	29.2	16.8	0.02	1.83	.000
				1.67	.007
				1.41	.015
				1.19	.035

Run **46** Date **10/21/66** Surface **Solid Polished S.S.**

Liquid **N_2** Pressure **13.9 psia** Orientation **Downwards**

Average Depth of Liquid _____ Convection Shield **Yes**

$q_M \times 10^3$ (watts)	$q_L \times 10^3$ (watts)	$\frac{q_{net}}{A} \times 10^3$ ($\frac{watts}{cm^2}$)	δT_{corr} (°K)	ΔT_s (°K)	Comments
144.2	36.3	21.3	0.03	2.27	Distances from surface = .000 in.
				2.07	.007
				1.74	.015
				1.43	.035
160.9	40.1	23.9	0.03	2.51	.000
				2.27	.007
				1.90	.015
				1.55	.035

Run __89__   Date __3/28/67__   Surface __NASA__

Liquid __N₂__   Pressure __17.0 psia__   Orientation __Upwards__

Average Depth of Liquid _____   Convection Shield __Yes__

$q_M \times 10^3$ (watts)	$q_L \times 10^3$ (watts)	$\dfrac{q_{net}}{A} \times 10^3$ $(\frac{watts}{cm^2})$	δT_{corr} (°K)	ΔT_s (°K)	Comments
19.0	4.2	3.7	0.11	0.10	From Run 90—1 active site
43.8	9.8	6.7	0.20	0.29	1 active site
65.2	14.4	10.0	0.30	0.42	From Run 90—1 active site
70.8	15.4	10.9	0.35	0.44	2 active sites
96.2	20.8	14.9	0.45	0.59	Some sites with large bubbles and low frequency and some
133	28.4	20.5	0.62	0.80	sites with small bubbles and high frequency
172	36.4	26.8	0.80	1.02	
200	42.2	31.1	0.94	1.17	
249	52.2	38.9	1.16	1.45	
309	64.2	48.2	1.45	1.76	
384	79.2	60.2	1.86	2.10	
511	104	80.3	2.41	2.79	
660	133	104	3.12	3.54	Site density increasing noticably
824	165	130	3.90	4.34	
1380	270	219	6.57	6.91	
2110	399	338	10.1	10.0	
2960	538	478	14.4	12.6	
4040	694	660	19.8	14.9	
5890	940	976	29.4	17.6	
4520	759	741	22.3	15.7	
3560	627	578	17.3	14.0	
2770	506	447	13.4	11.9	
1710	325	272	8.16	8.08	
1040	199	165	4.97	4.96	
591	117	93.6	2.84	2.99	
421	84.0	66.5	2.00	2.20	
274	55.2	43.2	1.29	1.47	
193	39.2	30.4	0.91	1.05	
137	28.2	21.5	0.65	0.86	
101	21.0	15.8	0.47	0.58	
78.1	16.2	12.2	0.36	0.45	
45.4	9.8	7.0	0.21	0.28	

Note: q_L and δT_{corr} are only guesses as the thermal properties of the glue used were not available. This run was not plotted because of the large uncertainties, but is included here for completeness.

Run____91____ Date____1/12/67____ Surface____CF-2a____

Liquid____N₂____ Pressure____17.1 psia____ Orientation____Upwards____

Average Depth of Liquid_____ Convection Shield____Yes____

$q_M \times 10^3$ (watts)	$q_L \times 10^3$ (watts)	$\frac{q_{net}}{A} \times 10^3$ ($\frac{watts}{cm^2}$)	δT_{corr} (°K)	ΔT_s (°K)	Comments
42.5	7.36	6.80	0.00	0.24	
70.2	11.5	11.5	0.00	0.37	
109	17.2	18.1	0.00	0.55	
177	25.6	29.9	0.00	0.82	
257	34.9	43.8	0.00	1.12	
435	54.3	75.1	0.00	1.74	
680	77.7	119	0.00	2.49	
965	103	170	0.00	3.29	
1340	135	239	0.00	4.31	
1650	157	295	0.00	5.02	2 steady sites right together
1580	151	282	0.00	4.84	1 steady site—bubble size Much smaller than above
1530	146	273	0.00	4.68	Site intermittently active
1470	142	262	0.00	4.55	
1390	138	247	0.00	4.41	
1360	135	242	0.00	4.34	Site inactive
1390	138	247	0.00	4.43	
1470	143	262	0.00	4.57	Same site active again
1980	175	356	0.01	5.59	1 group of 3 sites and 1 of 4
2280	168	417	0.01	5.36	A small patch, not at above sites
2990	185	552	0.01	5.92	
4070	179	767	0.01	5.71	
5560	190	1060	0.02	6.06	
8130	200	1560	0.03	6.37	
11000	190	2120	0.03	6.05	
14100	217	2730	0.04	6.90	
16100	216	3130	0.05	6.87	
19800	225	3860	0.06	7.14	
17200	217	3350	0.05	6.89	
14500	208	2830	0.05	6.63	
11600	200	2240	0.04	6.36	
9480	193	1830	0.03	6.16	
7960	185	1530	0.02	5.90	
6500	184	1250	0.02	5.89	
5330	179	1020	0.02	5.73	
3870	170	729	0.01	5.43	
2900	159	541	0.01	5.07	
1810	128	332	0.01	4.10	
1210	108	217	0.00	3.47	2 sites
853	89.5	151	0.00	2.87	no sites
362	47.1	62.1	0.00	1.51	
89.0	15.6	14.5	0.00	0.50	

Run __94__   Date __4/25/67__   Surface __CSF-1__

Liquid __N₂__   Pressure __17.2 psia__   Oriéntation __Upwards__

Average Depth of Liquid _____   Convection Shield __Yes__

$q_M \times 10^3$ (watts)	$q_L \times 10^3$ (watts)	$\dfrac{q_{net}}{A} \times 10^3$ $\left(\dfrac{watts}{cm^2}\right)$	δT_{corr} (°K)	ΔT_s (°K)	Comments
89.0	17.1	14.2	0.00	0.55	Taken from Run 92
137	23.0	22.6	0.00	0.74	Taken from Run 93
179	30.4	29.3	0.00	0.97	
315	44.2	53.3	0.01	1.44	Taken from Run 93
531	69.5	91.0	0.01	2.22	
984	110	172	0.02	3.51	Taken from Run 93
1,450	148	257	0.03	4.71	
1,570	157	279	0.03	5.01	
1,700	168	303	0.04	5.36	
1,910	184	340	0.04	5.84	
2,080	196	372	0.05	6.23	
2,220	206	397	0.05	6.55	1 site
2,380	213	427	0.05	6.77	2 clusters of sites
2,530	215	456	0.06	6.84	
2,940	222	536	0.07	7.05	
3,600	224	667	0.08	7.10	
4,760	228	894	0.11	7.21	
6,540	236	1,240	0.15	7.40	
8,770	240	1,680	0.21	7.49	
12,500	243	2,420	0.30	7.51	
18,400	252	3,580	0.44	7.65	
24,700	263	4,820	0.59	7.85	
32,200	278	6,290	0.77	8.13	
42,300	298	8,280	1.01	8.54	
59,700	332	11,700	1.43	9.20	
67,600	346	13,300	1.62	9.48	
50,000	305	9,800	1.19	8.58	
37,100	278	7,270	0.89	8.04	
27,100	259	5,290	0.65	7.66	
21,300	249	4,150	0.51	7.48	
15,300	240	2,960	0.36	7.33	
10,700	232	2,060	0.25	7.20	
7,000	224	1,340	0.16	7.02	
4,520	216	848	0.10	6.83	
2,820	208	515	0.06	6.60	
2,220	202	398	0.05	6.44	
2,120	199	380	0.05	6.33	3 active sites
2,010	193	358	0.04	6.15	1 active site
1,900	184	338	0.04	5.85	
1,740	174	309	0.04	5.53	No sites
516	68.7	88.3	0.01	2.19	

Run __108__   Date __6/6/67__   Surface __CSF-1__

Liquid __H_2__   Pressure __17.1 psia__   Orientation __Upwards__

Average Depth of Liquid __8 in.__   Convection Shield __Yes__

q_M x 10^3 (watts)	q_L x 10^3 (watts)	$\dfrac{q_{net}}{A}$ x 10^3 ($\dfrac{watts}{cm^2}$)	δT_{corr} (°K)	ΔT_s (°K)	Comments
22.9	3.93	4.3	0.00	0.15	
54.1	7.86	9.1	0.00	0.30	
85.3	11.8	14.5	0.01	0.45	
135	17.0	23.2	0.01	0.65	
212	24.6	37.0	0.01	0.94	1 site
238	27.2	41.5	0.01	1.03	Above site inactive—another site intermittently active
293	30.9	51.7	0.01	1.17	2 steady sites
348	34.8	61.7	0.01	1.32	
426	39.8	76.3	0.01	1.51	Small patch
515	43.8	93.0	0.01	1.66	Additional sites and clusters
623	45.9	114	0.01	1.74	
772	47.9	143	0.02	1.81	
975	50.3	182	0.02	1.90	
1,400	53.4	284	0.03	2.01	Sites cover ~40% of surface area
1,980	57.1	379	0.05	2.13	
2,480	60.8	476	0.06	2.26	Sites cover ~80% of surface area
3,050	65.5	589	0.07	2.43	Surface appears to be covered with sites
3,570	68.1	690	0.08	2.52	
4,400	72.3	854	0.10	2.66	
5,170	75.7	1,000	0.12	2.77	
5,980	79.4	1,160	0.14	2.89	
5,550	77.3	1,080	0.13	2.82	
4,810	74.1	935	0.10	2.73	
3,950	70.2	766	0.09	2.59	
3,360	67.3	650	0.08	2.49	
2,800	63.7	538	0.07	2.36	
2,170	60.3	417	0.05	2.25	
1,620	56.3	309	0.04	2.11	
1,200	52.9	226	0.03	1.99	
823	48.7	153	0.02	1.84	
540	42.2	98.2	0.01	1.60	~20 active sites
397	36.2	71.1	0.01	1.37	
296	29.9	52.5	0.01	1.13	
221	24.6	38.7	0.00	0.94	8 active sites
195	22.5	34.1	0.00	0.86	
173	20.7	30.0	0.00	0.79	
136	17.0	23.4	0.00	0.65	2 active sites
122	16.5	20.8	0.00	0.63	
110	15.2	18.7	0.00	0.58	2 active sites—very small bubbles
101	14.4	17.1	0.00	0.55	1 active site
92.0	13.1	15.6	0.00	0.50	No active sites
64.0	10.5	10.6	0.00	0.40	
36.5	6.8	5.9	0.00	0.26	

Run **111**   Date **6/7/67**   Surface **CSF-1**

Liquid **H$_2$**   Pressure **17.3 psia**   Orientation **Upwards**

Average Depth of Liquid **12 in.**   Convection Shield **No**

$q_M \times 10^3$ (watts)	$q_L \times 10^3$ (watts)	$\dfrac{q_{net}}{A} \times 10^3$ $\left(\dfrac{watts}{cm^2}\right)$	δT_{corr} (°K)	ΔT_s (°K)	Comments
29.4	5.76	4.7	0.00	0.22	
46.5	8.12	7.6	0.00	0.31	
61.9	11.0	10.0	0.00	0.42	
90.6	14.4	15.0	0.00	0.55	
134	19.9	22.5	0.00	0.76	
198	26.7	33.8	0.00	1.02	
248	32.0	42.5	0.01	1.21	
319	38.8	55.3	0.01	1.47	3 well separated sites
286	35.6	49.4	0.01	1.35	2 sites
245	31.4	42.0	0.01	1.20	4 sites—all separate
229	29.3	39.3	0.00	1.12	4 sites
350	39.6	61.2	0.01	1.50	More individual sites
388	40.9	68.5	0.01	1.55	Clusters developing
425	41.7	75.6	0.01	1.58	
463	43.2	82.7	0.01	1.64	
515	44.0	92.8	0.01	1.67	Patches developing
584	45.3	106	0.01	1.72	
649	46.1	119	0.01	1.75	
718	48.2	132	0.02	1.82	
793	49.0	147	0.02	1.85	
875	50.8	163	0.02	1.92	
970	52.4	181	0.02	1.98	
1,090	54.2	204	0.02	2.05	
1,190	55.5	224	0.03	2.09	Sites cover ~40% of surface area
1,310	57.6	247	0.03	2.17	
1,490	58.7	282	0.03	2.21	
1,620	60.5	308	0.04	2.27	
1,810	62.9	345	0.04	2.36	
1,980	64.5	379	0.05	2.41	
2,240	65.8	429	0.05	2.46	
2,780	69.7	535	0.07	2.59	Surface appears to be covered with sites
3,560	74.9	687	0.08	2.78	
4,390	78.9	851	0.10	2.91	
5,030	82.3	975	0.12	3.02	
5,970	86.2	1,160	0.14	3.15	
5,530	84.6	1,070	0.13	3.10	
4,690	81.2	908	0.11	2.99	
3,860	77.3	745	0.09	2.86	
3,050	72.6	587	0.07	2.70	
2,350	67.6	450	0.05	2.53	
2,070	65.2	396	0.05	2.44	
1,780	62.9	338	0.04	2.36	
1,450	60.0	274	0.03	2.26	

Run 111 (Continued)

q_M x 10^3 (watts)	q_L x 10^3 (watts)	$\dfrac{q_{net}}{A}$ x 10^3 ($\dfrac{watts}{cm^2}$)	δT_{corr} (°K)	ΔT_s (°K)	Comments
1,080	56.3	203	0.02	2.13	Site density decreasing uniformly over surface
857	52.7	159	0.02	1.99	
689	49.0	126	0.02	1.85	
548	45.3	99.1	0.01	1.72	
443	41.4	79.2	0.01	1.57	~30 active sites
345	37.7	60.6	0.01	1.43	~20 active sites
268	33.0	46.3	0.01	1.26	12 active sites
230	29.6	39.4	0.00	1.13	8 active sites
192	26.2	32.6	0.00	1.00	4 active sites
173	23.8	29.4	0.00	0.91	3 active sites
152	21.5	25.7	0.00	0.82	No active sites
124	17.6	21.0	0.00	0.67	
89.6	14.4	14.8	0.00	0.55	
66.7	11.0	10.9	0.00	0.42	
51.8	8.91	8.4	0.00	0.34	
35.9	6.29	5.8	0.00	0.24	

Run 112   Date 6/7/67   Surface CSF-1

Liquid H_2 Pressure 17.1 lbf/in.^{2} Orientation Upward

Average Depth of Liquid 7 in.   Convection Shield No

q_M x 10^3 (watts)	q_L x 10^3 (watts)	$\frac{q_{net}}{A}$ x 10^3 ($\frac{watts}{cm^2}$)	δT_{corr} (°K)	ΔT_s (°K)	Comments
23.2	5.24	3.5	0.00	0.20	Outer dewar rotated 90°
36.4	7.07	5.7	0.00	0.27	
47.8	9.17	7.6	0.00	0.35	
70.8	14.9	11.0	0.00	0.57	
99.0	16.2	16.3	0.00	0.62	
122	18.6	20.3	0.00	0.71	
161	23.8	27.0	0.00	0.91	
198	27.8	33.6	0.00	1.06	
345	31.4	40.1	0.00	1.20	
286	36.2	49.3	0.01	1.37	
344	41.4	59.6	0.01	1.57	
403	45.9	70.4	0.01	1.74	
476	48.7	84.2	0.01	1.85	
549	48.2	98.7	0.01	1.83	
672	49.5	123	0.01	1.88	
764	50.8	141	0.02	1.92	
893	51.9	166	0.02	1.96	
1,060	54.0	198	0.02	2.04	
1,250	54.8	236	0.03	2.06	
1,420	56.9	268	0.03	2.14	
1,620	59.2	308	0.04	2.22	
1,860	61.8	355	0.04	2.32	
2,160	65.0	414	0.05	2.43	
2,880	70.2	555	0.07	2.61	
3,770	75.7	729	0.09	2.81	
4,790	81.2	929	0.11	2.99	
5,960	86.7	1,160	0.14	3.17	
5,260	83.6	1,020	0.12	3.07	
4,190	78.6	811	0.10	2.90	
3,280	73.4	633	0.08	2.72	
2,470	67.6	473	0.06	2.53	
2,070	64.2	396	0.05	2.40	
1,840	62.6	351	0.04	2.35	
1,660	61.3	316	0.04	2.30	
1,490	59.7	282	0.03	2.25	
1,340	57.6	254	0.03	2.17	
1,140	55.5	213	0.03	2.09	
971	53.2	181	0.02	2.01	
824	51.1	152	0.02	1.93	
685	48.7	126	0.02	1.84	
540	45.6	97.4	0.01	1.73	
418	42.7	74.1	0.01	1.62	
343	38.5	60.0	0.01	1.46	
314	36.9	54.5	0.01	1.40	
245	32.0	42.0	0.01	1.21	
193	26.7	32.8	0.00	1.02	

Run 112 (Continued)

q_M x 10^3 (watts)	q_L x 10^3 (watts)	$\dfrac{q_{net}}{A}$ x 10^3 ($\dfrac{watts}{cm^2}$)	δT_{corr} (°K)	ΔT_s (°K)	Comments
163	23.6	27.4	0.00	0.90	
135	20.2	22.6	0.00	0.77	
113	18.1	18.6	0.00	0.69	
89.8	14.7	14.8	0.00	0.56	
72.5	12.3	11.8	0.00	0.47	
58.2	11.0	9.3	0.00	0.42	
40.3	8.1	6.3	0.00	0.31	

Run __116__   Date __6/29/67__   Surface __CTF-1__

Liquid __H_2__   Pressure __17.0 psia__   Orientation __Upward__

Average Depth of Liquid __12 in.__   Convection Shield __No__

$q_M \times 10^3$ (watts)	$q_L \times 10^3$ (watts)	$\dfrac{q_{net}}{A} \times 10^3$ ($\dfrac{watts}{cm^2}$)	δT_{corr} (°K)	ΔT_s (°K)	Comments
25.4	6.04	3.82	0.01	0.22	
39.1	8.39	6.07	0.02	0.31	
52.1	10.5	8.21	0.02	0.38	1 site
56.9	11.4	8.98	0.02	0.42	
64.3	12.6	10.2	0.03	0.46	
69.6	13.4	11.1	0.03	0.49	
76.2	14.4	12.2	0.03	0.52	
83.4	15.4	13.4	0.04	0.56	
93.2	16.6	15.1	0.04	0.60	
102	17.7	16.6	0.04	0.64	
114	19.1	18.6	0.05	0.69	
123	20.2	20.3	0.05	0.73	3 sites
135	21.6	22.3	0.06	0.78	
148	23.3	24.7	0.07	0.84	2 of the above sites inactive— 2 other sites active
179	26.7	30.1	0.08	0.95	
216	30.4	36.5	0.10	1.08	6 sites
257	34.6	43.9	0.12	1.22	7 sites
308	38.7	53.0	0.14	1.35	12 sites
348	42.0	60.3	0.16	1.46	17 sites
423	46.9	74.2	0.20	1.61	
489	50.5	86.4	0.23	1.72	
613	54.6	110	0.29	1.81	
742	60.2	134	0.36	1.97	Individual sites distributed over entire surface
861	63.8	157	0.42	2.04	
1,060	68.9	196	0.52	2.14	
1,280	73.2	238	0.63	2.20	
1,560	72.1	294	0.78	2.00	
1,840	77.6	348	0.92	2.07	
2,250	83.4	428	1.14	2.08	
2,970	93.3	568	1.51	2.10	
3,880	102	746	1.98	1.97	
4,890	114	943	2.50	1.91	
6,020	128	1,160	3.08	1.86	
5,270	117	1,020	2.70	1.80	
4,200	100	809	2.15	1.72	
3,310	86.1	636	1.69	1.63	
2,430	72.1	465	1.23	1.55	

Run 116 (Continued)

q_M x 10^3 (watts)	q_L x 10^3 (watts)	$\frac{q_{net}}{A}$ x 10^3 ($\frac{watts}{cm^2}$)	δT_{corr} (°K)	ΔT_s (°K)	Comments
1,790	61.4	341	0.91	1.46	
1,240	51.7	235	0.62	1.37	
918	44.8	172	0.46	1.27	
672	39.1	125	0.33	1.18	
512	34.6	94.1	0.25	1.09	
383	29.6	69.7	0.19	0.96	Small partical of something in liquid moving around the surface and acting as a site
293	25.8	52.6	0.14	0.86	
244	23.3	43.5	0.12	0.79	Bubbles from sites are very small—almost appear to be a mist
197	20.6	34.7	0.09	0.70	
161	18.4	28.1	0.07	0.64	Many sites
134	16.1	23.2	0.06	0.56	
111	14.3	19.1	0.05	0.50	
89.9	12.2	15.3	0.04	0.43	
76.2	10.7	12.9	0.03	0.38	~50 sites—small bubbles
65.3	9.67	11.0	0.03	0.34	
54.1	8.43	9.01	0.02	0.30	
44.2	7.45	7.25	0.02	0.27	
33.9	6.13	5.48	0.01	0.22	~40 sites
23.8	4.88	3.73	0.01	0.18	~30 sites

Run ___120___   Date ___6/30/67___   Surface ___CTF-1___

Liquid ___H₂___   Pressure ___17.1 psia___   Orientation ___Upward___

Average Depth of Liquid ___9 in.___   Convection Shield ___No___

$q_M \times 10^3$ (watts)	$q_L \times 10^3$ (watts)	$\dfrac{q_{net}}{A} \times 10^3$ $\left(\dfrac{watts}{cm^2}\right)$	δT_{corr} (°K)	ΔT_s (°K)	Comments
0.0	0.0	0.0	0.00	0.00	Time = 0
2,022	104	378	1.00	2.97	0.5 min
				2.94	1
				2.79	2
				2.73	3
				2.61	5
				2.49	7
				2.42	11
				2.35	15
				2.27	20
2,035	82.0	385	1.02	2.11	35
				2.05	66
				2.00	81
				1.94	130
2,036	78.1	386	1.03	1.92	144
				1.90	166
				1.90	177

Run __121__   Date __6/30/67__   Surface __CTF-1__

Liquid __H$_2$__   Pressure __17.3 lbf/in.^{2}__   Orientation __Upward__

Average Depth of Liquid __5 in.__   Convection Shield __No__

q_M x 10^3 (watts)	q_L x 10^3 (watts)	$\frac{q_{net}}{A}$ x 10^3 ($\frac{watts}{cm^2}$)	δT_{corr} (°K)	ΔT_s (°K)	Comments
8,320	161	1,610	4.27	1.95	
7,090	144	1,370	3.64	1.92	
5,930	127	1,140	3.04	1.87	
4,810	110	927	2.46	1.79	
3,890	95.8	748	1.99	1.71	
3,150	83.6	604	1.60	1.62	
2,560	74.3	490	1.30	1.57	
2,090	66.4	399	1.06	1.51	
1,710	59.7	325	0.86	1.44	
1,370	53.3	261	0.69	1.36	
1,130	48.0	214	0.57	1.29	
921	43.5	173	0.46	1.22	
746	39.5	139	0.37	1.15	
612	36.2	114	0.31	1.09	
492	32.4	90.6	0.24	1.01	Many sites producing small bubbles
402	29.5	73.5	0.20	0.95	
328	26.6	59.5	0.16	0.87	
269	23.7	48.4	0.13	0.79	
223	21.6	39.7	0.11	0.73	
181	19.3	32.0	0.08	0.66	
151	17.3	26.3	0.07	0.60	
123	15.4	21.3	0.06	0.54	
102	13.6	17.4	0.05	0.48	
84.6	12.1	14.3	0.04	0.43	
68.4	10.4	11.4	0.03	0.37	
55.8	9.15	9.21	0.02	0.33	~50-60 sites
45.3	8.07	7.35	0.02	0.29	
37.0	7.18	5.87	0.02	0.26	
29.7	6.41	4.60	0.01	0.24	~30-40 sites
24.1	5.69	3.63	0.01	0.21	~30 sites
21.0	5.26	3.10	0.01	0.19	~25 sites

Run 122   Date 7/5/67   Surface CSF-4

Liquid H_2 Pressure 17.2 psia   Orientation Upward

Average Depth of Liquid 7 in.   Convection Shield No

$q_M \times 10^3$ (watts)	$q_L \times 10^3$ (watts)	$\dfrac{q_{net}}{A} \times 10^3$ $\left(\dfrac{watts}{cm^2}\right)$	δT_{corr} (°K)	ΔT_s (°K)	Comments
20.9	4.63	3.20	0.00	0.18	
26.4	5.67	4.09	0.00	0.22	
31.9	6.54	5.00	0.00	0.25	
38.9	7.31	6.23	0.00	0.28	
47.4	8.44	7.68	0.00	0.32	
58.2	10.0	9.49	0.00	0.38	
70.5	12.1	11.5	0.00	0.46	
85.1	13.7	14.1	0.00	0.52	
101	15.8	16.8	0.00	0.60	
122	18.3	20.5	0.00	0.70	
148	21.4	25.0	0.00	0.82	
178	24.3	30.4	0.00	0.93	
214	28.2	36.7	0.00	1.07	
259	32.8	44.5	0.00	1.25	
313	37.8	54.3	0.00	1.44	
376	43.6	65.6	0.00	1.66	
454	50.6	79.5	0.01	1.92	
394	36.5	107	0.01	1.38	Patch of 40-50 sites covering ~5% of surface
663	39.0	123	0.01	1.48	
794	37.4	149	0.01	1.42	Patch growing
970	36.5	184	0.01	1.38	Second patch of 10-20 sites. Most likely from runner of first patch.
1,190	37.4	226	0.01	1.41	
1,440	38.6	276	0.02	1.45	
1,750	39.4	338	0.02	1.48	
2,180	40.7	423	0.03	1.52	Sites on ~50% of surface
2,960	41.9	576	0.04	1.56	
3,860	43.6	753	0.05	1.61	Surface almost coverered with sites
4,790	46.5	936	0.06	1.72	Surface appears to be covered with sites
5,920	50.2	1,160	0.07	1.86	
7,110	53.5	1,390	0.09	1.95	
8,320	56.7	1,630	0.10	2.06	
7,720	53.9	1,510	0.10	1.96	
6,400	48.5	1,250	0.08	1.77	
5,250	44.0	1,030	0.07	1.61	
4,200	39.4	821	0.05	1.46	

Run 122 (Continued)

q_M x 10^3 (watts)	q_L x 10^3 (watts)	$\dfrac{q_{net}}{A}$ x 10^3 $\left(\dfrac{watts}{cm^2}\right)$	δT_{corr} (°K)	ΔT_s (°K)	Comments
3,300	35.7	645	0.04	1.32	
2,500	32.4	486	0.03	1.20	
1,860	29.4	361	0.02	1.10	
1,370	26.9	265	0.02	1.00	Site density decreasing uniformly
1,130	25.6	218	0.01	0.97	
859	24.3	165	0.01	0.92	
643	22.2	122	0.01	0.84	
482	21.1	90.9	0.01	0.79	Many sites producing small bubbles
371	20.0	69.2	0.00	0.76	
286	18.9	52.7	0.00	0.72	~100 active sites
206	17.4	37.3	0.00	0.66	
165	16.3	29.4	0.00	0.62	~60-80 active sites distributed over surface
130	15.1	22.6	0.00	0.58	
99.8	13.8	17.0	0.00	0.53	~40 active sites
76.1	12.0	12.6	0.00	0.46	~25 active sites
56.0	10.5	8.98	0.00	0.40	16 active sites
45.9	9.30	7.23	0.00	0.36	10 active sites
37.2	8.26	5.71	0.00	0.32	4 active sites
31.3	7.14	4.77	0.00	0.27	3 active sites
26.5	6.58	3.93	0.00	0.25	1 active site
23.3	5.93	3.44	0.00	0.23	1 active site
20.7	5.54	3.00	0.00	0.21	1 active site
15.7	4.72	2.17	0.00	0.18	No sites

Run 125   Date 7/11/67   Surface CSF-3

Liquid H$_2$ Pressure 17.1 psia   Orientation Upward

Average Depth of Liquid 12 in.   Convection Shield No

q_M x 10^3 (watts)	q_L x 10^3 (watts)	$\frac{q_{net}}{A}$ x 10^3 ($\frac{watts}{cm^2}$)	δT_{corr} (°K)	ΔT_s (°K)	Comments
20.4	5.63	2.91	0.00	0.21	
26.1	6.71	3.82	0.00	0.26	
31.7	7.75	4.73	0.00	0.30	
38.7	9.13	5.83	0.00	0.35	
47.6	10.6	7.30	0.00	0.40	
57.8	11.8	9.08	0.00	0.45	
70.4	13.8	11.2	0.00	0.53	
85.6	15.8	13.8	0.00	0.60	
105	18.1	17.1	0.00	0.69	
127	20.4	21.0	0.00	0.78	
154	23.8	25.6	0.00	0.91	Approximate initial vapor point— exact point missed
187	26.7	31.7	0.00	1.02	
228	30.5	38.9	0.00	1.16	
274	33.0	47.5	0.00	1.26	~20 sites distributed over surface
334	34.3	59.2	0.00	1.31	Individual sites and clusters of 3 and 4 sites
407	35.1	73.3	0.00	1.34	
494	35.1	90.5	0.01	1.33	
607	35.6	113	0.01	1.35	
737	35.1	138	0.01	1.33	
892	35.6	169	0.01	1.35	
1,160	37.2	221	0.01	1.41	Individual sites and clusters over the entire surfac
1,550	39.3	297	0.02	1.48	
2,130	41.0	412	0.03	1.53	
2,900	43.4	564	0.04	1.61	
3,850	46.3	750	0.05	1.71	
4,780	49.2	933	0.06	1.82	
5,920	53.3	1,160	0.07	1.97	
5,220	50.4	1,020	0.07	1.86	
4,280	45.9	835	0.05	1.71	
3,290	41.8	641	0.04	1.55	
2,530	38.5	491	0.03	1.44	
1,780	34.7	343	0.02	1.30	
1,370	32.2	263	0.02	1.21	
1,050	30.5	202	0.01	1.15	

Run 125 (Continued)

$q_M \times 10^3$ (watts)	$q_L \times 10^3$ (watts)	$\dfrac{q_{net}}{A} \times 10^3$ $(\dfrac{watts}{cm^2})$	δT_{corr} (°K)	ΔT_s (°K)	Comments
780	28.0	148	0.01	1.06	Site density and bubble size decreasing
608	26.3	115	0.01	0.99	
470	24.2	88.0	0.01	0.91	
356	22.1	65.9	0.00	0.84	
268	19.5	49.0	0.00	0.74	
194	17.4	34.9	0.00	0.66	
153	15.5	27.2	0.00	0.59	
122	13.9	21.2	0.00	0.53	
94.3	12.2	16.2	0.00	0.47	~100 active sites
70.6	10.3	11.9	0.00	0.39	
53.8	8.66	8.89	0.00	0.33	~40-50 active sites
41.0	7.57	6.59	0.00	0.29	~30 active sites
31.7	6.32	5.00	0.00	0.24	~25 active sites
26.4	5.76	4.07	0.00	0.22	~20 active sites
20.7	4.98	3.10	0.00	0.19	16 active sites
15.7	4.20	2.26	0.00	0.16	12 active sites

Run ___134___   Date ___7/18/67___   Surface ___CSF-4___

Liquid ___N_2___   Pressure ___17.2 lbf/in.^{2}___   Orientation ___Downward___

Average Depth of Liquid ___8 in.___   Convection Shield ___Yes___

q_M x 10^3 (watts)	q_L x 10^3 (watts)	$\frac{q_{net}}{A}$ x 10^3 ($\frac{watts}{cm^2}$)	δT_{corr} (°K)	ΔT_s (°K)	Comments
20.6	4.87	3.10	0.00	0.56	
48.3	10.2	7.52	0.00	1.17	
89.4	17.8	14.1	0.00	2.04	
190	36.2	30.3	0.00	4.16	
236	40.6	38.6	0.00	4.67	Vapor formed sometime after 4.67°K

Run __146__   Date __7/20/67__   Surface __CSF-1__

Liquid __N₂__   Pressure __17.6 psia__   Orientation __Downward__

Average Depth of Liquid __9 in.__   Convection Shield __Yes__

$q_M \times 10^3$ (watts)	$q_L \times 10^3$ (watts)	$\dfrac{q_{net}}{A} \times 10^3$ ($\dfrac{watts}{cm^2}$)	δT_{corr} (°K)	ΔT_s (°K)	Comments
21.9	4.40	3.45	0.00	0.51	
54.8	10.9	8.67	0.00	1.25	
87.0	17.8	13.7	0.00	2.04	
172	31.2	27.9	0.00	3.58	Formed vapor sometime after 3.58°K

Run __147__   Date __7/21/67__   Surface __CSF-4__

Liquid __N₂__   Pressure __17.2 psia__   Orientation __Upward__

Average Depth of Liquid __8 in.__   Convection Shield __No__

$q_M \times 10^3$ (watts)	$q_L \times 10^3$ (watts)	$\dfrac{q_{net}}{A} \times 10^3$ $\left(\dfrac{watts}{cm^2}\right)$	δT_{corr} (°K)	ΔT_s (°K)	Comments
37.0	9.47	5.43	0.00	0.30	
77.3	16.4	12.0	0.00	0.53	
175	30.9	28.3	0.00	0.99	
389	57.5	65.5	0.00	1.84	
788	98.4	136	0.00	3.15	
1,030	119	180	0.00	3.81	
1,280	141	224	0.00	4.53	
1,560	137	281	0.00	4.40	
2,030	138	372	0.00	4.42	Patch covering about 5% of surface.
2,830	140	530	0.00	4.48	Patch spreading.
4,520	148	861	0.00	4.74	Patch covers about 65% of surface.
7,540	160	1,460	0.00	5.12	Surface almost covered with active sites
12,600	176	2,460	0.01	5.62	
18,500	192	3,610	0.01	6.14	
27,700	211	5,410	0.02	6.74	
42,900	242	8,420	0.03	7.72	Temperatures might not have reached steady state values as readings were rushed
62,600	278	12,300	0.04	8.88	
50,500	259	9,910	0.03	8.26	
39,400	240	7,730	0.02	7.67	
30,900	225	6,050	0.02	7.19	
23,700	212	4,630	0.01	6.76	
17,700	199	3,450	0.01	6.38	
13,000	187	2,530	0.01	6.00	
8,300	173	1,600	0.01	5.55	
5,270	160	1,010	0.00	5.12	
3,850	152	730	0.00	4.88	
2,650	145	494	0.00	4.66	
1,840	140	336	0.00	4.48	~50 active sites
1,140	121	201	0.00	3.88	~25 active sites
909	105	158	0.00	3.38	~15 active sites
698	90.1	120	0.00	2.89	1 steady, 5-6 intermittent sites
567	74.4	97.2	0.00	2.38	No sites
123	23.8	19.6	0.00	0.76	

Run __151__   Date __7/31/67__   Surface __CF-2__

Liquid __H2__   Pressure __17.2 psia__   Orientation __Upward__

Average Depth of Liquid __11 in.__   Convection Shield __No__

$q_M \times 10^3$ (watts)	$q_L \times 10^3$ (watts)	$\dfrac{q_{net}}{A} \times 10^3$ ($\dfrac{watts}{cm^2}$)	δT_{corr} (°K)	ΔT_s (°K)	Comments
90.5	15.1	14.9	0.00	0.57	
109	17.4	18.0	0.00	0.66	1 intermittent site
129	13.7	22.8	0.00	0.52	Patch of ~10 sites, above site inactive.
166	12.8	30.2	0.00	0.49	Patch growing, site density in patch not great.
225	13.3	41.8	0.00	0.51	
554	15.7	106	0.00	0.60	Patch covers ~25% of surface.
989	17.5	192	0.00	0.67	Patch covers ~60% of surface.
2,010	21.3	393	0.00	0.81	Patch cover ~85% of surface.
3,310	25.9	647	0.00	0.98	Surface appears to be covered with sites.
4,050	27.8	794	0.00	1.06	
4,780	28.6	938	0.01	1.09	
5,580	29.0	1,100	0.01	1.10	
4,870	26.7	955	0.01	1.01	
3,800	24.6	745	0.00	0.94	
3,060	22.9	599	0.00	0.87	
2,330	21.2	455	0.00	0.81	Site density decreasing.
1,930	20.1	377	0.00	0.77	
1,580	19.2	308	0.00	0.73	
1,270	18.2	247	0.00	0.69	
1,020	17.4	198	0.00	0.66	Site density uniform over surface
798	16.5	154	0.00	0.63	
648	15.8	125	0.00	0.60	
527	15.1	101	0.00	0.58	
429	14.5	81.8	0.00	0.55	
341	14.0	64.5	0.00	0.53	
271	13.6	50.7	0.00	0.52	
215	12.7	39.8	0.00	0.48	
177	12.2	32.4	0.00	0.46	
145	11.5	26.3	0.00	0.44	~100 sites, large bubbles, low frequency.
117	10.9	21.0	0.00	0.42	
95.9	10.1	16.9	0.00	0.39	
79.7	9.81	13.8	0.00	0.37	
64.2	9.34	10.8	0.00	0.36	~40-50 intermittent sites
52.7	8.74	8.68	0.00	0.33	~30 intermittent sites
43.5	8.18	6.97	0.00	0.31	
35.5	7.44	5.54	0.00	0.28	2 steady sites, ~25 intermittent sites
28.5	6.67	4.31	0.00	0.25	
22.2	5.93	3.20	0.00	0.23	1 steady site

Run __154__   Date __8/1/78__   Surface __CSF-1__

Liquid __H₂__   Pressure __17.7 psia__   Orientation __Vertical__

Average Depth of Liquid __11 in.__   Convection Shield __No__

$q_M \times 10^3$ (watts)	$q_L \times 10^3$ (watts)	$\dfrac{q_{net}}{A} \times 10^3$ ($\frac{watts}{cm^2}$)	δT_{corr} (°K)	ΔT_s (°K)	Comments
20.3	3.64	3.28	0.00	0.11	
29.5	5.34	4.77	0.00	0.17	
59.9	10.4	9.77	0.00	0.37	
139	21.4	23.2	0.00	0.78	
162	23.4	27.4	0.00	0.86	
194	27.0	32.9	0.00	1.00	
220	28.7	37.7	0.00	1.06	
246	32.4	42.2	0.01	1.20	
297	38.9	50.9	0.01	1.45	
375	46.5	64.9	0.01	1.74	1 site near top of surface.
495	52.9	87.2	0.01	1.98	5-6 sites on top 1/3 of surface.
661	54.4	120	0.01	2.03	Sites on top 1/2 of surface.
824	47.7	153	0.02	180	1 site at very bottom of surface, sites in triangle above it.
1,060	53.7	198	0.02	2.02	
1,330	58.0	250	0.03	2.18	
1,730	64.6	329	0.04	2.43	Sites cover ~60% of surface.
2,280	72.0	435	0.05	2.69	
2,950	76.9	567	0.07	2.87	Sites cover ~80% of surface.
3,770	86.3	726	0.09	3.21	
4,840	94.9	937	0.11	3.51	
6,230	109	1,200	0.15	4.03	Sites appear to cover entire surface
8,290	117	1,610	0.20	4.26	
6,530	103	1,270	0.15	3.76	
5,360	91.6	1,040	0.13	3.37	
4,280	81.1	828	0.10	2.99	
3,360	70.4	649	0.08	2.61	About 2 mm along bottom. Almost void of sites.
2,570	61.5	495	0.06	2.29	
1,900	53.7	363	0.04	2.00	
1,350	45.3	258	0.03	1.70	
969	39.3	183	0.02	1.48	
675	32.8	127	0.02	1.23	
503	27.8	93.7	0.01	1.05	Sites in triangle with 60° angle, located at bottom of surface.
347	24.5	63.5	0.01	0.93	3 areas with sites
241	20.8	43.5	0.01	0.79	
196	18.6	35.0	0.00	0.71	~10 steady sites on top 1/2 of surface

Run 154 (Continued)

$q_M \times 10^3$ (watts)	$q_L \times 10^3$ (watts)	$\dfrac{q_{net}}{A} \times 10^3$ $\left(\dfrac{watts}{cm^2}\right)$	δT_{corr} (°K)	ΔT_s (°K)	Comments
162	17.0	28.6	0.00	0.64	
132	14.0	23.4	0.00	0.53	7 steady sites
108	13.1	18.8	0.00	0.50	6 steady sites
89.8	12.1	15.3	0.00	0.46	4 steady sites, all on top 1/2 of surface.
72.8	10.5	12.3	0.00	0.40	3 steady sites
62.4	9.28	10.5	0.00	0.35	3 steady sites
49.8	7.93	3.25	0.00	0.30	2 steady sites
43.3	7.30	7.11	0.00	0.28	2 steady sites
35.0	6.11	5.69	0.00	0.23	No sites

Run __158__   Date __8/3/67__   Surface __CF-4__

Liquid __H_2__   Pressure __17.7 psia__   Orientation __Upward__

Average Depth of Liquid __10 in.__   Convection Shield __No__

$q_M \times 10^3$ (watts)	$q_L \times 10^3$ (watts)	$\dfrac{q_{net}}{A} \times 10^3$ ($\frac{watts}{cm^2}$)	δT_{corr} (°K)	ΔT_s (°K)	Comments
22.1	0.974	4.16	0.00	0.11	
36.1	2.90	6.56	0.00	0.18	
60.7	4.72	11.0	0.00	0.30	
91.4	7.89	16.5	0.00	0.40	Patch of 7-8 sites.
106	10.4	18.8	0.00	0.40	
146	10.4	26.8	0.00	0.39	~20 sites in patch.
241	10.3	45.5	0.00	0.40	~10% of surface covered.
471	10.4	90.9	0.00	0.40	
700	10.6	136	0.00	0.40	~35% of surface covered.
1,290	10.6	253	0.00	0.49	~60% of surface covered.
2,300	12.9	450	0.00	0.60	Patch appears to cover the entire surface.
3,120	15.9	613	0.00	0.69	
4,470	18.1	878	0.01	0.84	
6,000	22.2	1,180	0.01	1.02	
7,650	27.0	1,500	0.01	1.21	
6,810	31.9	1,340	0.01	1.13	
5,590	29.7	1,100	0.01	0.98	
4,590	25.9	899	0.01	0.83	
3,760	22.0	767	0.00	0.74	
3,080	19.4	603	0.00	0.65	Site density very large.
2,490	17.1	487	0.00	0.56	
2,040	14.8	400	0.00	0.50	
1,660	13.1	324	0.00	0.45	
1,360	11.9	265	0.00	0.42	
1,110	11.0	217	0.00	0.39	
905	10.1	177	0.00	0.36	
726	9.52	141	0.00	0.34	
587	8.83	114	0.00	0.32	Many sites, bubble size getting smaller.
484	8.35	93.8	0.00	0.30	
397	7.88	76.7	0.00	0.29	
317	7.54	61.1	0.00	0.27	
253	7.19	48.5	0.00	0.27	
207	6.97	39.4	0.00	0.25	
170	6.67	32.3	0.00	0.24	
140	6.32	26.4	0.00	0.22	~150 sites distributed over surface.
113	5.72	21.1	0.00	0.21	
90.3	5.59	16.7	0.00	0.20	~100 active sites.
74.2	5.28	13.6	0.00	0.19	
50.8	5.11	9.02	0.00	0.18	~50-60 active sites.

Run 165   Date 8/7/67   Surface CSF-3

Liquid H_2 Pressure 17.1 psia   Orientation Vertical

Average Depth of Liquid 9 in.   Convection Shield No

$q_M \times 10^3$ (watts)	$q_L \times 10^3$ (watts)	$\dfrac{q_{net}}{A} \times 10^3$ ($\dfrac{watts}{cm^2}$)	δT_{corr} (°K)	ΔT_s (°K)	Comments
21.8	7.10	2.90	0.00	0.27	
45.1	11.7	6.58	0.00	0.45	
94.4	19.1	14.9	0.00	0.73	
104	20.5	16.5	0.00	0.78	
113	21.3	18.1	0.00	0.81	
124	22.6	20.0	0.00	0.86	
137	24.3	22.2	0.00	0.93	
152	25.5	25.0	0.00	0.97	
167	26.8	27.6	0.00	1.02	1 site ~1/2 way from top of surface.
187	28.4	31.2	0.00	1.08	
197	28.8	33.1	0.00	1.10	4 sites above previous site.
243	31.3	41.8	0.00	1.19	
280	25.9	50.1	0.00	0.99	2 additional sites 1/4 way from top, sites near top.
438	29.7	80.6	0.01	1.12	1 site near bottom center, sites in triangle above it.
833	35.4	157	0.01	1.34	Surface ~30% covered with sites.
1,390	40.7	267	0.02	1.53	Surface ~50% covered with sites.
2,130	45.1	411	0.03	1.69	Surface ~65% covered with sites.
2,910	48.8	565	0.04	1.82	Surface ~80% covered with sites.
3,980	52.0	774	0.05	1.93	
5,650	57.5	1,102	0.07	2.13	Surface appears to be covered with sites.
7,700	61.8	1,507	0.10	2.26	
6,160	48.0	1,205	0.08	1.75	
5,070	43.9	992	0.06	1.61	
3,960	39.1	774	0.05	1.44	
3,280	35.4	641	0.04	1.31	Surface still covered with sties.
2,680	31.7	522	0.03	1.18	
2,220	29.2	433	0.03	1.08	Site density decreasing, especially near bottom.
1,860	26.3	362	0.02	0.98	
1,490	23.9	290	0.02	0.89	
1,210	21.8	234	0.01	0.82	
976	19.3	189	0.01	0.72	Few sites on bottom 2mm of surface.

Run 165 (Continued)

q_M x 10^3 (watts)	q_L x 10^3 (watts)	$\dfrac{q_{net}}{A}$ x 10^3 ($\dfrac{watts}{cm^2}$)	δT_{corr} (°K)	ΔT_s (°K)	Comments
791	17.7	152	0.01	0.66	
635	15.8	122	0.01	0.59	Few sites on bottom 5mm of surface.
526	14.6	101	0.01	0.55	
428	13.4	81.7	0.01	0.50	
333	12.2	63.2	0.00	0.47	
267	11.0	50.5	0.00	0.42	Few sites on bottom 6 mm of surface.
220	10.2	41.5	0.00	0.39	
179	9.48	33.4	0.00	0.36	
143	8.62	26.5	0.00	0.33	
114	8.07	21.0	0.00	0.31	
76.3	7.26	13.6	0.00	0.28	
57.0	6.84	9.89	0.00	0.26	~15 sites, mostly 1/2 way from top.
40.4	6.50	6.68	0.00	0.25	~10 steady sites.
32.4	5.90	5.22	0.00	0.23	5 steady sites.
22.0	5.34	3.29	0.00	0.20	3 steady sites.

Run 169   Date 8/10/67   Surface CSF-4a

Liquid H$_2$ Pressure 17.2 psia   Orientation Vertical

Average Depth of Liquid 13 in.   Convection Shield No

$q_M \times 10^3$ (watts)	$q_L \times 10^3$ (watts)	$\dfrac{q_{net}}{A} \times 10^3$ ($\frac{watts}{cm^2}$)	δT_{corr} (°K)	ΔT_s (°K)	Comments
22.2	4.72	3.44	0.00	0.18	
34.9	6.73	5.55	0.00	0.26	
59.4	10.6	9.62	0.00	0.41	
93.3	15.2	15.4	0.00	0.58	
125	18.0	21.0	0.00	0.69	
139	12.7	24.8	0.00	0.49	~8-10 sites on same side of surface, bottom ones 1/3 way up.
181	14.0	32.9	0.00	0.53	
298	15.6	55.7	0.00	0.60	Sites in same area cover ~20% of surface.
522	17.9	99.4	0.01	0.67	
912	19.9	176	0.01	0.75	Sites cover ~50% of surface.
1,450	22.1	282	0.02	0.82	Sites cover ~60% of surface.
2,260	25.2	442	0.03	0.93	Sites cover ~95% of surface.
3,320	35.0	648	0.04	1.29	Sites appear to cover surface.
3,920	37.8	765	0.05	1.39	
5,270	30.9	1,030	0.07	1.11	
7,240	34.6	1,420	0.09	1.24	
6,420	33.3	1,260	0.08	1.19	
5,290	30.9	1,040	0.07	1.11	
4,470	28.8	876	0.06	1.04	
3,490	26.3	684	0.04	.96	
2,910	24.7	570	0.04	0.90	
2,210	22.1	431	0.03	0.81	
1,700	20.2	332	0.02	0.75	
1,180	17.9	230	0.01	0.67	
838	16.3	162	0.01	0.61	
588	14.8	113	0.01	0.55	Few sites on bottom 2mm
396	13.6	75.4	0.00	0.52	
260	12.4	48.8	0.00	0.47	
184	11.4	34.0	0.00	0.43	Most sites on top 1/3 of surface.
139	10.4	25.4	0.00	0.40	~75 sites
102	9.96	18.2	0.00	0.38	~50 sites
68.9	9.07	11.8	0.00	0.35	~25 sites
55.3	8.51	9.23	0.00	0.32	~15 sites
45.4	8.04	8.79	0.00	0.31	10 sites
37.4	7.52	7.23	0.00	0.29	5-7 sites
22.4	5.66	4.31	0.00	0.22	3 steady sites.

REFERENCES

1. Westwater, J. W. "Boiling of Liquids," T. B. Drew and J. W. Hoopes, Jr. Ed., Advances in Chemical Engineering, 1, Academic Press Inc., 1956.

2. Rohsenow, W. M., "Heat Transfer with Boiling," W. M. Rohsenow Ed., Developments in Heat Transfer, Press, 1964.

3. Leppert, C. and Pitts, C. C., "Boiling," T. F. Irvine, Jr. and J. P. Hartnett Ed., Advances in Heat Transfer, 1, Academic Press Inc., 1964.

4. Zuber, N., "Recent Trends in Boiling Heat Transfer Research, Part I: Nucleate Pool Boiling," Applied Mechanics Review, 17, No. 9, p. 663, 1964.

5. Bankoff, S. G., "Ebullition from Solid Surfaces in the Absence of a Pre-existing Gaseous Phase," Trans, ASME, 79, p. 735, May, 1957.

6. Clark, H. B., Strenge, P. S., and Westwater, J. W., "Active Sites for Nucleate Boiling," Chemical Engineering Progress Symposium Series, 55 No. 29, p. 103, 1959.

7. Corty, C. and Foust, A. S., "Surface Variables in Nucleate Boiling," Chemical Engineering Progress Symposium Series, 51, No. 17, p. 1, 1955.

8. Griffith, P. and Wallis, J. D., "The Role of Surface Condition in Nucleate Boiling," Chemical Engineering Progress Symposium Series, 56, No. 30, p. 49, 1960.

9. Hsu, Y. Y. and Graham, R. W., "An Analytical and Experimental Study of the Thermal Boundary Layer and Ebullition Cycle in Nucleat Boiling," NASA TN D-594 (1961).

10. Hsu, Y. Y., "On the Size Range of Active Nucleation Cavities on a Heating Surface," Trans. ASME, Series C, J. of Heat Transfer, 85, p. 207, 1963.

11. Bergles, A. E. and Rohsenow, W. M., "The Determination of Forced-Convection Surface-Boiling Heat Transfer," Trans. ASME, Series C, J. of Heat Transfer, 86, No. 3, p. 365, Aug. 1964.

12. Han, C. Y. and Griffith, P., "The Mechanism of Heat Transfer in Nucleate Pool Boiling, Part I: Bubble Initiation, Growth and Departure," Int. J. Heat Mass Transfer, 8, No. 6, p. 887, June 1965.

REFERENCES (Continued)

13. Howell, J. R. and Siegel, R., "Incipience, Growth and Detachment of Boiling Bubbles in Saturated Water from Artificial Nucleation Sites of Known Geometry and Size," Presented at the Third International Heat Transfer Conference, Chicago, Ill., Aug. 7-12, 1966.

14. Bankoff, S. G., "Entrapment of Gas in the Spreading of a Liquid Over a Rough Surface," AIChE Jour. 4, No. 1, p. 24, March 1958.

15. Marto, P. J. and Rohsenow, W. M., "Effects of Surface Conditions on Nucleate Pool Boiling of Sodium," Trans. ASME, Series C, J. of Heat Transfer, 88, No. 2, p. 196, May 1966.

16. Hatton, A. P. and Hall, I. S., "Photographic Study of Boiling on Prepared Surfaces," Presented at the Third International Heat Transfer Conference, Chicago, I.., Aug. 7-12, 1966.

17. Merte, H. Jr. and Clark, J. A., "Pool Boiling in an Accelerating System," Trans. ASME, Series C, J. of Heat Transfer, 83, p. 233, Aug. 1961.

18. Raben, I. A., Beaubouef, R. T., and Commerford, G., "A Study of Nucleate Pool Boiling of Water at Low Pressure," Chemical Engineering Progress Symposium Series, 61, No. 57, p. 249, 1965.

19. Gaertner, R. F., "Distribution of Active Sites in the Nucleate Boiling of Liquids," Chemical Engineering Progress Symposium Series, 59, No. 41, p. 52, 1963.

20. Berenson, P. J., "Experiments on Pool-Boiling Heat Transfer," Int. J. Heat Mass Transfer, 5, p. 985, 1962.

21. Kurihara, H. M. and Myers, J. E., "The Effect of Superheat and Surface Roughness on Boiling Coefficients," AIChE Jour., 6, No. 1, p. 83, March 1960.

22. Lyon, D. N., "Boiling Heat Transfer and Peak Nucleation Boiling Fluxes in Saturated Liquid Helium Between the λ and Critical Temperatures," K. D. Timmerhaus, Ed., International Advances in Cryogenic Engineering, 10, Plenum Press, p. 371, 1965.

23. Githinji, P. M. and Sabersky, R. H., "Some Effects of Orientation of the Heating Surface in Nucleate Boiling," Trans. ASME, Series C, J. of Heat Transfer, 85, No. 4, p. 379, Nov. 1963.

REFERENCES (Continued)

24. Marcus, B. D. and Dropkin, "The Effect of Surface Configuration on Nucleate Boiling Heat Transfer," *Int. J. Heat Mass Transfer*, 6, p. 683, 1963.

25. Richards, R. J., Steward, W. G., and Jacobs, R. B., "A Survey of the Literature on Heat Transfer from Solid Surfaces to Cyrogenic Fluids," NBS TN-122, 1961.

26. Mulford, R. N. and Nigon, J. P., "Heat Exchange Between a Copper Surface and Liquid Hydrogen and Nitrogen," Los Alamos Scientific Laboratory, LA-1416, 1952.

27. Class, C. R., DeHann, J. R., Piccone, M., and Cost, R. B., "Boiling Heat Transfer to Liquid Hydrogen from Flat Surfaces," K. D. Timmerhaus, *Advances in Cryogenic Liquids*, 5, Plenum Press, p. 254, 1960.

28. Class, C. R., DeHann, J. R., Piccone, M., and Cost, R. B., "Pool Boiling Heat Transfer to a Cryogenic Liquid," WADC Technical Report 58-528, 1958.

29. Drayer, D. E. and Timmerhaus, K. D., "An Experimental Investigation of the Individual Boiling and Condensing Heat Transfer Coefficients for Hydrogen," K. D. Timmerhaus, Ed., *Advances in Cryogenic Engineering*, 7, Plenum Press, p. 401, 1962.

30. Graham, R. W., Hendricks, R. C., and Ehlers, R. C., "An Experimental Study of the Pool Heating of Liquid Hydrogen in the Subcritical and Supercritical Pressure Regimes over a Range of Accelerations," K. D. Timmerhaus, Ed., *International Advances in Cryogenic Engineering*, 10, Plenum Press, p. 342, 1965.

31. Fredrickson, G. O. and Schweikle, J. D., "Thermo and Hydrodynamic Experiment Research Module in Orbit—Final Report," Douglas Missile and Space Systems Division, DAC-60594, March 1967.

32. Sherley, J. E., "Nucleate Boiling Heat Transfer Data for Liquid Hydrogen at Standard and Zero Gravity," K. D. Timmerhaus, Ed., *Advances in Cryogenic Engineering*, 8, Plenum Press, p. 495, 1963.

33. Steinle, H. F., "Review of Zero-G Studies Performed at General Dynamics/ Astronautics," *Advances in the Astronautical Sciences*, 14, p. 95.

34. Tusk, G., "Zero-G Report—LH$_2$ Boiling Threshold," GD/A Report 55D 859- 3, May 1962.

REFERENCES (Continued)

35. Drayer, D. E., "Nucleate Boiling of Hydrogen," I and EC Fundamentals, 4, No. 2, p. 167, May 1965.

36. Zuber, N. and Fried, E., "Two-Phase Flow and Boiling Heat Transfer to Cryogenic Liquids," Americal Rocket Society Jour., 32, No. 9, p. 1332, Sept. 1962.

37. Forster, H. K. and Zuber, N., "Dynamics of Vapor Bubbles and Boiling Heat Transfer," AIChE Jour., 1, No. 4, p. 531, Dec. 1955.

38. Forster, H. K. and Greif, R., "Heat Transfer to a Boiling Liquid—Mechanism and Correlations," Trans. ASME, Series C, J. of Heat Transfer, 81, No. 1, p. 42, Feb. 1959.

39. Cryder, D. S. and Gilliland, E. R., Ind. Eng. Chem., 24, p. 1382, 1932.

40. Hord, J., Jacobs, R. B., Robinson, C. C., and Sparks, L. L., "Nucleation Characteristics of Static Liquid Nitrogen and Liquid Hydrogen," Trans ASME, Series A, J. of Engineering for Power, 86, No. 4, p. 485, 1964.

41. Good, R. J. and Ferry, G. V., "The Wetting of Solids by Liquid Hydrogen," K. D. Timmerhaus, Ed., Advances in Cryogenic Engineering, 8, Plenum Press, p. 306, 1963.

42. Brentari, E. G. and Smith, R. V., "Nucleate and Film Pool Foiling Design Correlations for O_2, H_2, N_2, and He," K. D. Timmerhaus, Ed., International Advances in Cryogenic Engineering, 10, Plenum Press, p. 325, 1965.

43. McAdams, W. H., Heat Transmission, McGraw-Hill Book Co., 1954.

44. Scott, R. B., Cryogenic Engineering, D. Van Nostrand Co., Inc., 1959.

45. Powell, R. L. and Bunch,   Nat. Bur. of Standards Publ., R-188.

46. Feller, W., Probability Theory and Its Applications, 1, John Wiley and Sons, Inc., New York, 1950.

47. Corruccini, R. J., "Properties of Liquid Hydrogen," Nat. Bur. of Standards Publication, R412, 1965.

48. Scott, R. B., Denton, W. H., and Nicholls, C. M., Technology and Uses of Liquid Hydrogen, Pergamon Press, 1964.

REFERENCES (Concluded)

49.   Strobridge, T. R., "The Thermodynamic Properties of Nitrogen from 64 to 300°K Between 0.1 and 200 Atmospheres," Nat. Bur of Standards, TN129, 1962.

50.   Handbook of Chemistry and Physics, 40th ed., Chemical Rubber Publishing Co., Cleveland, Ohio, 1959.

51.   Kreith, F., Principles of Heat Transfer, 2nd ed., International Textbook Co., Scranton, Pa., 1966.

52.   Goodwin, R. D., Diller, D. E., Roder, H. M., and Weber, L. A., "The Densities of Saturated Liquid Hydrogen," Nat. Bur. of Standards Publication, R226, 1961.